

ENGINEERING INTRAVAGINAL RINGS FOR HIV
PREVENTION AND CONTRACEPTION

by

Justin Thomas Clark

A dissertation submitted to the faculty of
The University of Utah
in partial fulfillment of the requirements for the degree of

Doctor of Philosophy

Department of Bioengineering

The University of Utah

May 2014

Copyright © Justin Thomas Clark 2014

All Rights Reserved

The University of Utah Graduate School

STATEMENT OF DISSERTATION APPROVAL

The dissertation of Justin Thomas Clark
has been approved by the following supervisory committee members:

<u>Patrick F. Kiser</u>	, Chair	<u>12/12/2013</u> Date Approved
<u>David W. Grainger</u>	, Member	<u>12/12/2013</u> Date Approved
<u>Vladimir Hlady</u>	, Member	<u>12/12/2013</u> Date Approved
<u>Leonard F. Pease</u>	, Member	<u>12/12/2013</u> Date Approved
<u>Anil V. Virkar</u>	, Member	<u>12/12/2013</u> Date Approved

and by Patrick A. Tresco, Chair/Dean of
the Department of Bioengineering

and by David B. Kieda, Dean of The Graduate School.

ABSTRACT

Three decades have passed since the discovery of HIV and still no viable vaccine technologies exist to prevent the spread of the virus. The concept of interrupting HIV transmission with oral or topical antiretroviral drugs (ARV), also known as pre-exposure prophylaxis (PrEP), has been proven in several clinical efficacy trials. One PrEP strategy has been to formulate the ARV tenofovir (TFV) into topically applied vaginal gels. However, the vaginal gel approach has met with mixed results, likely due to poor user adherence. Globally, high incidence of HIV infection correlates with high incidence of unintended pregnancy, especially in resource-poor regions. Combining HIV PrEP with contraception into a single, easy-to-use product could have a synergistic effect, further motivating women to protect themselves against HIV infection. Thus, a concerted effort is underway to develop long-acting multipurpose prevention technologies (MPT) capable of simultaneously preventing sexual HIV transmission and pregnancy.

The nearly half-century-old technology of the intravaginal ring (IVR) has undergone a renaissance in the past decade due to the potential of IVR to leverage both the principles of topical HIV PrEP and of long-acting controlled drug release systems. This dissertation details several new observations and innovations regarding drug delivery from intravaginal rings (IVR). First, an injection-molded, hydrophilic poly(ether urethane) (HPEU) matrix IVR capable of sustained release of milligram-per-day quantities of TFV over 90 days is described. In the final two chapters, a second-

generation reservoir TFV IVR is combined with a reservoir poly(ether urethane) segment that releases microdoses of the contraceptive progestin levonorgestrel (LNG), in a multisegment IVR design, concluding with assessments of product stability and *in vivo* pharmacokinetics in order to confirm the suitability of the IVR for clinical investigation. This dissertation represents an engineer's approach to designing and testing IVR, which are most commonly considered a pharmaceutical product rather than a medical device. Accordingly, much attention is given to the development and usage of mathematical models for drug release and mechanical properties from IVR, and in general to a mechanistic understanding of the underlying mechanisms of their operation.

To Jenny, and all who encouraged me to see this through to the end

TABLE OF CONTENTS

ABSTRACT.....	iii
NOMENCLATURE	viii
ACKNOWLEDGEMENTS	xiii
1 INTRODUCTION	1
1.1 HIV/AIDS Pandemic and ARV Therapy.....	2
1.2 HIV Pre-Exposure Prophylaxis.....	3
1.3 Contraception and Modern Contraceptive Methods.....	5
1.4 Multipurpose Prevention Technologies	7
1.5 History of Intravaginal Rings.....	8
1.6 IVR Dimensions, Design, Materials, and Manufacturing.....	11
1.7 Drug Release from IVR	14
1.8 Biotransport Description of HIV Pre-Exposure Prophylaxis.....	17
1.9 Mechanical Properties of IVR	21
1.10 Dissertation Chapter Overview.....	23
1.11 References.....	25
2 QUANTITATIVE EVALUATION OF A HYDROPHILIC MATRIX INTRAVAGINAL RING FOR THE SUSTAINED DELIVERY OF TENOFOVIR	34
2.1 Abstract.....	35
2.2 Introduction.....	35
2.3 Theory	36
2.4 Materials and Methods.....	37
2.5 Results and Discussion	38
2.6 Conclusion	42
2.7 Acknowledgements.....	42
2.8 References.....	42
2.9 Supplementary Data.....	44
3 ENGINEERING A SEGMENTED DUAL-RESERVOIR POLYURETHANE INTRAVAGINAL RING FOR SIMULTANEOUS PREVENTION OF HIV TRANSMISSION AND UNWANTED PREGNANCY	47

3.1 Abstract.....	48
3.2 Introduction.....	48
3.3 Design.....	49
3.4 Theory.....	50
3.5 Materials and Methods.....	52
3.6 Results and Discussion.....	54
3.7 Conclusions.....	59
3.8 Acknowledgements.....	60
3.9 References.....	60
3.10 Supporting Information.....	62
4 PRECLINICAL EVALUATION OF A MULTIPURPOSE PREVENTION INTRAVAGINAL RING: ASSESSMENTS OF STABILITY AND IN VIVO PERFORMANCE.....	71
4.1 Abstract.....	72
4.2 Introduction.....	72
4.3 Materials and Methods.....	75
4.4 Results.....	84
4.5 Discussion.....	91
4.6 Conclusions.....	97
4.7 Acknowledgements.....	98
4.8 References.....	98
4.9 Figures.....	102
5 SUMMARY AND FUTURE DIRECTIONS.....	108
5.1 Research Summary and Context.....	109
5.2 Discussion and Future Recommendations.....	111
5.3 References.....	116
APPENDIX: PROPOSED SPATIAL PK MODEL FOR PREDICTION OF DRUG AND VIRUS TRANSPORT IN THE VAGINAL TRACT.....	118

NOMENCLATURE

a	exponential time constant decay of drug release rates from reservoirs
ACN	acetonitrile
AIDS	acquired immunodeficiency syndrome
α	fractional equilibrium polymer swelling
ARV	antiretroviral drug
AUC	area under the curve
β	linear constant for implicit solution for drug release from matrix devices
c_0	initial concentration
CAD	computer-aided design
c_{in}	reservoir core concentration
c_{max}	maximum drug concentration
COC	combined oral contraceptive (progestin + estrogen)
c_p	drug concentration in blood plasma
DDI	doubly de-ionized
D, D_{eff}	effective diffusivity
dM/dt	drug release rate
DPV	dapivirine (TMC-120)
E	Young's modulus, modulus of elasticity
EE	ethinyl estradiol

ENG	etonogestrel
EVA	poly(ethylene-co-vinyl acetate)
F	force, load
F_1	force required to compress a ring by 1% of its initial outer diameter
F_{10}	force required to compress a ring by 10% of its initial outer diameter
FDA	United States Food and Drug Administration
FGT	female genital tract
FTC	emtricitabine
f_2	similarity factor (for comparison two drug release profiles)
HEC	hydroxyethyl cellulose
HIV, HIV-1	human immunodeficiency virus, type 1
HPEU	hydrophilic poly(ether urethane)
HPLC	high performance liquid chromatography
IUS	intrauterine system
IVR	intravaginal ring
k	linear regression constant for force vs. ring compression (Chapter 2), linear regression constant for drug release against the square-root-of-time (Chapter 3)
k_{12}	rate constant for elimination of drug from tissue to plasma
K ₃ EDTA	tripotassium ethylenediaminetetraacetic acid
l	length
LNG	levonorgestrel
LOQ	limit of quantification

LP	lamina propria
$M, M(t)$	cumulative drug release
M_0	initial total drug mass
MALDI	matrix-assisted laser desorption/ionization
M_b	total maximal burst release from a reservoir device
MPT	multipurpose prevention technology
MS	mass spectroscopy
N9	nonoxynol-9
NHP	nonhuman primate
NNRTI	nonnucleoside reverse transcriptase inhibitor
NRTI	nucleoside reverse transcriptase inhibitor
NtRTI	nucleotide reverse transcriptase inhibitor
OD	outer ring diameter
ODE	ordinary differential equation
ω_s	mass/weight fraction solubility
ω_s^*	porosity adjusted mass/weight fraction solubility
ω_T	total fractional drug loading (by mass/weight)
PBS	phosphate buffered saline
PDE	partial differential equation
PEO	poly(ethylene oxide), poly(ethylene glycol)
PEU	poly(ether urethane)
PK	pharmacokinetic, pharmacokinetics
PLDT	product-log difference transform

POP	progestin-only pill
PrEP	pre-exposure prophylaxis
PSS	pseudo-steady-state
PTFE	poly(tetrafluoroethylene)
PTM	pig-tailed (pigtail) macaque
PTMO	poly(tetramethylene oxide)
R	outer ring radius
R'	outer ring radius (measured to center of cross-section)
RCM	rate-controlling membrane
r_d	diffusion front, distance from center to diffusion front
r_i	inner cross-sectional radius, reservoir core radius
r_o	outer cross-sectional radius, cross-sectional radius
RTI	reverse transcriptase inhibitor
SHIV	simian/human immunodeficiency virus
SSE	single screw extruder
STI	sexually transmitted infection
t_b	burst duration from reservoir devices
TDF	tenofovir disoproxil fumarate
TFV	tenofovir
TFV-DP	tenofovir disphosphate
t_{lag}	lag time
TSE	twin screw extruder
UP	unintended pregnancy, unwanted pregnancy

USDA	United States Department of Agriculture
UTL	upper testing limit
VE	vaginal epithelium
VF	vaginal fluid
v/v	volume per volume
W	Lambert W-function, product log function
W_0	upper real valued branch of Lambert W-function
W_{-1}	lower real valued branch of Lambert W-function
w/v	weight per volume
w/w	weight per weight
WHO	World Health Organization
XD	cross-sectional diameter

ACKNOWLEDGEMENTS

First and foremost, I thank my soon-to-be wife, Jennifer Wall, without whose boundless love and unwavering moral support this manuscript may have never been completed. I also thank my mother and father, Gaye Clark and Dr. Kevin Clark, for their unconditional support throughout the entirety of this endeavor, for always encouraging me to embrace and explore my abilities, and for insisting that I never settle for less than my best.

Next, I must thank my advisor, Dr. Patrick Kiser, for his continual guidance, mentorship, and honest criticism and critique throughout my graduate career and for lending me (at least some portion of) his unparalleled dedication. Dr. Kiser always encouraged me to expand my thinking, examine problems critically, and abandon dogmatic tendencies. Above all technical specificities, I feel that I improved innumerable as a critical and rational thinker through this experience. I thank my "scientific big brother", Dr. Todd Johnson, for helping to pave the way for this work, and for his patience and thoughtfulness. I also thank my "scientific big sister", Dr. Meredith Clark, for her continual motivation, encouragement, and mentorship. I thank Drs. Tyler McCabe and Rachna Rastogi for their wise council and rational perspective. I thank *anyone* who worked in the Kiser Lab from 2009 to 2013 for helping to shape it into the incredible collaborative space in which I was fortunate to perform my dissertation work.

Specifically, I thank Judit Fabian, Dr. Namdev Shelke, Eric Smith, Andrew Andreasen

and Joel Nebeker, without whose contributions this body of work would not have been possible. I also thank the remainder of my supervisory committee, Drs. David Grainger, Vladimir Hlady, Leonard Pease, and Anil Virkar, for their council and for their critical audit of the scientific merit of this dissertation.

I must also acknowledge the wonderful team at CONRAD of Eastern Virginia Medical School, especially Dr. Clark and Dr. David Friend. Without their financial support, collaboration, and commitment, the large body of data in this dissertation could never have been collected. I thank CONRAD and their funding sources, as well as Dr. Kiser for allowing me to participate in such important projects as these with real-world significance. It has been a truly remarkable experience.

Lastly (but not "leastly"), I thank our (Jenny's and my) families and our incredible group of loyal friends for their constant encouragement and genuine interest in this work throughout the past few years. This goes out to all of you.

CHAPTER 1

INTRODUCTION

This chapter includes excerpts from the manuscript:

STATE OF THE ART IN INTRAVAGINAL RING TECHNOLOGY FOR TOPICAL PROPHYLAXIS OF HIV INFECTION

Patrick F. Kiser, Todd J. Johnson, and Justin T. Clark

AIDS Reviews 2012; 14(1): 62-77

Reproduced with permission from Permanyer Publishing

1.1 HIV/AIDS Pandemic and ARV Therapy

The human immunodeficiency virus (HIV) was clinically identified as the causative agent of acquired immunodeficiency syndrome (AIDS) in 1983. Primarily by sexual transmission, HIV propagated rapidly both in the developed and developing world, eventually resulting in the classification of HIV/AIDS as a global pandemic. HIV is a retrovirus that causes a loss in cell-mediated immunity by attacking CD4+ T cells. The virus is notoriously difficult to eradicate from the body due to its high genetic variability and highly glycosylated envelope that protects genetically conserved receptor sites [1], as well as its ability to lie latent in cellular reservoirs [2]. Three decades following its discovery, no efficacious vaccine strategies have been identified to prevent infection. The WHO estimates that approximately 70 million people have been infected with HIV since the beginning of the epidemic, half of whom (35 million) have died due to AIDS-related complications.

Through the diligent use of antiretroviral (ARV) drug therapy, HIV infection is no longer universally fatal. Over two dozen ARV drugs have been approved by the FDA to date [3]. ARV are generally classified by their mechanisms of action, with reverse transcriptase inhibitors (RTI) being among the earliest and most common. These RTI act by inhibiting HIV reverse transcriptase (RT) and preventing DNA transcription of the viral RNA genome. RTI are further subdivided into three main categories: nucleoside analogs (NRTI), nucleotide analogs (NtRTI), and nonnucleosides (NNRTI). NtRTI and NRTI are phosphorylated two or three times intracellularly, respectively, to their active forms which compete with deoxyribonucleotide triphosphate binding to prevent transcription of the viral genome [4]. In contrast, NNRTI are delivered in their active form and prevent transcription by binding to a specific pocket on HIV RT. Although this

dissertation will focus on RTI, there are several other classes of ARV utilized for HIV treatment, including protease inhibitors, integrase inhibitors, and cell entry inhibitors. Even with the advent of ARV therapy, HIV/AIDS remains a global pandemic, with 35 million living with HIV infection, 2.3 million new infections per year, and 1.6 million annual deaths resulting from AIDS-related complications [5]. HIV/AIDS disproportionately affects resource-poor settings, such as sub-Saharan Africa, where nearly 5% of the population (age 15-49) is infected, compared to less than 1% in most other parts of the world. National prevalence is even more staggering in specific Southern African countries; more than 15% of the population (age 15-49) lives with HIV in South Africa (18%), Botswana and Lesotho (23%), and Swaziland (27%, the highest observed globally) [5].

1.2 HIV Pre-Exposure Prophylaxis

The continued absence of an HIV vaccine has motivated the investigation of woman-controlled strategies that can interrupt the early events of male-to-female sexual transmission. Early studies employed vaginal gels formulated with nonspecific polymeric agents (e.g. carrageenan, cellulose sulfate) designed to prevent infection and were categorically unsuccessful [6]. More recent efforts have proven the concept of pre-exposure prophylaxis (PrEP), whereby ARV drugs are administered prior to sexual exposure. To date, HIV PrEP has met with mixed results. In the CAPRISA 004 study, women were instructed to use a hydroxyethylcellulose (HEC) vaginal gel containing the NtRTI tenofovir (TFV) up to 12 hours before and after sexual intercourse (twice per act of intercourse, often referred to as BAT24 dosing). Use of this TFV 1% gel resulted in a 39% reduction in HIV infection compared to use of a placebo (non-TFV) gel [7]. The

TFV gel prevented transmission more effectively (54%) in women who reported at least 80% adherence to the trial protocol. Furthermore, the gel was 74% effective in women who exhibited vaginal fluid concentrations of TFV greater than 1000 ng/g [8].

Unfortunately, once-daily, coitally-independent administration of the same TFV 1% gel failed to demonstrate a statistically significant reduction in male-to-female transmission in the VOICE study [9]. Another PrEP strategy, also met with mixed results, has been once-daily oral administration of the existing HIV therapy Truvada, a fixed dose combination of tenofovir disoproxil fumarate (TDF, an oral prodrug of TFV) and the NRTI emtricitabine (FTC). In the Partners PrEP study, oral Truvada was 75% effective in preventing HIV-negative men and women from becoming infected by their seropositive partner [10]. This result was confirmed in another study termed TDF2, where a general population of men and women were 62% less likely to become infected when using Truvada. These results contributed to the FDA approval of oral Truvada as the first clinical PrEP intervention [11]. However, oral Truvada was unsuccessful in the aforementioned VOICE study and in the FEM-PrEP study that was discontinued due to low user-reported adherence [12]; also likely contributing to the failure of VOICE. In total, these results demonstrate that PrEP has great promise to impact the pandemic, but that products need to be developed that women are highly motivated to use. It is impossible to demonstrate clinical efficacy if a majority of participants do not use the product as instructed.

Although it has been difficult to show effectiveness in human PrEP studies to-date, the promise of PrEP has been strengthened by several demonstrations of HIV chemoprophylaxis in nonhuman primate (NHP) models. In the only true preclinical

measure of HIV PrEP efficacy, NHP (generally pig-tailed or rhesus macaques) are repeatedly exposed to the recombinant simian-human immunodeficiency virus (SHIV) during the implementation of a PrEP dosing strategy. Dobard *et al.* challenged pig-tailed macaques twice-weekly for 10 weeks during once-weekly 1% TFV gel dosing (SHIV exposure both 30 minutes and 72 hours after exposure) and demonstrated 74% efficacy of TFV gel in preventing SHIV infection [13]. ARV-releasing intravaginal rings (IVR, which will be the focus of this manuscript and are introduced in detail below) have also shown high rates of efficacy in NHP challenge studies. An IVR releasing the NNRTI MIV-150 demonstrated 80% efficacy in preventing SHIV infection in rhesus macaques [14], while another IVR releasing TDF was 100% effective (no infections in the active IVR group) in preventing SHIV infection in pig-tailed macaques challenged weekly for 4 months during continuous IVR use [15].

1.3 Contraception and Modern Contraceptive Methods

Nearly inseparable from a discussion of the HIV/AIDS pandemic is the staggering global incidence of unintended pregnancy (UP). Over 50 years after the advent of daily hormonal contraception and with several highly-effective contraceptive options available worldwide, nearly half of all pregnancies worldwide are still unintended, equating to approximately 80 million pregnancies per year that result in nearly 100,000 maternal deaths due to unsafe abortions and pregnancy- or delivery-related complications [16]. These statistics are startling considering the wide variety of contraceptive options available to women. Contraceptive methods are typically classified as either modern or traditional, where "traditional methods" include lower effectiveness user interventions such as withdrawal and periodic abstinence (the "rhythm" method). Modern methods can

be either reversible or nonreversible (e.g. sterilization). Most reversible methods can be further subdivided into two main categories: barrier methods, such as the male and female condom that employ a physical polymeric barrier to prevent the transport of sperm through the cervix, and hormonal methods that employ the periodic or continuous administration of various hormone analogs to prevent ovulation and/or fertilization. With the exception of the male condom and male sterilization, all modern methods are woman-controlled. No approved drug products exist for male contraception, although several compounds with various mechanisms of action are under investigation. In daily combined oral contraceptive (COC) strategies (colloquially known as "the pill"), a fixed-dose combination pill containing a synthetic progestogen (progestin) and an estrogen analog is taken once-daily in a 21 day on, 7 day off cycle that simultaneously prevents ovulation and regulates the menstrual cycle. COC is still the most popular modern method in the U.S. [17] and the most popular reversible modern method in some regions around the world [18]. Progestin-only pills (POP) are also available that may or may not inhibit ovulation, depending on the dose, but also may rely on the thickening of cervical mucus to inhibit sperm transport and prevent fertilization [19].

As with any periodic interventions, daily oral contraception is subject to varying degrees of user adherence which may ultimately reduce effectiveness. Several highly-effective alternative drug delivery systems exist which can provide reliable contraception for extended durations with little or no user intervention. As discussed below, NuvaRing is a 99% effective combined contraceptive IVR applied once every 28 days and follows COC pattern of 21 days in, 7 days out to regulate the menstrual cycle [20]. Other, even more effective methods employ the progestin-only strategy, including the Depo-Provera

injection (effective for 3 months), progestin-releasing subcutaneous implants (i.e. Norplant and Jadelle, effective for up to 3-5 years), and progestin-releasing intrauterine systems (IUS). The Mirena and Skyla IUS both deliver very small doses (up to 14 and 20 $\mu\text{g}/\text{d}$, respectively) of the progestin levonorgestrel (LNG) in the uterus for up to 3 and 5 years, respectively, and achieve contraception largely through local effects (e.g. cervical mucus thickening and inhibition of sperm function) [21]. Both Mirena and Skyla are over 99% effective in preventing pregnancy [22, 23]. The one product perhaps not classified as either a barrier or hormonal method is Paragard, a copper-releasing IUS that is also over 99% effective and can remain in place for up to 10 years [24].

UN models estimate that worldwide prevalence of modern contraception among married or in-union women between the ages of 15 and 49 was 57% in 2013. As with the HIV statistics presented above, a large regional disparity exists in the use of modern methods, with the same models predicting 71% and 74% use in North America and Northern Europe, respectively, but only 21% use throughout Sub-Saharan Africa [25].

1.4 Multipurpose Prevention Technologies

Through the statistics presented thus far, the reader will recognize the simultaneous need for HIV prevention technologies and reliable contraception in resource-poor settings, such as the often-discussed Sub-Saharan Africa. Biomedical interventions designed to simultaneously address multiple reproductive health needs are commonly termed multipurpose prevention technologies (MPT) [16]. MPT can include products that protect against multiple sexually transmitted infections (STI) or contraception and an STI. The only existing commercially available MPT are the barrier contraceptives discussed above (male and female condoms), which exhibit reasonable

efficacy in providing a barrier to both agents of infection (i.e. viruses and bacteria) and sperm cells, but are prone to misuse and inconsistent use. Condoms are particularly problematic in developing areas with high HIV prevalence, in part due to men's unwillingness to comply with a woman's desire for their use [26].

A single product that combines HIV PrEP and contraception has been identified as an urgently needed MPT by the global health community [27]. It has been hypothesized that the inclusion of a contraceptive into an HIV PrEP could increase user demand for PrEP products, due to the familiarity of contraceptive products whereas HIV PrEP is a relatively new concept. Combination of the two indications could also provide significant cost amortization, greatly needed in the development of publically-funded developing world products.

1.5 History of Intravaginal Rings

Intravaginal rings (IVR) have taken center stage in the PrEP discussion as an alternative to the inconvenient and undesirable once-daily application of ARV using oral tablets or vaginal gels. IVR are promising as they can directly deliver ARV to the potential site of HIV infection in a sustained or controlled fashion for months or even years from a single device [28]. Similarly, IVR have been identified as one of the two most viable options for a long-acting MPT platform along with injectable depot formulations [16].

IVR were among the first in the class now referred to as "combination devices" or "drug/device combinations". Combination devices can either be regulated as drugs or medical devices by the FDA, depending on the primary mechanism of action. All IVR to date have been classified as drug products, as their primary function is to deliver drugs to

the vaginal tract, and their secondary function is to remain in place in the upper vaginal tract via a mechanical force balance between the IVR and the vaginal musculature. IVR were first investigated for the sustained delivery of contraceptive hormones to systemic circulation in the late 1960s [29, 30], exploiting the effective systemic absorption of small molecules through the vaginal mucosa, a phenomenon discovered nearly a century ago [31]. Mishell *et al.* were the first to clinically demonstrate the potential of contraception via IVR by testing a silicone IVR impregnated with the progestin medroxyprogesterone acetate, the same active ingredient as in the commonly used Depo-Provera contraceptive injection, in a small PK/PD pilot trial [32]. In a series of seminal papers, Chien *et al.* used similar silicone IVR as a case study for the discussion of controlled drug release in the context of vaginal delivery, describing methods for *in vitro* release testing [33], mechanisms of drug release [34], and *in vivo* evaluation of vaginal devices using the rabbit model [35]. The WHO developed a "microdose" progestin IVR that released approximately 20 µg/d LNG for up to 3 months [36-39]. This LNG IVR was tested in a large clinical multicenter clinical trial and was shown to be over 95% effective in preventing pregnancy. This IVR showed promise, but development was discontinued for multiple reasons, one being that use of the IVR was associated with formation of vaginal lesions, potentially due to excessive device stiffness [40] (IVR mechanical properties are discussed in detail in Section 1.9). The first contraceptive IVR to market was the progestin/estrogen NuvaRing, a poly(ethylene-co-vinyl acetate) (EVA) ring that releases the progestin etonogestrel (ENG) and ethinyl estradiol (EE) at near constant rates over 21 days. The inclusion of EE and the 3 week in/1 week out cycle generally results in a normal menstrual cycle, as in progestin/estrogen oral contraceptives that adhere to a

similar 3 week/1 week cycle. Several important insights to IVR design and development gained from the NuvaRing work were published by van Laarhoven and colleagues in the early 2000s [41-43]. Four silicone-based IVR are currently available worldwide for various indications other than general contraception. Estring and Femring, both available in the US, deliver estrogen analogs (estradiol and estradiol acetate, respectively) for postmenopausal hormone replacement. Progering and Fertiring both release natural progesterone and are approved only in select Central and South American countries. Progering is indicated for contraception in lactating women, while Fertiring is indicated for hormone supplementation and pregnancy maintenance during *in vitro* fertilization [44].

IVR for HIV PrEP can be traced back to the nonoxynol-9 (N9) releasing silicone IVR reported by Malcolm and Woolfson at Queen's University Belfast in the early 2000s [45]. N9 is a nonionic surfactant that was indicated for use as a spermicide and investigated for use as anti-HIV ("microbicide") agent. However, all hope of using N9 as a microbicide ceased with observations that N9 use could result in higher risk for HIV infection, regardless of its potential anti-HIV activity. This group went on to formulate the NNRTI dapivirine (DPV, often referred to by its laboratory designation, TMC120) into silicone IVRs [46, 47], research that ultimately led to clinical testing [48-50] and an ongoing Phase III clinical trial, the first of its kind to test the efficacy of an IVR for HIV PrEP. In the mid-to-late 2000s, Kiser *et al.* at the University of Utah published several papers reporting the *in vitro* and *in vivo* investigation of polyurethane IVR for the delivery of several ARV [51, 51-55], including an innovative multisegment IVR for the combination delivery of TFV and DPV [56]. Chapters 2, 3, and 4 of this manuscript

detail the continuation of this work, including the incorporation of a contraceptive-releasing component in what will likely become the first clinically-viable MPT IVR.

1.6 IVR Dimensions, Design, Materials, and Manufacturing

IVR are flexible torus-shaped devices typically classified by two characteristic dimensions: outer diameter (OD), or the overall maximum width of the entire ring, and cross-sectional diameter (XD), the width of the ring forming strand. IVR OD are somewhat constrained by the width of the vaginal canal, observed to vary from 48 to 63 mm in one study [57], although the fit and comfort of IVR are truly constrained by the overall balance of elastic properties between the compressible ring and the vaginal musculature (see Section 1.9). Clinical IVR OD do not vary greatly, ranging from 54 mm (NuvaRing) to 56 mm (Femring); however, sizes of 50 to 61 mm are thought to be well-tolerated based on clinical investigation [29]. Interestingly, the first silicone IVR tested by Mishell had OD of up to 80 mm [32]. Clinical IVR XD vary more significantly than OD, ranging from 4 mm (NuvaRing) to 9 mm (Estring).

Most IVR fall into two design classes, matrix and reservoir. Matrix IVR are simple, monolithic devices where drug is dissolved and/or dispersed evenly throughout the polymer matrix, whereas reservoir IVRs employ a rate-controlling membrane (RCM) to control the rate of drug release. Drug release from matrix IVR usually decreases significantly with time, due to an increase in the effective diffusion path length following progressive inward drug depletion. Drug release rates from reservoir IVR are linearly dependent on the dissolved core drug concentration, and thus can be constant (if an excess of undissolved drug is present), or can decay in a first-order exponential fashion (if the entirety of drug is completely dissolved). Mathematical models for drug release

from IVR are a focus of this dissertation, and are given a detailed introduction in Section 1.7. Most clinical IVR are reservoirs, but matrix IVR have seen significant investigation by the HIV PrEP field, likely due to their potential manufacturing simplicity and reduced cost. More advanced designs have been investigated which ease the challenge of delivering multiple drugs simultaneously, although this was achieved in the standard reservoir NuvaRing, likely due to the chemical similarity of the two molecules delivered. These advanced designs include the segmented or multisegment IVR (discussed in Chapters 3 and 4) which theoretically can incorporate both matrix and reservoir components, and the pod-insert IVR wherein a placebo injection molded ring is fitted with several reservoir-type controlled release inserts [58].

When designing an IVR for drug delivery, one must first estimate the desired daily drug dose and duration, the product of which results in the minimum necessary drug load, although a significant overage would be required for matrix IVR that exhibit time-dependent drug release behavior. The total drug load in an IVR (M_0) is calculated as follows:

$$M_0 = 2\omega_T\rho\pi^2r_o^2(R - r_o) \quad (1.1)$$

where ω_T is the drug weight fraction loaded in the matrix, ρ is the matrix density and R and r_o are the IVR outer and cross-sectional radii, respectively (or half of the outer and cross-sectional diameters). In cases where drug is only loaded into the core of a reservoir IVR, the first instance (but not the second) of r_o is replaced with r_i , or the core cross-sectional radius.

In theory, any elastomer that proves biocompatible in contact with the vaginal mucosa can be used as an IVR matrix, provided that it meets two basic criteria. First, it

must not erode or degrade on relevant time-scales for IVR drug delivery (i.e. weeks to months, depending on the specific system), and second, it must possess appropriate continuum-scale properties, namely compatible values of effective drug-polymer diffusivity (D_{eff} , used interchangeably with D in this dissertation) and elastic modulus (E). The interdependence of D_{eff} and E is further explored in Chapter 2. As detailed in the previous section, 4 of the 5 commercially-available IVR are fabricated from thermosetting silicone elastomers, with the one exception (NuvaRing) being fabricated from the thermoplastic poly(ethylene-co-vinyl acetate) (EVA). The DPV IVR under clinical investigation for HIV PrEP is also synthesized from a silicone elastomer. Kiser and colleagues have extensively investigated thermoplastic polyurethane elastomers as IVR matrices, particularly poly(ether urethanes) (PEU), which are synthesized from the condensation polymerization of isocyanates and oligomeric poly(ether diols), typically poly(tetramethylene oxide) (PTMO). These PEU can be synthesized in water-swelling and nonswelling variants, with the former, referred to as hydrophilic PEU (HPEU), achieving tunable hydrophilicity through the modulation of the ratio between PTMO and poly(ethylene oxide) (PEO). Use of HPEU and PEU in segmented IVR has proven useful as the two types are chemically very similar on the microscopic scale, and thus can easily be welded together to form mechanically sound IVR, while the HPEU ring components allow for delivery of hydrophilic drugs which do not possess sufficient solubility and/or permeability in the nonswelling elastomers. Most IVR designs are limited to the delivery of small molecule drugs due to similar solubility/permeability constraints; however, several designs have been investigated, including the aforementioned pod-insert ring, that could allow for delivery of larger molecules [58, 59]. Saxena *et al.* investigated a

biodegradable hydrogel IVR formed from a co-polymer of 2-hydroxyethyl methacrylate and acrylic acid, although not much is known about the practicality or acceptability of such a device [60, 61].

IVR manufacturing is usually limited to reaction injection molding as most IVR are comprised of thermosetting silicones. NuvaRing manufacturing leverages the thermoplastic nature of EVA by using a continuous co-axial hot melt extrusion process to manufacture a drug-loaded reservoir strand that is cut to length and welded to form a ring by induction welding. The PEU IVR designed by Kiser *et al.* are also typically made by hot-melt extrusion and melt-welding. The use of extrusion and injection molding are described in Chapter 2, and use of co-axial extrusion and induction welding are described in Chapter 3.

Sections 1.7, 1.8, and 1.9 contain excerpts from "State of the Art in Intravaginal Ring Technology for Topical Prophylaxis of HIV Infection", authored by Patrick F. Kiser, Todd J. Johnson, and Justin T. Clark, and published in *AIDS Reviews* Volume 14 (2012) (pages 62-77).

1.7 Drug Release from IVR

The release rates of drugs from IVR can be limited by one or more physical processes. Assuming a physiological sink condition exists for the drug in the vaginal tract, drug release is limited by diffusional flux away from the surface of the IVR. As described above, this flux can be steady-state in the case of a reservoir ring, or unsteady in the case of a matrix ring. Models describing these types of release mechanisms generally assume that a "sink" boundary condition is maintained at the outer surface of the device. That is, the effective concentration of drug in the surrounding medium is very

low with respect to its solubility. Most *in vitro* IVR drug-release studies are performed under sink conditions, where the volume and stirring of the release medium is sufficient to prevent the local and/or overall drug concentration from approaching the drug solubility in the medium. It is unclear, however, whether a sink is maintained for some hydrophobic antiviral compounds *in vivo*. It may be that zero-order release would be possible *in vivo* for certain devices that exhibited diffusion/dissolution limited kinetics *in vitro* if the vaginal fluid concentration remains saturated or supersaturated at a value limited by its solubility [34]. Illustrating this phenomena, a study comparing drug release behavior of matrix-type UC781-containing IVR segments from various polymeric matrices showed large differences in release rates between formulations under sink conditions in the lab, yet very few pharmacokinetic differences in a rabbit model, with UC781 release rates significantly less *in vivo* as compared to *in vitro* [51, 62].

Drug release from IVR can be mechanistically described by solutions to diffusion equations. Since axial diffusion can generally be neglected, IVR diffusion problems can be reduced to one dimension by transforming to polar coordinates. For matrix IVR, the mathematical approach depends on the physical nature of the drug inside the polymer matrix. When the entirety of the drug load is dissolved, Fick's Second Law can be solved on the circular IVR cross-section with a sink outer boundary and uniform initial condition, resulting in the following series approximation [63]:

$$\frac{M}{M_0} \approx \frac{4}{r_0} \sqrt{\frac{Dt}{\pi}} - \frac{Dt}{r_0^2} - \frac{1}{3\sqrt{\pi}} \left(\frac{Dt}{r_0^2}\right)^{3/2} + \dots \quad (1.2)$$

where M is the cumulative release of drug as a function of time, and D is the effective diffusivity of the drug in the polymer matrix. When considering values of M/M_0 less than

0.2-0.3, the first term is sufficiently accurate and the remaining terms may be neglected. Equation 1.2 can also be used if a saturation equilibrium is reached outside the ring by replacing M_0 with the total mass released when equilibrium is reached. If the majority of drug molecules are undissolved, meaning that the drug loading far exceeds the solubility in the polymer matrix, a pseudo-steady-state moving diffusion boundary approach leads to an implicit solution for cumulative release [64-66]:

$$\frac{M}{M_0} + \left(1 - \frac{M}{M_0}\right) \ln \left(1 - \frac{M}{M_0}\right) = \frac{4D\omega_s}{\omega_T r_o^2} \quad (1.3)$$

where ω_s is the mass fraction solubility of the drug in the polymer matrix. Equation 1.3 is derived by a similar approach used by T. Higuchi to arrive at the classic equation for thin films [67], and is further discussed in Chapter 2. For long-acting systems, including IVR, it is more useful to express results as release rates (dM/dt) than as a cumulative release quantity. Instantaneous release rates can be obtained by a simple time-derivative of $M(t)$, or often-used daily release rates can be obtained by subtracting $M(t)$ across a 24-hour interval. Although Equation 1.3 is simplified in that it neglects the change in the amount of dissolved drug with time outside the diffusion front (appropriate for some systems), Helbling and Cabrera corrected for this by integrating the concentration profile outside the diffusion front in their more comprehensive analytical model [68].

For reservoir-type IVR, the steady-state form of Fick's Second Law can be solved on the rate-controlling membrane (RCM), and applying Fick's First Law at the outer boundary reveals a simple formula for instantaneous drug release rate as a function of core concentration (c_{in}) [43]:

$$\frac{dM}{dt} = \frac{2\pi l D c_{in}}{\ln\left(\frac{r_o}{r_i}\right)} \quad (1.4)$$

It should be noted that D (or D_{eff}) refers to a macroscopic Fickian approximation of diffusivity. Also, the derivation of Equation 1.4 assumes that no drug partitioning exists between the core and RCM polymers at their interface, which should be appropriate if drug solubility is the same in the two materials. When this is not the case, a linear partition coefficient K (equal to the ratio of drug solubilities between the membrane and core) is applied to the boundary condition and ultimately appears in the numerator of Equation 1.4. This model is further discussed in Chapter 3.

1.8 Biotransport Description of HIV Pre-Exposure Prophylaxis

Although the characterization of drug release from an IVR into an *in vitro* release media sink condition is a critical step in the design and optimization process, understanding drug transport through vaginal tissue is of equal practical importance. There are three basic compartments of importance when considering spatial drug distributions following PrEP administration in women: vaginal fluid, vaginal tissue, and blood circulation. For topical delivery (e.g. from IVR), vaginal fluid is the dissolution medium, and acts as a relay from dosage form to tissue. Fluid can be a sink-type boundary in the case of water-soluble drugs, or can become a saturated (or partially-saturated) rate-controlling impediment for release in the case of less water-soluble drugs [34, 51]. In either case, the fluid serves as a source for drug transport throughout the tissues. It is thought that fluid convection in the vaginal tract serves to effectively spread drugs longitudinally from the device to the introitus [69], which is particularly advantageous for devices that provide a constant drug source from a fixed point in the

vaginal tract (such as an IVR). It is likely that a fraction of any dose delivered vaginally remains dissolved in the fluid and is lost through the introitus [70], which could lead to a reduction in dose availability for bolus-type doses (such as gels). It has also been suggested that drugs can partition directly into the epithelial layer from an IVR, thus bypassing the fluid compartment completely [29]. However, a fraction of the surface area is not in direct contact with the tissue, so only a fraction of the total flux from the ring would be described by this phenomenon. The vaginal tissue compartment can be further stratified into various sub-compartments. When considering continuum-scale drug transport, the tissue can be divided into the epithelium (nonvascularized), and the lamina propria (vascularized). For vaginal delivery, a linear concentration reduction in drug concentration can be expected across the epithelium (by Fick's laws, approximating the epithelium as a thin plane), while combined diffusion and elimination to the bloodstream should result in an exponential decay of drug concentration throughout the vascularized tissues [71]. Any vaginal PrEP delivery strategy must ensure that a sufficient drug source is maintained in the fluid compartment to ensure an effective drug level surrounding infectable cells at various depths in the tissue [72]. For drugs that are activated intracellularly (NtRTI and NRTI), the tissue can be further stratified at the cellular level and chemical reactions must be considered along with diffusion and elimination.

The plasma compartment acts as a sink for vaginal delivery, in contrast to its function as a source for oral delivery. In either case, drugs or their byproducts will likely be eliminated by renal or hepatic clearance mechanisms. For oral delivery of antiretrovirals, local tissue protection is likely achieved by the same mechanism described above, only in reverse. The vascularized (lower) tissue layer will become

loaded with drug, which can then diffuse into the epithelial layers and vaginal fluid. However, it is likely that large temporal fluctuations in local tissue drug concentrations are experienced in the tissue compartment with intermittent oral dosing, leading to the same drawbacks experienced with intermittent gel dosing. Through this analysis, it is readily apparent, as with many local drug delivery schemes, that vaginal delivery of PrEP agents can have two advantages over oral delivery: 1) Greatly reduced systemic drug concentrations are required to deliver the tissue a protective level; and 2) The potential for establishing constant vaginal tissue levels through controlled-release dosage forms (e.g. an IVR), which would be impossible to achieve through intermittent oral dosing [73].

When considering the mass transport of PrEP agents, several physicochemical properties are of interest including aqueous solubility, tissue permeability, and hydrophobicity. Aqueous solubility is important since the concentration dissolved in the vaginal fluid will ultimately serve as the boundary condition for transport across the tissue compartment. Compounds also must have sufficient diffusivity in the tissue compartment for them to reach their potential sites of action (inside and surrounding target immune cells). Although hydrophobic compounds generally have better permeability across epithelial cell membranes, small hydrophilic compounds can rapidly diffuse in the extracellular space, quickly reaching continuum-level steady state concentrations. The extracellular concentration at any point then serves as a drug source across individual cell membranes. Aqueous solubility is potentially more important for long-term delivery from an IVR because local tissue concentrations should be directly related to the source concentration dissolved in the vaginal fluid.

Several models of local PK for vaginal delivery have been reported. Kuo *et al.* used a steady-state solution to a one-dimensional diffusion-elimination model to predict the vaginal transport of ^{125}I -labeled IgG antibodies released from EVA discs [71], but measured the concentration as a function of distance experimentally. This treats the vaginal fluid as a thin conducting surface with constant API concentration. However, this model neglects the advective transport of drugs longitudinally through the vaginal tract. Saltzman later published an improved, compartmental, vaginal pharmacokinetic model that also considered vaginal fluid advection [74]. Geonnotti and Katz constructed a finite-element model of a two-dimensional cross-section of an IVR and the vaginal tract and surrounding tissues [69]. Although this 2D model is not fully representative of vaginal anatomy, it was the first *in silico* attempt to assess the spatial pharmacokinetics of drugs released from an IVR. The results of the model indicate that the thickness and fluid velocity of the vaginal fluid boundary layer has much greater impact on drug distribution through tissue than the effective diffusivity of the drug through the tissue. A proposed three-dimensional PK model to describe IVR drug transport is discussed in Appendix A.

Another variable often not considered is the effect of menstrual cycle variation and sexual intercourse on drug release from an IVR. In cases where the flux of a drug from the IVR surface is limited by its solubility in the surrounding fluid, it is conceivable that changes in the vaginal environment could affect drug release. For instance, drug release could be reduced in the case of peri-menopausal vaginal dryness, or increased upon the introduction of semen to the insertion site due to changes in the available dilution volume. The increase in vaginal pH following intercourse could also result in a temporary modulation of the release rate of drugs which exhibit pH-dependent aqueous

solubility. Some IVR dosing regimens currently under consideration involve the user leaving the ring in place for one or more menstrual cycles. During this time, drug release rates could be modulated by the composition of the vaginal fluid, which may contain various drug-solubilizing factors, such as hemoglobin, as well as by an increase in the vaginal fluid volume, as already mentioned. A full analytical treatment of vaginal transport through the tissue, where both bulk diffusion and surface convection are considered along with first-order elimination, is not likely feasible, but finite-element or other numerical approximations could aid in the design of IVR or other topical microbicide sustained-delivery systems, provided that they can be sufficiently validated by correlation to experimental data.

1.9 Mechanical Properties of IVR

In general, the efficacy of long-term controlled release drug-device combinations is dependent on their ability to remain in place for the duration of use. IVR differ from other long-term delivery systems in that they are not surgically implanted and are designed to be inserted and removed by the user. An elastic IVR under compression will be in a force balance with the vaginal wall, the magnitude of which is determined by ring geometry and matrix material properties and the biomechanical environment provided by the underlying musculature. Provided the force applied on the tissue as a result of ring relaxation is of sufficient magnitude, the ring will remain in place. Under normal physiological conditions, the vaginal tract is a low-friction environment due to the presence of vaginal fluid and cervicovaginal mucus. If an IVR is too easily deformed, the ring may be expelled as a result of day-to-day activities of the user that apply force to the ring, like defecation, coughing, or running [37]. However, if this retractile force is too

great, it may be difficult for the user to compress the ring prior to insertion or it may cause damage to the vaginal epithelium proximal to the ring site [40]. Logically, there exists an optimum range of compressibility for an IVR of given dimensions, keeping in mind that there will be a wide range of vaginal shapes and sizes among the user population [57, 75, 76]. A mechanical model for the point compression of thin elastic rings is derived in engineering literature [77]. The most interesting feature of the model result is the fourth-power dependence of compressive load on the cross-sectional diameter of the ring. Thus, increasing the cross-sectional diameter of an IVR from 5 to 6 mm will result in a 107% increase in the force required to deform the ring by a given amount. Also, IVR compression force is linearly related to the elastic modulus of the IVR matrix, which can be affected by the incorporation of drugs and/or other excipients. This mechanical model is discussed in further detail in Chapter 2. The addition of nondissolved solids to the matrix can greatly increase the elastic modulus [78], whereas dissolution of polymer-soluble compounds can cause a plasticizing effect, effectively reducing the elastic modulus of the material [79]. Although this mechanical model assumes linear stress-strain behavior, which is invalid for high ring deformations such as during ring insertion, the model can still be a useful tool for ring design, especially when considering small ring deformations such as those seen in an MRI assessment of NuvaRing retention *in vivo* [80]. Complete mechanical analysis of complex IVR designs, such as the dual-segmented polyurethane IVR described by Johnson *et al.* [56] or pod-insert-type IVR [58], would most likely require a numerical approximation or finite-element simulation. An even larger difficulty in designing new IVR products is the interpretation of such mechanical modeling and testing results. Other than performing

side-by-side comparison tests with existing clinical IVR which have shown high user acceptability, there is no quantitative model to directly determine the ideal range for mechanical IVR acceptability. Recent studies have begun to quantitatively examine the vaginal musculature [81, 82]. Developing a model which couples ring elastic mechanics with vaginal biomechanics could prove useful in future IVR design and in the design of dosage forms with shapes other than the symmetric torus, such as the SILCS diaphragm.

1.10 Dissertation Chapter Overview

Chapters 2, 3, and 4 of this dissertation are separate manuscripts in various stages of publication. Chapters 2 and 3 are published, peer-reviewed articles, and Chapter 4 is a manuscript in preparation for publication.

1.10.1 Chapter 2 Overview

Chapter 2 describes an injection-molded hydrophilic polyether urethane (HPEU) matrix intravaginal ring (IVR) for the sustained delivery of tenofovir (TFV) for up to 90 days, as well as mathematical models for *in vitro* release and mechanical properties. The drug release model is an explicit solution of implicit model for limited-solubility cylindrical dosage forms originally derived by Roseman and W. Higuchi [64, 65]. An explicit solution was obtained by use of the Lambert-W (product log) function, the first such use in the drug delivery literature. Described is the first device capable of the sustained vaginal delivery of milligram per day quantities of TFV, a molecule that proved effective in early HIV prevention studies as detailed above. This article also established a foundation for the prediction of IVR mechanical properties using a model that had not yet been described in the drug delivery literature.

Publication: Clark JT, Johnson TJ, Clark MR, Nebeker JS, Fabian J, Tuitupou AL, Ponnappalli S, Smith EM, Friend DR, Kiser PF. Quantitative evaluation of a hydrophilic matrix intravaginal ring for the sustained delivery of tenofovir. *Journal of Controlled Release*, 2012, 163(2), pages 240-248.

1.10.2 Chapter 3 Overview

Chapter 3 describes the design and *in silico*, *in vitro*, and *in vivo* evaluation of a two-segment, dual-reservoir polyurethane IVR which delivers TFV and the contraceptive progestin levonorgestrel (LNG) at near-constant rates for 90 days. Several aspects of the work are presented, including a new diffusion model for drug release, *in vitro* release testing, *in vivo* pharmacokinetic testing in a rabbit model, manufacturing methods, and mechanical testing. This article presents a novel solution for the delivery of two physicochemically different drugs at up to 700-fold different rates through the use of the chemically diverse PEU/HPEU platform. The IVR described is one of the first devices in its class designed for simultaneous long-acting HIV prevention and contraception. The mathematical model presented is an improvement over those existing in the literature and is useful in the design of cylindrical reservoir devices, including IVR. This chapter focuses primarily on the design and testing of a solid, co-axially extruded 1 to 2 cm length PEU reservoir for the delivery of LNG and its incorporation into a two-segment ring that also delivers TFV. The TFV delivery system is a hollow-tube HPEU reservoir and represents the "second generation" of the technology presented in Chapter 2, but is not a primary topic of this dissertation. For a detailed description of the TFV reservoir,

the reader is referred to the Ph.D. dissertation of Todd Johnson, also of the University of Utah Department of Bioengineering.

Publication: Clark JT, Clark MR, Shelke NB, Johnson TJ, Smith EM, Andreasen AK, Nebeker JS, Fabian J, Friend DR, Kiser PF. Engineering a segmented dual-reservoir polyurethane intravaginal ring for simultaneous prevention of HIV transmission and unwanted pregnancy. PLoS ONE 2014; 9(3): e88509.

1.10.3 Chapter 4 Overview

Chapter 4 continues in the description of the TFV/LNG dual-reservoir IVR presented in Chapter 3. In this manuscript, the physical and chemical stability of the system are evaluated, as well as the pharmacokinetics of TFV and LNG in the sheep model.

Publication: Clark JT, Shelke NS, Clark MR, Johnson TJ, McCabe RT, Meidell KZ, Fabian J, Friend DR, Kiser PF. Preclinical evaluation of a multipurpose prevention intravaginal ring: Assessments of stability and in vivo performance. In preparation for submission to the European Journal of Pharmaceutics and Biopharmaceutics.

1.11 References

- [1] M.P. Girard, S.K. Osmanov, M.P. Kieny, A review of vaccine research and development: the human immunodeficiency virus (HIV). *Vaccine* 24(19) (2006) 4062-4081.
- [2] D.M. Margolis, Mechanisms of HIV latency: an emerging picture of complexity. *Curr HIV/AIDS Rep* 7(1) (2010) 37-43.
- [3] E. De Clercq, Anti-HIV drugs: 25 compounds approved within 25 years after the discovery of HIV. *Int J Antimicrob Agents* 33(4) (2009) 307-320.

- [4] J. Balzarini, L. Naesens, E. De Clercq, New antivirals - mechanism of action and resistance development. *Curr Opin Microbiol* 1(5) (1998) 535-546.
- [5] UNAIDS, Global report: UNAIDS report on the global AIDS epidemic 2013, Joint United Nations Programme on HIV/AIDS (UNAIDS), 2013.
- [6] R.M. Grant, D. Hamer, T. Hope, R. Johnston, J. Lange, M.M. Lederman, J. Lieberman, C.J. Miller, J.P. Moore, D.E. Mosier, D.D. Richman, R.T. Schooley, M.S. Springer, R.S. Veazey, M.A. Wainberg, Whither or wither microbicides? *Science* 321(5888) (2008) 532-534.
- [7] Q. Abdool Karim, S.S. Abdool Karim, J.A. Frohlich, A.C. Grobler, C. Baxter, L.E. Mansoor, A.B. Kharsany, S. Sibeko, K.P. Mlisana, Z. Omar, T.N. Gengiah, S. Maarschalk, N. Arulappan, M. Mlotshwa, L. Morris, D. Taylor, Effectiveness and safety of tenofovir gel, an antiretroviral microbicide, for the prevention of HIV infection in women. *Science* 329(5996) (2010) 1168-1174.
- [8] S.S. Abdool Karim, A.D. Kashuba, L. Werner, Q. Abdool Karim, Drug concentrations after topical and oral antiretroviral pre-exposure prophylaxis: implications for HIV prevention in women. *Lancet* 378(9787) (2011) 279-281.
- [9] J. Marrazzo, G. Ramjee, G. Nair, T. Palanee, B. Mkhize, C. Nakabiito, M. Taljaard, J. Piper, K. Gomez Feliciano, M. Chirenje, Pre-exposure Prophylaxis for HIV in Women: Daily Oral Tenofovir, Oral Tenofovir/Emtricitabine, or Vaginal Tenofovir Gel in the VOICE Study (MTN 003) (Paper 26LB). 20th Conference on Retroviruses and Opportunistic Infections, Atlanta, Georgia, 2013.
- [10] J.M. Baeten, D. Donnell, P. Ndase, N.R. Mugo, J.D. Campbell, J. Wangisi, J.W. Tappero, E.A. Bukusi, C.R. Cohen, E. Katabira, A. Ronald, E. Tumwesigye, E. Were, K.H. Fife, J. Kiarie, C. Farquhar, G. John-Stewart, A. Kakia, J. Odoyo, A. Mucunguzi, E. Nakku-Joloba, R. Twesigye, K. Ngure, C. Apaka, H. Tamooh, F. Gabona, A. Mujugira, D. Panteleeff, K.K. Thomas, L. Kidoguchi, M. Krows, J. Revall, S. Morrison, H. Haugen, M. Emmanuel-Ogier, L. Ondrejcek, R.W. Coombs, L. Frenkel, C. Hendrix, N.N. Bumpus, D. Bangsberg, J.E. Haberer, W.S. Stevens, J.R. Lingappa, C. Celum, Antiretroviral prophylaxis for HIV prevention in heterosexual men and women. *N Engl J Med* 367(5) (2012) 399-410.
- [11] J. Cohen, FDA Panel Recommends Anti-HIV Drug for Prevention. *Science* 336(6083) (2012) 792.
- [12] L. Van Damme, A. Corneli, K. Ahmed, K. Agot, J. Lombaard, S. Kapiga, M. Malahleha, F. Owino, R. Manongi, J. Onyango, L. Temu, M.C. Monedi, P. Mak'Oketch, M. Makanda, I. Reblin, S.E. Makatu, L. Saylor, H. Kiernan, S. Kirkendale, C. Wong, R. Grant, A. Kashuba, K. Nanda, J. Mandala, K. Fransen, J. Deese, T. Crucitti, T.D. Mastro, D. Taylor, Preexposure prophylaxis for HIV infection among African women. *N Engl J Med* 367(5) (2012) 411-422.

- [13] C. Dobard, S. Sharma, A. Martin, C.P. Pau, A. Holder, Z. Kuklennyik, J. Lipscomb, D.L. Hanson, J. Smith, F.J. Novembre, J.G. Garcia-Lerma, W. Heneine, Durable protection from vaginal simian-human immunodeficiency virus infection in macaques by tenofovir gel and its relationship to drug levels in tissue. *J Virol* 86(2) (2012) 718-725.
- [14] R. Singer, P. Mawson, N. Derby, A. Rodriguez, L. Kizima, R. Menon, D. Goldman, J. Kenney, M. Aravantinou, S. Seidor, A. Gettie, J. Blanchard, M. Piatak, Jr., J.D. Lifson, J.A. Fernandez-Romero, M. Robbiani, T.M. Zydowsky, An intravaginal ring that releases the NNRTI MIV-150 reduces SHIV transmission in macaques. *Sci Transl Med* 4(150) (2012) 150ra123.
- [15] J.M. Smith, R. Rastogi, R.S. Teller, P. Srinivasan, P.M. Mesquita, U. Nagaraja, J.M. McNicholl, R.M. Hendry, C.T. Dinh, A. Martin, B.C. Herold, P.F. Kiser, Intravaginal ring eluting tenofovir disoproxil fumarate completely protects macaques from multiple vaginal simian-HIV challenges. *Proc Natl Acad Sci U S A* (2013).
- [16] D.R. Friend, J.T. Clark, P.F. Kiser, M.R. Clark, Multipurpose prevention technologies: Products in development. *Antiviral Res* (2013).
- [17] Guttmacher Institute, Contraceptive Use in the United States (Fact Sheet), August 2013.
- [18] E.E. Seiber, J.T. Bertrand, T.M. Sullivan, Changes in contraceptive method mix in developing countries. *Int Fam Plan Perspect* 33(3) (2007) 117-123.
- [19] R. Rivera, I. Yacobson, D. Grimes, The mechanism of action of hormonal contraceptives and intrauterine contraceptive devices. *Am J Obstet Gynecol* 181(5 Pt 1) (1999) 1263-1269.
- [20] Merck Sharp & Dohme B.V., NuvaRing: highlights of prescribing information, Whitehouse Station, NJ, 2013.
- [21] S. Rose, A. Chaudhari, C.M. Peterson, Mirena (Levonorgestrel intrauterine system): a successful novel drug delivery option in contraception. *Adv Drug Deliv Rev* 61(10) (2009) 808-812.
- [22] Bayer HealthCare Pharmaceuticals Inc., Mirena: highlights of prescribing information, Wayne, NJ, 2009.
- [23] Bayer HealthCare Pharmaceuticals Inc., Skyla: highlights of prescribing information, Wayne, NJ, 2013.

- [24] Teva Women's Health, Inc., ParaGard T 380A: prescribing information, Sellersville, PA.
- [25] United Nations, Department of Economic and Social Affairs, Population Division, Fertility and Family Planning Section, World contraceptive use 2012: model-based estimates: regions: contraceptive prevalence: any modern method: percentage of married or in-union women aged 15 to 49 who are currently using any modern method of contraception. 2012.
- [26] D. Kacanek, A. Dennis, N.N. Sahin-Hodoglugil, E.T. Montgomery, N. Morar, S. Mtetwa, B. Nkala, J. Phillip, C. Watadzaushe, A. van der Straten, A qualitative study of obstacles to diaphragm and condom use in an HIV prevention trial in sub-Saharan Africa. *AIDS Educ Prev* 24(1) (2012) 54-67.
- [27] P.F. Harrison, A. Hemmerling, J. Romano, K.J. Whaley, B. Young Holt, Developing multipurpose reproductive health technologies: an integrated strategy. *AIDS Res Treat* 2013 (2013) 790154.
- [28] R.K. Malcolm, S.M. Fetherston, C.F. McCoy, P. Boyd, I. Major, Vaginal rings for delivery of HIV microbicides. *Int J Womens Health* 4 (2012) 595-605.
- [29] B. Harwood, D.R. Mishell, Jr., Contraceptive vaginal rings. *Semin Reprod Med* 19(4) (2001) 381-390.
- [30] D.R. Mishell, Jr., M.E. Lumkin, Contraceptive effect of varying dosages of progesterone in silastic vaginal rings. *Fertil Steril* 21(2) (1970) 99-103.
- [31] D.I. Macht, The absorption of drugs and poison through the vagina. *J Pharmacol Exp Ther* 10(7) (1918) 509-522.
- [32] D.R. Mishell, M. Talas, A.F. Parlow, D.L. Moyer, Contraception by means of a silastic vaginal ring impregnated with medroxyprogesterone acetate. *Am J Obstet Gynecol* 107(1) (1970) 100-107.
- [33] Y.W. Chien, H.J. Lambert, D.E. Grant, Controlled drug release from polymeric devices. I. Technique for rapid in vitro release studies. *J Pharm Sci* 63(3) (1974) 365-369.
- [34] Y.W. Chien, H.J. Lambert, Controlled drug release from polymeric delivery devices. II. Differentiation between partition-controlled and matrix-controlled drug release mechanisms. *J Pharm Sci* 63(4) (1974) 515-519.
- [35] Y.W. Chien, S.E. Mares, J. Berg, S. Huber, H.J. Lambert, K.F. King, Controlled drug release from polymeric delivery devices. III: In vitro-in vivo correlation for intravaginal release of ethynodiol diacetate from silicone devices in rabbits. *J Pharm Sci* 64(11) (1975) 1776-1781.

- [36] S. Koetsawang, G. Ji, U. Krishna, A. Cuadros, G.I. Dhall, R. Wyss, J. Rodriguez la Puente, A.T. Andrade, T. Khan, E.S. Kononova, et al., Microdose intravaginal levonorgestrel contraception: a multicentre clinical trial. III. The relationship between pregnancy rate and body weight. World Health Organization. Task Force on Long-Acting Systemic Agents for Fertility Regulation. *Contraception* 41(2) (1990) 143-150.
- [37] S. Koetsawang, G. Ji, U. Krishna, A. Cuadros, G.I. Dhall, R. Wyss, J. Rodriguez la Puente, A.T. Andrade, T. Khan, E.S. Kononova, et al., Microdose intravaginal levonorgestrel contraception: a multicentre clinical trial. II. Expulsions and removals. World Health Organization. Task Force on Long-Acting Systemic Agents for Fertility Regulation. *Contraception* 41(2) (1990) 125-141.
- [38] S. Koetsawang, G. Ji, U. Krishna, A. Cuadros, G.I. Dhall, R. Wyss, J. Rodriguez la Puente, A.T. Andrade, T. Khan, E.S. Kononova, et al., Microdose intravaginal levonorgestrel contraception: a multicentre clinical trial. I. Contraceptive efficacy and side effects. World Health Organization. Task Force on Long-Acting Systemic Agents for Fertility Regulation. *Contraception* 41(2) (1990) 105-124.
- [39] S. Koetsawang, G. Ji, U. Krishna, A. Cuadros, G.I. Dhall, R. Wyss, J. Rodriguez la Puente, A.T. Andrade, T. Khan, E.S. Kononova, et al., Microdose intravaginal levonorgestrel contraception: a multicentre clinical trial. IV. Bleeding patterns. World Health Organization. Task Force on Long-Acting Systemic Agents for Fertility Regulation. *Contraception* 41(2) (1990) 151-167.
- [40] E. Weisberg, I.S. Fraser, J. Baker, D. Archer, B.M. Landgren, S. Killick, P. Soutter, T. Krause, C. d'Arcangues, A randomized comparison of the effects on vaginal and cervical epithelium of a placebo vaginal ring with non-use of a ring. *Contraception* 62(2) (2000) 83-89.
- [41] H. van Laarhoven, J. Veurink, M.A. Krufft, H. Vromans, Influence of spinline stress on release properties of a coaxial controlled release device based on EVA polymers. *Pharm Res* 21(10) (2004) 1811-1817
- [42] J.A. van Laarhoven, M.A. Krufft, H. Vromans, Effect of supersaturation and crystallization phenomena on the release properties of a controlled release device based on EVA copolymer. *J Control Release* 82(2-3) (2002) 309-317.
- [43] J.A. van Laarhoven, M.A. Krufft, H. Vromans, In vitro release properties of etonogestrel and ethinyl estradiol from a contraceptive vaginal ring. *Int J Pharm* 232(1-2) (2002) 163-173.
- [44] A.R. Thurman, M.R. Clark, J.A. Hurlburt, G.F. Doncel, Intravaginal rings as delivery systems for microbicides and multipurpose prevention technologies. *Int J Womens Health* 5 (2013) 695-708.

- [45] K. Malcolm, D. Woolfson, J. Russell, C. Andrews, In vitro release of nonoxynol-9 from silicone matrix intravaginal rings. *J Control Release* 91(3) (2003) 355-364.
- [46] R.K. Malcolm, A.D. Woolfson, C.F. Toner, R.J. Morrow, S.D. McCullagh, Long-term, controlled release of the HIV microbicide TMC120 from silicone elastomer vaginal rings. *J Antimicrob Chemother* 56(5) (2005) 954-956.
- [47] A.D. Woolfson, R.K. Malcolm, R.J. Morrow, C.F. Toner, S.D. McCullagh, Intravaginal ring delivery of the reverse transcriptase inhibitor TMC 120 as an HIV microbicide. *Int J Pharm* 325(1-2) (2006) 82-89.
- [48] B. Devlin, J. Nuttall, S. Wilder, C. Woodson, Z. Rosenberg, Development of dapivirine vaginal ring for HIV prevention. *Antiviral Res* (2013).
- [49] A. Nel, S. Smythe, K. Young, K. Malcolm, C. McCoy, Z. Rosenberg, J. Romano, Safety and pharmacokinetics of dapivirine delivery from matrix and reservoir intravaginal rings to HIV-negative women. *Journal of acquired immune deficiency syndromes* 51(4) (2009) 416-423.
- [50] J. Romano, B. Variano, P. Coplan, J. Van Roey, K. Douville, Z. Rosenberg, M. Temmerman, H. Verstraelen, L. Van Bortel, S. Weyers, M. Mitchnick, Safety and availability of dapivirine (TMC120) delivered from an intravaginal ring. *AIDS Res Hum Retroviruses* 25(5) (2009) 483-488.
- [51] M.R. Clark, T.J. Johnson, R.T. McCabe, J.T. Clark, A. Tuitupou, H. Elgandy, D.R. Friend, P.F. Kiser, A hot-melt extruded intravaginal ring for the sustained delivery of the antiretroviral microbicide UC781. *J Pharm Sci* 101(2) (2012) 576-587.
- [52] K.M. Gupta, S.M. Pearce, A.E. Poursaid, H.A. Aliyar, P.A. Tresco, M.A. Mitchnik, P.F. Kiser, Polyurethane intravaginal ring for controlled delivery of dapivirine, a nonnucleoside reverse transcriptase inhibitor of HIV-1. *J Pharm Sci* 97(10) (2008) 4228-4239.
- [53] T.J. Johnson, J.S. Nebeker, A.L. Tuitupou, E.M. Smith, J.T. Clark, J. Fabian, N.B. Shelke, R.T. McCabe, M.R. Clark, D.R. Friend, P.F. Kiser, Engineering of a new intravaginal ring technology for HIV prophylaxis (Manuscript in Preparation). *Pharm Res* (2013).
- [54] T.J. Johnson, P. Srinivasan, T.H. Albright, K. Watson-Buckheit, L. Rabe, A. Martin, C.P. Pau, R.M. Hendry, R. Otten, J. McNicholl, R. Buckheit, Jr., J. Smith, P.F. Kiser, Safe and sustained vaginal delivery of pyrimidinedione HIV-1 inhibitors from polyurethane intravaginal rings. *Antimicrob Agents Chemother* 56(3) (2012) 1291-1299.

- [55] P.M. Mesquita, R. Rastogi, T.J. Segarra, R.S. Teller, N.M. Torres, A.M. Huber, P.F. Kiser, B.C. Herold, Intravaginal ring delivery of tenofovir disoproxil fumarate for prevention of HIV and herpes simplex virus infection. *J Antimicrob Chemother* 67(7) (2012) 1730-1738.
- [56] T.J. Johnson, K.M. Gupta, J. Fabian, T.H. Albright, P.F. Kiser, Segmented polyurethane intravaginal rings for the sustained combined delivery of antiretroviral agents dapivirine and tenofovir. *Eur J Pharm Sci* 39(4) (2010) 203-212.
- [57] P.B. Pendergrass, C.A. Reeves, M.W. Belovicz, D.J. Molter, J.H. White, The shape and dimensions of the human vagina as seen in three-dimensional vinyl polysiloxane casts. *Gynecol Obstet Invest* 42(3) (1996) 178-182.
- [58] J.A. Moss, A.M. Malone, T.J. Smith, S. Kennedy, E. Kopin, C. Nguyen, J. Gilman, I. Butkyavichene, K.L. Vincent, M. Motamedi, D.R. Friend, M.R. Clark, M.M. Baum, Simultaneous delivery of tenofovir and acyclovir via an intravaginal ring. *Antimicrob Agents Chemother* 56(2) (2012) 875-882.
- [59] R.J. Morrow, A.D. Woolfson, L. Donnelly, R. Curran, G. Andrews, D. Katinger, R.K. Malcolm, Sustained release of proteins from a modified vaginal ring device. *Eur J Pharm Biopharm* 77(1) (2011) 3-10.
- [60] Y.A. Han, M. Singh, B.B. Saxena, Development of vaginal rings for sustained release of nonhormonal contraceptives and anti-HIV agents. *Contraception* 76(2) (2007) 132-138.
- [61] B.B. Saxena, Y.A. Han, D. Fu, P. Rathnam, M. Singh, J. Laurence, S. Lerner, Sustained release of microbicides by newly engineered vaginal rings. *AIDS* 23(8) (2009) 917-922.
- [62] M.R. Clark, P.F. Kiser, A. Loxley, C. McConville, R.K. Malcolm, D.R. Friend, Pharmacokinetics of UC781-loaded intravaginal ring segments in rabbits: a comparison of polymer matrices. *Drug Delivery and Translational Research* 1(3) (2011) 238-246.
- [63] J. Vergnaud, *Controlled Drug Release of Oral Dosage Forms*, CRC Press, Boca Raton, 1993.
- [64] T.J. Roseman, Release of steroids from a silicone polymer. *J Pharm Sci* 61(1) (1972) 46-50.
- [65] T.J. Roseman, W.I. Higuchi, Release of medroxyprogesterone acetate from a silicone polymer. *J Pharm Sci* 59(3) (1970) 353-357.

- [66] J. Siepmann, F. Siepmann, Modeling of diffusion controlled drug delivery. *J Control Release* 161(2) (2012) 351-362.
- [67] T. Higuchi, Mechanism of Sustained-Action Medication. Theoretical Analysis of Rate of Release of Solid Drugs Dispersed in Solid Matrices. *J Pharm Sci* 52 (1963) 1145-1149.
- [68] I.M. Helbling, J.A. Luna, M.I. Cabrera, Mathematical modeling of drug delivery from torus-shaped single-layer devices. *J Control Release* 149(3) (2011) 258-263.
- [69] A.R. Geonnotti, D.F. Katz, Compartmental transport model of microbicide delivery by an intravaginal ring. *J Pharm Sci* 99(8) (2010) 3514-3521.
- [70] K. Barnhart, E.S. Pretorius, A. Stolpen, D. Malamud, Distribution of topical medication in the human vagina as imaged by magnetic resonance imaging. *Fertil Steril* 76(1) (2001) 189-195.
- [71] P.Y. Kuo, J.K. Sherwood, W.M. Saltzman, Topical antibody delivery systems produce sustained levels in mucosal tissue and blood. *Nat Biotechnol* 16(2) (1998) 163-167.
- [72] P.F. Kiser, P.M. Mesquita, B.C. Herold, A perspective on progress and gaps in HIV prevention science. *AIDS Res Hum Retroviruses* 28(11) (2012) 1373-1378.
- [73] R.K. Malcolm, in: M. J. Rathbone (Ed.), *Modified-Release Drug Delivery Technology*, Informa Healthcare, New York, 2008, pp. 499-510.
- [74] W.M. Saltzman, J.K. Sherwood, D.R. Adams, P. Castle, P. Haller, Long-term vaginal antibody delivery: delivery systems and biodistribution. *Biotechnol Bioeng* 67(3) (2000) 253-264.
- [75] P.B. Pendergrass, M.W. Belovicz, C.A. Reeves, Surface area of the human vagina as measured from vinyl polysiloxane casts. *Gynecol Obstet Invest* 55(2) (2003) 110-113.
- [76] P.B. Pendergrass, C.A. Reeves, M.W. Belovicz, D.J. Molter, J.H. White, Comparison of vaginal shapes in Afro-American, caucasian and hispanic women as seen with vinyl polysiloxane casting. *Gynecol Obstet Invest* 50(1) (2000) 54-59.
- [77] R. Huston, *Practical Stress Analysis in Engineering Design*, CRC Press, Boca Raton, 2009.
- [78] S.H. Cypes, W.M. Saltzman, E.P. Giannelis, Organosilicate-polymer drug delivery systems: controlled release and enhanced mechanical properties. *J Control Release* 90(2) (2003) 163-169.

- [79] M.A. Repka, T.G. Gerding, S.L. Repka, J.W. McGinity, Influence of plasticizers and drugs on the physical-mechanical properties of hydroxypropylcellulose films prepared by hot melt extrusion. *Drug Dev Ind Pharm* 25(5) (1999) 625-633.
- [80] K.T. Barnhart, K. Timbers, E.S. Pretorius, K. Lin, A. Shaunik, In vivo assessment of NuvaRing placement. *Contraception* 72(3) (2005) 196-199.
- [81] J.A. Ashton-Miller, J.O. Delancey, On the biomechanics of vaginal birth and common sequelae. *Annu Rev Biomed Eng* 11 (2009) 163-176.
- [82] D.D. Rahn, M.D. Ruff, S.A. Brown, H.F. Tibbals, R.A. Word, Biomechanical properties of the vaginal wall: effect of pregnancy, elastic fiber deficiency, and pelvic organ prolapse. *Am J Obstet Gynecol* 198(5) (2008) 590 e591-596.

CHAPTER 2

QUANTITATIVE EVALUATION OF A HYDROPHILIC MATRIX INTRAVAGINAL RING FOR THE SUSTAINED DELIVERY OF TENOFOVIR

Justin T. Clark, Todd J. Johnson, Meredith R. Clark, Joel S. Nebeker, Judit Fabian,
Anthony L. Tuitupou, Satya Ponnappalli, Eric M. Smith, David R. Friend, Patrick F. Kiser

Journal of Controlled Release 2012; 163(2): 240-248

Reproduced with permission from Elsevier



Quantitative evaluation of a hydrophilic matrix intravaginal ring for the sustained delivery of tenofovir

Justin T. Clark^a, Todd J. Johnson^a, Meredith R. Clark^b, Joel S. Nebeker^a, Judit Fabian^a, Anthony L. Tuitupou^a, Satya Ponnappalli^a, Eric M. Smith^a, David R. Friend^b, Patrick F. Kiser^{a,c,*}

^a Department of Bioengineering, University of Utah, 20 South 2030 East, Salt Lake City, UT 84112, USA

^b CONRAD, Department of Obstetrics and Gynecology, Eastern Virginia Medical School, 1911 North Fort Myer Drive, Suite 900, Arlington, VA 22209, USA

^c Department of Pharmaceutics and Pharmaceutical Chemistry, University of Utah, 20 South 2030 East, Salt Lake City, UT 84112, USA

ARTICLE INFO

Article history:

Received 19 June 2012

Accepted 31 August 2012

Available online 7 September 2012

Keywords:

Drug release modeling

Hydrophilic polyether urethane

Intravaginal ring

Microbicides for HIV prevention

Tenofovir

ABSTRACT

In vitro testing and quantitative analysis of a matrix, hydrophilic polyether urethane (HPEU) intravaginal ring (IVR) for sustained delivery of the anti-HIV agent tenofovir (TFV) are described. To aid in device design, we employed a pseudo-steady-state diffusion model to describe drug release, as well as an elastic mechanical model for ring compression to predict mechanical properties. TFV-HPEU IVRs of varying sizes and drug loadings were fabricated by hot-melt extrusion and injection molding. *In vitro* release rates of TFV were measured at 37 °C and pH 4.2 for 30 or 90 days, during which times IVR mechanical properties and swelling kinetics were monitored. Experimental data for drug release and mechanical properties were compared to model predictions. IVRs loaded with 21% TFV (w/w) released greater than 2 mg TFV per day for 90 days. The diffusion model predicted 90 day release data by extrapolating forward from the first 7 days of data. Mechanical properties of IVRs were similar to NuvaRing®, although the matrix elastic modulus decreased up to three-fold following hydration. This is the first vaginal dosage form to provide sustained delivery of milligram quantities of TFV for 90 days. Drug release and mechanical properties were approximated by analytical models, which may prove useful for the continuing development of IVRs for HIV prevention or other women's health indications.

© 2012 Elsevier B.V. All rights reserved.

1. Introduction

The use of pre-exposure prophylaxis (PrEP) as a tool to combat the global HIV/AIDS pandemic is evolving from theory to practice with the successful completion of several clinical trials [1] and the recent FDA panel recommendation for approval of preventative oral administration of anti-HIV drugs [2]. All efficacious HIV PrEP strategies to date utilized either topical (i.e., microbicides) or oral prodrug formulations of tenofovir (TFV), an HIV-1 nucleotide reverse transcriptase inhibitor. The CAPRISA 004 trial tested a vaginal gel containing 1% TFV in a “before and after sex” dosing regimen. Overall, the trial showed a 39% reduction in the rate of HIV acquisition when compared to a placebo gel, and a 54% reduction among self-reported high-adherers (at least 80% use) [3]. This trial measured the first reduction in HIV infection rates in women using a topically applied dosage form [4]. Unfortunately, the once-daily TFV gel

arm of the VOICE trial (MTN-003) did not show a reduction in transmission [5]. Together, these results indicate that HIV chemoprevention may be achieved with topical TFV administration, but that dosing regimen can largely impact trial outcomes. They also highlight the need to develop alternative drug delivery systems for TFV and other antiretroviral agents.

Intravaginal rings (IVRs) provide several benefits over gels including sustained drug delivery and coitally independent use. IVRs are torus-shaped elastomeric devices commonly used for vaginal drug delivery in reproductive health applications [6–8], and are currently under investigation as HIV PrEP agents [9–12]. IVR systems may be capable of antiviral delivery for months or potentially years from a single device. Sustained, long-term delivery of TFV from an IVR may provide three substantial improvements over pericoital delivery systems. First, the high user acceptability observed with existing clinical IVRs [13] may translate to higher user adherence in IVR PrEP trials. Second, sustained delivery should provide more favorable pharmacokinetics than those provided by pericoital delivery systems [14]. Finally, as HIV PrEP likely will be implemented in low-income populations, the potential to spread IVR cost over weeks or months attracts interest in the public health community.

The hydrophilicity of TFV [15] presents a challenge for achieving sustained release from hydrophobic elastomers typically used to

* Corresponding author at: University of Utah, Department of Bioengineering, 20 S. 2030 E., Rm. 108, Salt Lake City, UT 84112–9458, USA. Tel.: +1 801 505 6881; fax: +1 801 585 5151.

E-mail address: patrick.kiser@utah.edu (P.F. Kiser).

manufacture IVRs (i.e., poly(ethylene-co-vinyl acetate), silicones) due to low drug-polymer solubility. Our previous article [16] describes a segmented, hydrophilic poly(ether urethane) (HPEU) IVR prototype which released TFV over 30 days. HPEUs differ from conventional poly(ether urethanes) by exhibiting moderate water swellability, owing to covalently incorporated polyethylene oxide segments [R. Ward, patent application 27959-WO-PCT]. When HPEUs are hydrated, hydrophilic small molecules can dissolve into the aqueous phase, allowing for their passive diffusion through the matrix.

Quantitative analysis of drug release mechanisms can yield useful tools for the design and development of drug delivery systems, especially those designed to release drugs for weeks or months. However, mathematical description of drug delivery systems may increase in complexity when both drug dissolution and matrix swelling are required for drug release due to potential time-dependent drug diffusivity [17–19].

In addition to drug release, one also must study mechanical properties when considering IVRs as drug delivery vehicles. Excessively inflexible IVRs may cause user discomfort or epithelial barrier damage, while excessively compressible IVRs may be expelled during use [20–22]. These problems are compounded in swellable systems as polymer properties will likely vary during swelling and drug dissolution.

In this article we describe the design and characterization of a monolithic, injection-molded, HPEU IVR that releases milligram-per-day quantities of TFV for up to 90 days *in vitro*. We also apply a simple pseudo-steady-state model that effectively describes TFV release from this IVR, and perform the first application of a solid mechanical model that provides a quantitative foundation for the description of IVR mechanical properties.

2. Theory

2.1. Model for drug release

Mathematical description of drug release from a swellable IVR with limited drug solubility requires consideration of three-dimensional drug diffusion and drug dissolution, both of which are affected by the spatially dependent kinetics of polymer matrix swelling. For this system, swelling has a minimal impact on long-term drug release modeling as HPEU IVRs typically reach equilibrium swelling within the first 2 to 3 days of drug release. In an IVR, diffusion should only occur in the radial direction, meaning that any constitutive equations can be solved on a circular cross-section (if the cross-sectional radius is small with respect to the outer radius), which is reduced to one-dimension in polar coordinates (Fig. 1). We assume an outer zero-concentration boundary (sink condition), and define two dimensionless weight fractions: the solubility of drug in the hydrated polymer matrix (ω_s), and the total IVR drug loading (ω_r). We also assume that an excess of undissolved drug will maintain the dissolved concentration at ω_s inside the diffusion front (r_d), resulting in a constant-value moving boundary. Our approach follows the pseudo-steady-state method used by Higuchi when considering drug release from spheres with limited drug solubility [23]. If $\omega_s \ll \omega_r$, this model setup is identical to that of Roseman and W. Higuchi for matrix-controlled drug release from cylindrical dosage forms with no axial drug transport [24,25]. Their solution to the model, which is achieved via the steady-state solution of Fick's second law [8] on the annular drug depletion zone ($r_d < r < r_o$) and application of Fick's first law at the outer radius ($r = r_o$), results in an implicit solution for cumulative release (M) drug release as a function of time (t) [26]:

$$\frac{M}{M_0} + \left(1 - \frac{M}{M_0}\right) \ln\left(1 - \frac{M}{M_0}\right) = \frac{4D_{eff}\omega_s}{\omega_r r_o^2} t \quad (1)$$

where M_0 is the initial drug load (assuming all drug is eventually released from the device) and D_{eff} is the effective diffusivity of the drug in the hydrated, depleted polymer matrix (outside the diffusion front). For further simplification and analysis, we will revert Eq. (1) to an earlier point in its derivation by replacing M/M_0 by the fractional residual drug mass (M_r/M_0 , equal to $1 - (M/M_0)$) which yields through simple algebraic rearrangement:

$$\frac{M_r}{M_0} \ln\left(\frac{M_r}{M_0}\right) - \frac{M_r}{M_0} + 1 = \beta t \quad (2a)$$

$$\beta = \frac{4D_{eff}\omega_s}{\omega_r r_o^2} \quad (2b)$$

We refer to the left-hand-side of Eq. (2a) as the product-log-difference (PLDT) of cumulative release. Further analysis reveals that the right-hand-side of Eq. (2a) represents dimensionless time and can be used to estimate the duration of drug release (t_f):

$$t_f = \frac{1}{\beta} = \frac{\omega_r r_o^2}{4D_{eff}\omega_s} \quad (3)$$

It should be noted that this model is only valid when undissolved drug still remains in the device. However, when $\omega_s \ll \omega_r$, the amount of dissolved drug at total depletion is very small with respect to M_0 and negligible error should result from this simplification. An explicit solution for cumulative drug release can be computed using the lower real-valued branch of the Lambert W-function (W_{-1}) [27]:

$$\frac{M}{M_0} = 1 - \frac{M_r}{M_0} = 1 - e^{(W_{-1}(\frac{\beta t}{\omega_r r_o^2}) + 1)} \quad (4)$$

where β is as defined above. Eq. (4) was computed algebraically using Maple 13 (Maplesoft, Waterloo, Ontario). By comparison of the input domains and output values of the two real-valued branches of W (W_0 and W_{-1}), it is obvious that using W_{-1} in Eq. (4) lends a physical solution to Eq. (2a) while W_0 does not. The W-function, also called the product log function, was first discussed by Euler and Lambert in the 18th century, but did not see much practical use by physicists until the 1990s. To our knowledge this is the first

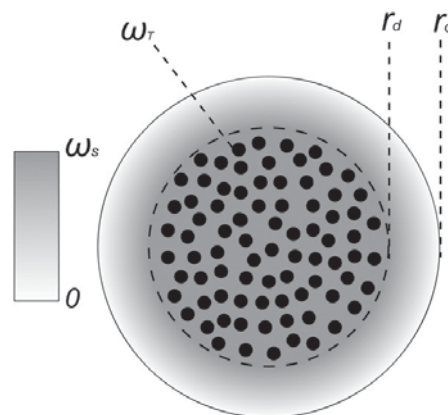


Fig. 1. Drug release model. Pseudo-steady-state, sink diffusion model setup for a circular IVR cross-section. Dots inside the diffusion front (r_d) represent undissolved drug loaded at ω_r , resulting in constant dissolved drug concentration ω_s for $r \leq r_d$. Drug flux at the device boundary (r_o) decreases with inward movement of r_d .

use of the W-function in a drug delivery application. Eqs. (2a)–(4) should apply to drug release from any IVR (whether swellable or not) where $\omega_s \ll \omega_T$. For systems where the $\omega_s \ll \omega_T$ assumption does not hold, the reader is referred to the analysis of Helbling et al. [28], which accounts for the change in dissolved drug mass with movement of the diffusion front. In Roseman's initial analysis [25], it was noted that use of a planar (Higuchi-style) approximation for cylindrical drug release was accurate to within 10% for the first 50% of cumulative release ($M/M_0 \leq 0.5$), which may explain any references to the Higuchi Equation for thin films when discussing drug release from matrix IVRs.

2.2. Model for IVR deformation

An expression for the point deflection Y of a thin elastic torus with radius R' under an applied load F can be found in the engineering literature [29]:

$$Y = \frac{FR^2(\pi^2 - 8)}{4\pi EI} \quad (5)$$

where E is the Young's modulus of the ring-forming material and I is the area moment of inertia of the ring-forming beam ($\pi r_o^4/4$ for a circular cross-section of radius r_o). Since Eq. (5) only considers the cross-section as a massless beam, R' represents the distance to the beam's center and can be replaced by $R - r_o$ for an IVR with outer radius R . Solving for F we obtain an expression for IVR compression force (F) as a function of compression distance (Y):

$$F = \frac{\pi^2 E r_o^4}{(\pi^2 - 8)(R - r_o)^3} Y \quad (6)$$

There are limitations to the utility of this model in IVR design. First, the model considers only the stresses from bending, and thus is most accurate for low values of r_o/R . Also, the model assumes linear elasticity, and is therefore only accurate for small values of Y when considering viscoelastic polymers, such as HPEUs.

3. Materials and methods

3.1. Materials

A custom-designed HPEU (HPEU 20) (Fig. 2A) was provided by DSM Biomedical (formerly DSM-PTG) (Berkeley, CA) [R. Ward, patent application 27959-WO-PCT]. TFV (Fig. 2B) was provided by CONRAD (Arlington,

VA). NuvaRing® was obtained from a local pharmacy. Dimethyl acetamide (HPLC grade) was obtained from Honeywell Burdick & Jackson (Morristown, NJ). Acetonitrile (HPLC grade) was obtained from EMD Chemicals (Gibbstown, NJ). DDI or USP grade water was used to prepare all aqueous stock solutions. All other reagents used were ACS or USP grade.

3.2. IVR fabrication

TFV was ground using an M20 universal mill (IKA Works, Wilmington, NC) and passed through a 425 μ m U.S. standard brass sieve to remove large aggregates (VWR International, Radnor, PA). Milled TFV and HPEU 20 pellets were fed into a HAAKE MiniLab twin-screw extruder (Thermo Scientific, Newington, NH) at varying ratios to achieve a range of drug loadings. Prior to extrusion, HPEU 20 was placed in a CAFM series compressed air dryer (Dri-Air Industries, East Windsor, CT) overnight at 66 °C to remove excess moisture. Batch sizes ranged from 150 to 500 g. The extruder barrel temperature and screw speed were set to 147 °C and 50 rpm, respectively. Each mixture was extruded and then pelletized using a variable-speed pelletizer (Randcastle Extrusion Systems, Cedar Grove, NJ). To ensure batch homogeneity, the pelletized sample was then re-extruded (147 °C, 70 rpm) and re-pelletized. The pelletized extrudate was molded into rings using a Babyplast 6/10P micro-injection molding system (ALBA Enterprises, Rancho Cucamonga, CA) using custom-fabricated, water-cooled, torus-shaped aluminum molds (Sorenson Mold, Inc., Midvale, UT). Target IVR dimensions were 55 mm outer diameter (OD) with 5.0, 5.5 or 6.0 mm cross-sectional diameter (XD). Injection-molding temperatures ranged from 130 °C to 135 °C and mold temperatures ranged from 12 °C to 14 °C. The XD and OD of each ring were measured with digital calipers and the mass of each ring was measured using an analytical balance. HPEU 20 pellets were also injection-molded to produce placebo IVRs.

3.3. TFV quantification by HPLC

TFV was quantified in extraction and release media samples by HPLC analysis using methods similar to those reported previously [16]. Detailed methods are described in the supplementary data section.

3.4. Determination of drug loading in IVRs

The TFV mass fraction (ω_T) in each IVR batch was determined by performing drug extractions similar to those reported previously [16]. Detailed methods are described in the supplementary data section.

3.5. IVR swelling

Both placebo and TFV-loaded IVRs were incubated for 7 days in 25 mM sodium acetate buffer (pH 4.2) in a MaxQ 6000 shaker cabinet set to 37 °C and 80 rpm (Thermo Scientific, Asheville, NC). Masses were measured using a digital balance.

3.6. Estimation of TFV solubility in hydrated HPEU

A slurry of TFV was prepared at 20% (w/w) in 50 mL of 25 mM sodium acetate buffer (pH 4.2), and incubated at 37 °C and 80 rpm for approximately 24 h to allow for TFV dissolution, at which time it was passed through an Express PLUS 0.22 μ m filter (Millipore, Billerica, MA), resulting in a saturated TFV solution. In a separate container, 5 g of HPEU 20 pellets were hydrated in 25 mM sodium acetate buffer (pH 4.2) for 24 h, and the pellets were removed and added to the saturated TFV solution described above and returned to the shaker at

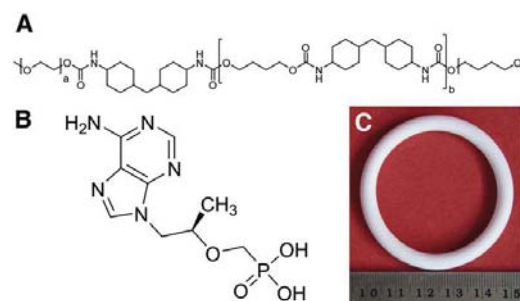


Fig. 2. IVR composition. Structural formulae for HPEU 20 (A) and tenofovir (TFV) (B), along with a photograph of an example injection molded 21% TFV, HPEU 20 IVR (C) (scale in cm).

37 °C and 80 rpm. Approximately 100 mg HPEU 20 were removed daily and massed directly into a tared 10 mL volumetric flask on an analytical balance, which subsequently was filled with approximately 7 mL of buffer. Flasks were shaken on a large capacity mixer (Glas-Col®, Terre Haute, IN) for 24 h to leach all TFV from the pellets, at which time the pellets were removed, flasks were filled to volume with buffer, and the solution was analyzed by HPLC for TFV content. After steady-state TFV concentration had been achieved, similar leaching was repeated with replicates to estimate ω_s . In a separate experiment, it was determined that 24 h incubation was sufficient to reach TFV saturation in HPEU 20. To determine the aqueous solubility of TFV in 25 mM sodium acetate buffer, another TFV slurry (20% w/w in 25 mM sodium acetate buffer, pH 4.2) was prepared in parallel. Aliquots were drawn into plastic syringes and passed through 0.2 μ m nylon syringe filters daily and analyzed by HPLC. Again, the solubility was measured with replicates after steady-state had been reached. Since placebo pellets were used to estimate ω_s , porosity-adjusted solubility values (ω_s^*) were calculated using the fractional equilibrium swelling (α):

$$\omega_s^* = \omega_s \left(\frac{\omega_r + \alpha}{\alpha} \right) \quad (7)$$

3.7. In vitro release testing of IVRs

IVRs were incubated for either 30 or 90 days in 25 mM sodium acetate buffer (pH 4.2) in a MaxQ 6000 shaker set to 37 °C and 80 rpm. Sink conditions (TFV concentrations below 10% of solubility) were maintained throughout. Release media were changed daily, aliquots of which were collected at various times throughout the study (following approximately 24 h incubation) and analyzed by HPLC for TFV content. Cumulative release was estimated by linear interpolation of daily release rate profiles (see supplementary data section). To observe the inward movement of the diffusion front during release testing, photomicrographs of IVR cross-sections were obtained with a Stemi 2000-C Stereo Microscope with a Stereo CL 1500 ECO light source (Carl Zeiss Microimaging, Thornwood, NY) and CFW-1312C color digital camera (Scion Corporation, Frederick, MD).

3.8. Drug release prediction

For each TFV release test a linear interpolation of product-log-difference transform (PLDT) versus time data from day 3 to day 7 was used to compute the time constant (β) in Eqs. (2a) and (2b). Effective lag-time (caused by matrix hydration) was calculated by subtracting the experimental and theoretical 24 hour PLDT values:

$$t_{\text{lag}} = \frac{PLDT_{\text{theoretical}} - PLDT_{\text{experimental}}}{\beta} \quad (8)$$

A modified form of Eq. (4), obtained by replacing 't' with 't - t_{lag}' (see supplementary data section) was then evaluated using the MATLAB 2011b Symbolic Math Toolbox (MathWorks, Natick, MA) to predict cumulative release (MATLAB code can be found in the supplementary section). The expected daily release rate profile $Q(t)$, calculated by sequentially subtracting the cumulative profile, was then compared to experimental data. Coefficients of determination (R^2) were calculated by comparing measured and predicted data from day 10 onward. The mean error in model prediction ($\mu(\epsilon)$) also was calculated from day 10 onward by computing the arithmetic mean of percentage discrepancies between experimental and theoretical release rates. R^2 values were also used to assess the linearity of PLDT versus time from day 3 onward. Time constants (β) and porosity-adjusted solubility values (ω_s^*) were used to estimate the

effective diffusivity (D_{eff}) of TFV in the hydrated matrix by rearranging Eq. (2b):

$$D_{\text{eff}} = \frac{\beta \omega_r r_0^2}{4\omega_s^*} \quad (9)$$

3.9. Compression testing of IVRs

Before and during drug release testing, the force required to compress TFV-loaded and placebo HPEU IVRs to up to 25% of their OD was measured using an Instron 3342 materials testing system, with 500 N load cell and Bluehill Lite software (Instron, Norwood, MA) using methods similar to those previously described [16,30]. IVRs were positioned in a rectangular aluminum cradle (6 mm in width), and a cylindrical aluminum probe (6 mm diameter) was placed directly above the IVR. The probe was moved downward at a velocity of 1 mm/s, during which time load and displacement values were measured. F_{10} was defined as the applied load following displacement by 10% of OD, which approximates *in situ* compression for NuvaRing® [31]. An F_{10} value also was determined for NuvaRing® by a similar test. To calculate elastic moduli for both dry and hydrated matrices, linear regressions of force vs. compression data were performed for the first 1 mm of compression. By rearranging Eq. (6), the elastic modulus for each IVR was then calculated using the slope (k) of the linear regression:

$$E = \frac{(\pi^2 - 8)(R - r_0)^3 k}{\pi^2 r^4} \quad (10)$$

3.10. Mechanical model validation

To experimentally validate Eq. (6), the elastic modulus of TFV-loaded HPEU was first estimated by uniaxial tensile testing. Rod segments cut from 21% TFV IVRs were then annealed at 150 °C in a cylindrical aluminum mold, rolled flat with a stainless-steel cylinder and clamped between two aluminum plates to produce films with 1 mm thickness. Films were cut into strips approximately 11 mm in width and exact dimensions were measured using digital calipers. The Instron system was outfitted with 2710–203 screw-side action clamps at an initial vertical spacing of 10 mm. Films were extended by 1 mm at 1 mm/s. Elastic modulus values were derived by computing the slope of linear regressions ($R^2 \geq 0.999$) of the stress versus strain plots for extension values of 0.04 to 0.15 mm. The average modulus value was used in Eq. (6) to predict the required force for 1% compression (of initial OD) of an IVR with 53 mm OD. This model function was compared to compression data from IVR batches containing 21% TFV (w/w). R^2 values were calculated to assess model accuracy.

4. Results and discussion

4.1. IVR fabrication

We compounded up to 0.5 kg TFV-HPEU batches using hot-melt extrusion and fabricated IVRs using lab-scale injection molding. Five batches of TFV-loaded, injection-molded HPEU IVRs were produced (an example can be seen in Fig. 2C). Three batches had an average XD of 5.0 mm with varying TFV loadings (2%, 11% or 21% w/w). The two remaining batches had an average XD of 5.6 mm and 6.0 mm and were loaded with 21% (w/w) TFV. All batches had an average OD of 52 or 53 mm. All IVRs produced were opaque and white to off-white. The processing methods described herein represent a marked improvement from those reported previously [11,16]. The

weakness of many innovative drug delivery systems, particularly those intended for the developing world, is the lack of attention to cost and scalability. With this in mind, we developed a two-step process utilizing hot-melt extrusion and high-throughput injection-molding [32] technologies commonly used in high-throughput plastics production.

4.2. IVR swelling

As shown in Fig. 3A, TFV-HPEU IVRs reached equilibrium swelling within 48 h, indicating that the swelling front reaches the center of the IVR within the first two days of drug release, validating the rapid swelling assumption discussed above. Equilibrium swelling ratios, averaged from day 2 to day 7, were 20%, 22% and 25% of initial IVR mass for placebo (no TFV), 11% TFV and 21% TFV IVRs, respectively. A potential concern with use of a water-swellaible IVR is the initial size change upon insertion. The dry and hydrated dimensions of various IVR batches tested are shown in Table 1. The outer diameter of these IVRs increased between 6% and 9% upon initial hydration, resulting in rings with OD of up to 57 mm, which is in the range of ODs for IVRs currently in clinical use [33].

4.3. TFV solubility

Using HPLC analysis of TFV slurry filtrates, we determined that TFV solubility in 25 mM sodium acetate buffer was $0.66 \pm 0.01\%$ (w/w) (22.9 ± 0.2 mM) ($N=5$, mean \pm SD). The TFV solubility in HPEU 20 pellets was assessed by 24 h leaching following storage in a saturated TFV solution for 1, 2, 3, 4, 6 or 7 days, during which solubility varied from 0.015% to 0.021% (w/w), with no discernible upward trend. On day 8, HPEU 20 pellets were removed from the saturated TFV solution and subjected to the same test. The TFV solubility in hydrated HPEU 20 pellets (ω_s) was determined to be $0.020 \pm 0.003\%$ (w/w) ($N=5$, mean \pm SD); considerably less than the 0.1% (w/w) obtained by scaling TFV solubility by aqueous mass fraction. This suggests that TFV has limited solubility in the polymer phase of this HPEU, and furthermore supports that only a fraction of water molecules in the hydrated HPEU are free to solubilize TFV [34]. Porosity-adjusted TFV solubility values (ω_s^*) were calculated for each IVR batch using Eq. (7) (shown in Table 1). It should be noted that solubility measurements do not take into account the possibility for TFV dissolution into the polymer phase during the high temperatures experienced in melt processing, which could result in a

Table 1
Dimensions (dry/hydrated), TFV loading (ω_r), porosity-adjusted solubility (ω_s^*) and effective TFV diffusivities (D_{eff}) for TFV-HPEU IVRs. Loadings were determined by drug extraction, solubilities using Eq. (7), and diffusivities using Eq. (9).

OD (mm)	XD (mm)	ω_r (% w/w)	ω_s^* (% w/w)	D_{eff} (10^{-7} cm ² /s)
52/55	5.0/5.4	2.3	0.022	4.9
53/56	5.0/5.4	11.1	0.029	4.8
53/57	5.0/5.4	20.6	0.038	6.7
53/57	5.6/6.1	20.6	0.038	5.6

meta-stable, supersaturated TFV dispersion in HPEU 20 at 37 °C [8], thus increasing ω_s^* and decreasing D_{eff} .

4.4. IVR mechanical characterization

An evaluation of TFV-HPEU IVR mechanical properties is presented in Fig. 4. Load varied non-linearly with compression distance, as shown in Fig. 4A. Elastic moduli (Fig. 4B) were calculated using the linear low-displacement (~1 mm) region of load versus displacement curves and Eq. (6). For dry TFV-HPEU matrices, increasing the TFV loading from 2% to 21% resulted in an increase of the mean elastic modulus from 10 MPa to 26 MPa. Following hydration, the modulus of the 2% TFV-loaded matrix decreased to 7 MPa, while the modulus of the 21% TFV-loaded matrix decreased to 12 MPa. Using ring compression, the dry and hydrated elastic moduli of placebo HPEU 20 were determined to be 11 and 8 MPa, respectively. In general, the elastic moduli of the dry and hydrated HPEU matrices increased with incorporation of undissolved TFV particles, but the magnitude of this effect was markedly reduced following polymer hydration. Assuming no adhesion occurs between undissolved TFV aggregates and HPEU molecules, the particles are likely disengaged from the polymer matrix upon hydration [35]. If TFV aggregate surfaces are well-hydrated, the resulting TFV slurry formed within the porous matrix should likely have little-to-no effect on matrix elasticity, which would explain the results shown in Fig. 4B–D.

The force required to compress IVRs to 10% of OD (F_{10}) [31] was evaluated as a function of time during release testing (Fig. 4C and D). Nearly a two-fold drop in F_{10} was observed following matrix hydration, except for in 2% TFV (w/w) loaded IVRs, where the average F_{10} only dropped from 0.75 N to 0.64 N over the first three days. For 21% TFV IVRs, a gradual decrease in the F_{10} was observed over 90 days, which is likely due to continued depletion of undissolved TFV. The F_{10} increased by 82% (averaged over all measurements during release testing) when the XD of 21% TFV IVRs was increased from 5.0 mm to 5.6 mm (only a 12% increase). For the 5.0 mm, 21% TFV IVR group, the average F_{10} ranged from 1.6 N at $t=0$, to hydrated values of 0.9 N on day 2, 0.6 N on day 20, and 0.5 N on day 90. The F_{10} of the contraceptive IVR NuvaRing® tested under the same conditions (dry) was 0.7 N.

While the non-linear stress–strain behavior observed is unremarkable given the viscoelasticity inherent to such elastomers [36], the mechanical model presented in Eq. (6) does not account for such viscoelastic effects, as it is derived from a linear elastic constitutive model. Accordingly, 1% IVR compression force (F_1) values, rather than F_{10} values, were used for mechanical model validation (Fig. 4E). The elastic modulus value for HPEU 20 loaded with 21% TFV (w/w) was determined to be 24.9 ± 1.7 MPa ($N=3$, mean \pm SD) from uniaxial tensile testing. 53 mm OD, 21% TFV-HPEU 20 IVRs with either 5.0 mm, 5.6 mm or 6.0 mm XD had 1% compression force values which correlated to values calculated from Eq. (6) ($R^2=0.997$). Model predictions for F_1 as a function of XD for both dry and hydrated HPEU loaded with 21% TFV are shown in Fig. 4F to further illustrate the impact of IVR geometry and hydration state on IVR compressibility.

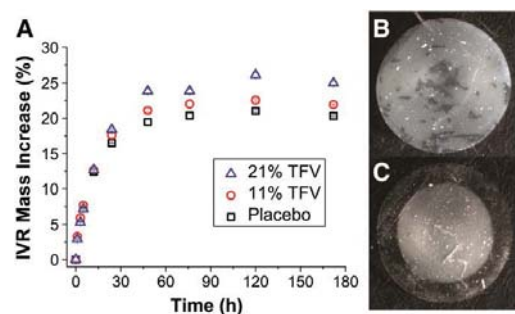


Fig. 3. Movement of the swelling and diffusion front. Percentage mass increase of TFV-HPEU 20 IVRs under aqueous sink conditions at 37 °C (A). Equilibrium swelling is reached within 48 h. Mass loss due to drug release is not considered. Data represent $N=3$, mean \pm SD. Photomicrographs of IVR cross-sections prior to (B) and following (C) 30 day drug release testing illustrating the movement of the diffusion front (r_d).

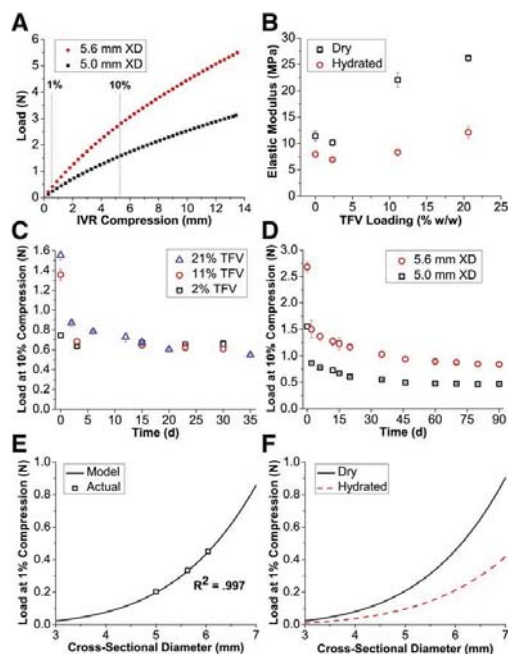


Fig. 4. Mechanical testing of IVRs. (A) Example load vs. compression profiles for 21% TFV IVRs with varying XD. The nonlinearity deviates from the model shown in Eq. (6). (B) HPEU 20 elastic moduli as a function of TFV loading estimated from IVR compression testing (Eq. (10)) either dry or hydrated (following 2–3 day drug release testing). (C,D) F_{10} values as a function of time during drug release testing showing both effects of increasing TFV loading with constant XD (5.0 mm) (C) and effects of increasing XD with constant TFV loading (21% TFV) (D). (E) Low-strain (compression by 1% of initial XD), validation of the IVR compression model presented in Eq. (6); average ($N = 3$) low-strain IVR compression data is well-correlated ($R^2 = 0.997$) to a model low-strain load vs. cross-sectional diameter curve. (F) Predicted 1% compression forces (F_1) are shown as a function of XD for 53 mm OD HPEU IVRs with 21% TFV, both dry and hydrated. Data represents $N = 3$, mean \pm SD for panels B–D (except $N = 6$ for 21% TFV points in panel B).

Despite the limitations of Eq. (6) in predicting behavior at high deformations, it can be used to predict low-deformation behavior directly from elastic modulus and IVR dimensions. Furthermore, the model can be used to generate first-order estimations of appropriate ring dimensions required to achieve targeted mechanical properties. The model could be improved by replacing the linear elastic constitutive model with a hyperelastic model (e.g., Mooney–Rivlin) suitable for elastomers. While an increase in drug loading will generally increase drug release rates and duration (discussed below), it will result in increased initial elastic modulus and a higher-magnitude drop in elastic modulus following initial hydration and throughout the duration of use. IVRs with 5.0 mm XD and 21% TFV loading had F_{10} values more than twice those of NuvaRing® prior to release testing and had F_{10} values approximately 30% less than NuvaRing® after release testing. Various reports from clinical literature [20–22] indicate an optimal range exists for IVR mechanical properties, however, there is no consensus as to the appropriate metric for quantitatively determining mechanical IVR acceptability. If the load under compression is insufficient, an IVR may be displaced or expelled by the user. However, if the compression force is unnecessarily high, it may cause user discomfort or even inflammation and/or damage to the vaginal

epithelium. We have introduced F_{10} as a metric for IVR acceptability based on MRI observations of *in vivo* ring placement [31]. Even given this metric, our approach for estimating mechanical acceptability was still limited to comparing F_{10} values to a commercially available IVR.

4.5. TFV release from HPEU IVRs

Release rates of TFV from HPEU IVRs, shown in Fig. 5, exhibited the time dependence generally associated with diffusion-limited matrices [12]. IVRs loaded with 21% TFV released greater than 2 mg/d for 90 days, although release rates decreased by more than an order of magnitude over this time period. IVRs loaded with 2%, 11% or 21% TFV (5.0 mm XD) were tested for 30 days (Fig. 5A). By interpolation, cumulative release was estimated to be 93%, 55% and 56% of the initial load from the 2%, 11% and 21% TFV-loaded IVRs, respectively, after 30 days (Fig. 5B). The increase in 30 day cumulative release from 2% to 11% TFV IVRs illustrates the correlation between release duration and loading (Eq. (3)), although it appeared that longer experiments would be needed to show this relationship between the 11% and 21% TFV groups, since linear loading-dependent release was observed for 30 days.

Example photomicrographs of IVR cross-sections before and after 30 day release testing (Fig. 3B and C) illustrate the movement of the diffusion front (r_d). IVRs containing 21% TFV with XD of either 5.0 or 5.6 mm were subjected to *in vitro* release testing for 90 days. It was estimated that 87% and 76% of the initial TFV loading was released from the 5.0 mm and 5.6 mm XD IVR groups, respectively, after 90 days (Fig. 5D). The product-log-difference transform (PLDT) of cumulative release was calculated for each IVR group. As shown in Fig. 6A, PLDT generally varies linearly with time, as predicted by Eq. (2a), ($R^2 > 0.997$).

Linear regressions of PLDT versus time data (Fig. 6B) were used to calculate time constants (β), which were used in a modified form of Eq. (4) (incorporating a lag time shift, see supplementary data) to construct 30 and 90 day release rate predictions, as shown in Fig. 6C and D. Coefficients of determination (R^2) from day 10 onward were greater than 0.8 in all cases. The mean error in prediction was less than 10% except for the 2% TFV IVR group, where the mean error was 14%. As shown in Fig. 6B, PLDT versus time fits, calculated from d3–d7, intercept the positive time axis when extrapolated to PLDT = 0, indicating that lag-type behavior occurs at early times during TFV release. Lag times, calculated by Eq. (8), ranged from 10 to 12 h. This suggests that, although 48 h were required for complete IVR swelling, the swelling front moved sufficiently inward in the first 12 h to achieve constant TFV diffusivity outside the diffusion front. Similar lag-time corrections have been employed to modify the Higuchi equation when considering early unsteady interfacial mass-transfer [37].

Porosity-adjusted matrix solubility values were used with time constants to calculate the effective diffusivity of TFV for each IVR batch using Eq. (9). All diffusivity values were between $5\text{--}7 \times 10^{-7} \text{ cm}^2/\text{s}$, indicating the architecture of the porous aqueous phase is similar regardless of drug loading. These effective diffusivities are functions of TFV aqueous diffusivity, TFV-polymer hydrodynamic interactions and pore tortuosity (neglecting any transport in the polymer phase) [38]. Fig. 6D shows that Eq. (4) (modified form) can be used to predict 90-day release from TFV HPEU IVRs given data from a 7-day drug release test. Although precise fits were not achieved between theoretical and experimental data, the mean error in model prediction across all model time points was less than 15%. This model can be used to reduce significantly the time-scale and experimental workload for the development of new IVR systems by eliminating the need to run full duration drug release studies during the formulation screening process. This model may prove useful for water-swallowable IVRs with negligible

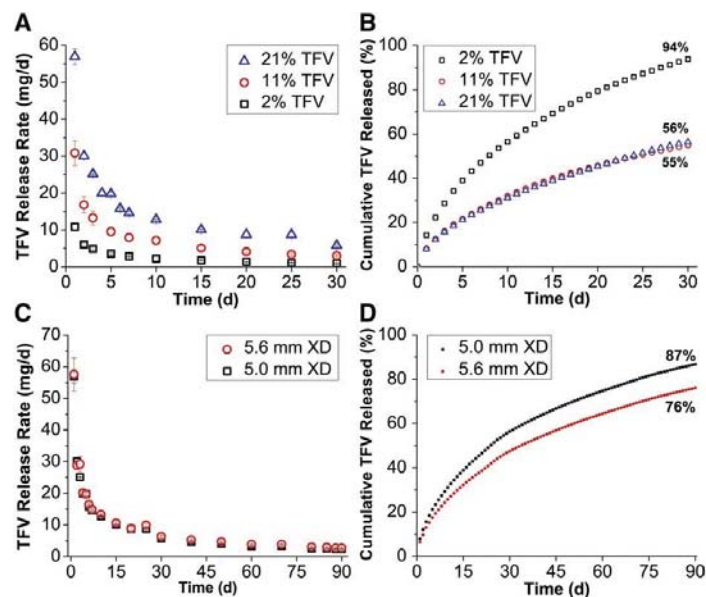


Fig. 5. Drug release testing. (A) Daily release rates measured by HPLC and (B) cumulative release estimated by linear interpolation from 5.0 mm XD IVRs with various TFV loadings (% w/w) for 30 days. (C) Daily release rates measured by HPLC and (D) cumulative release estimated by linear interpolation from 21% TFV IVRs with differing cross-sectional diameter (XD) for 90 days. All experiments were performed in 25 mM sodium acetate buffer (pH 4.2) at 37 °C and 80 rpm. Sink conditions were maintained throughout testing. Data represent N=3, mean \pm SD in panels A and C.

drug-polymer solubility, such as presented here, as well as for non-swelling matrix-type systems where the drug load far exceeds polymer solubility.

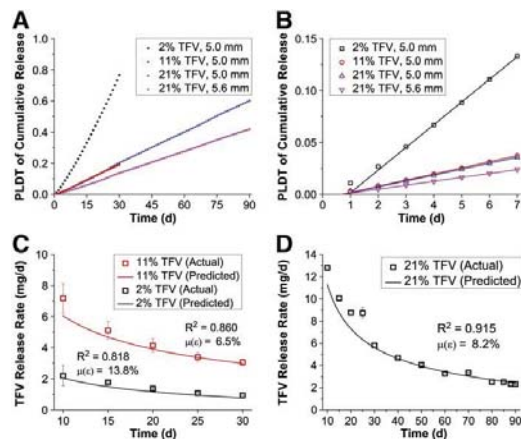


Fig. 6. Analysis of drug release. (A) Product-log-difference transforms (PLDT) of cumulative release data, as defined in Eq. (2a), are generally linear with time ($R^2 > 0.997$). (B) Linear regressions of early-time PLDT (calculated from d3–d7 and extrapolated to the x-axis) used to derive release time constants (β) ($R^2 > 0.999$). (C,D) Accuracy of the model presented in Eq. (4) in predicting TFV release rates from 5.0 mm XD IVRs using time constants extracted from regressions shown in panel B. The 5.6 mm, 21% TFV group (not shown) had R^2 and mean error ($\mu(\epsilon)$) values of 0.879 and 9.3%, respectively.

The exact release rate of TFV from an IVR required to achieve protection against HIV transmission in women is unknown. Efforts in the HIV prevention field are focused on correlating effective suppression of viral replication in tissue to antiviral drug concentrations measured in the vaginal vault using human trial data [39], as well as through pharmacokinetic [40] and challenge [41] studies in non-human primates. It is likely that when high bolus doses of TFV are administered vaginally, the efficiency of uptake into the vaginal tissue is low [14], meaning that the potential 80 mg TFV administered within a 24-hour period in CAPRISA 004 may not provide a dose metric on which to base long-duration delivery systems. Thus, matrix systems with increasing diffusion lengths and corresponding decreases in drug flux may not provide sustained levels of antiretrovirals to prevent viral invasion of the mucosa across multiple episodes of exposure at later time points. Furthermore, the high release rates (as high as ~50 mg/d) seen in the early part of the release profile may provide a loading dose but also could result in toxicity and potential loss of mucosal barrier function.

When testing this IVR in the pig-tailed macaque model, we have observed that similar milligram-per-day release rates of TFV can be replicated *in vivo* (unpublished data). While the 21% TFV IVR is capable of releasing greater than 2 mg/day for 90 days, there is a large drop in the release rate from day 1 to day 90. Depending on the release rate required for effective tissue protection, this IVR may not be effective over the complete 90 day profile, but could provide adequate protection for shorter durations (e.g., 30 days). To achieve the goal of developing an IVR which remains efficacious for longer durations, we are developing a reservoir-type IVR system for 90 day, zero-order TFV delivery [42].

Our theoretical and experimental presentation illustrates that co-optimization of drug release rates and IVR compressibility in a swellable matrix system containing a high weight fraction of undissolved drug is challenging. Drug release rates and IVR stiffness

are both positively correlated with initial drug loading and XD. This indicates that a very narrow design space of ring dimensions and drug loadings capable of yielding an IVR that performs within design specifications may exist, which may necessitate the investigation of different polymer systems and/or different IVR designs. Nonetheless, this work illustrates that a deep, quantitative understanding of relevant physical mechanisms is required to effectively design and develop long-acting dosage forms.

5. Conclusion

Here we present an HPEU intravaginal ring capable of sustained release of TFV, an inhibitor of HIV-1 reverse transcriptase, whose simple design may allow for easy scale-up to clinical production. However, there are several limitations to this IVR design that reduce its potential usefulness as a clinical product; notably the large decrease in TFV release with time, as well as the change in mechanical properties upon ring hydration. We also have presented drug release and solid mechanical models that can be used to optimize such an IVR system with minimal experimental work given inputs of desired mechanical properties and minimum release rates. Our model and simple resulting formulae should be extendable to any IVR system where the drug loading far exceeds polymer solubility.

Acknowledgements

This work was supported by CONRAD under a cooperative agreement with USAID (GPO-A-00-08-00005-00). The authors thank Shanger Wang, Ph.D. and Li Li, Ph.D. of DSM Biomedical for preparing and supplying HPEU 20. The authors also thank Jennifer Hurlburt (CONRAD), R. Tyler McCabe, Ph.D. and Krystin Meidell (University of Utah) for assistance in manuscript preparation, as well as David Katz, Ph.D. (Duke University) and Jeff Weiss, Ph.D. (University of Utah) for their critique of the drug release and mechanical models presented. Views expressed by the authors do not necessarily reflect those of USAID.

Appendix A. Supplementary data

Supplementary data to this article can be found online at <http://dx.doi.org/10.1016/j.jconrel.2012.08.033>.

References

- C. Celum, J.M. Baeten, Tenofovir-based pre-exposure prophylaxis for HIV prevention: evolving evidence, *Curr. Opin. Infect. Dis.* 25 (1) (2012) 51–57.
- J. Cohen, FDA panel recommends anti-HIV drug for prevention, *Science* 336 (6083) (2012) 792.
- Q. Abdoal Karim, S.S. Abdoal Karim, J.A. Frohlich, A.C. Grobler, C. Baxter, L.E. Mansoor, A.B. Kharsany, S. Sibeko, K.P. Mlisana, Z. Omar, T.N. Gengiah, S. Maarschalk, N. Arulappan, M. Mlotshwa, L. Morris, D. Taylor, Effectiveness and safety of tenofovir gel, an antiretroviral microbicide, for the prevention of HIV infection in women, *Science* 329 (5996) (2010) 1168–1174.
- R.M. Grant, D. Hamer, T. Hope, R. Johnston, J. Lange, M.M. Lederman, J. Lieberman, C.J. Miller, J.P. Moore, D.E. Mosier, D.D. Richman, R.T. Schooley, M.S. Springer, R.S. Veazey, M.A. Wainberg, Whither or wither microbicides? *Science* 321 (5888) (2008) 532–534.
- L. Rossi, Microbicide trials network statement on decision to discontinue use of tenofovir gel in VOICE, a major HIV prevention study in women, *Microbicide Trials Network*, 2011.
- Y.W. Chien, H.J. Lambert, D.E. Grant, Controlled drug release from polymeric devices. I. Technique for rapid in vitro release studies, *J. Pharm. Sci.* 63 (3) (1974) 365–369.
- D.R. Mishell, M. Talas, A.F. Parlow, D.L. Moyer, Contraception by means of a silastic vaginal ring impregnated with medroxyprogesterone acetate, *Am. J. Obstet. Gynecol.* 107 (1) (1970) 100–107.
- J.A. van Laarhoven, M.A. Kruft, H. Vromans, In vitro release properties of etonogestrel and ethinyl estradiol from a contraceptive vaginal ring, *Int. J. Pharm.* 232 (1–2) (2002) 163–173.
- R.K. Malcolm, A.D. Woolfson, C.F. Toner, R.J. Morrow, S.D. McCullagh, Long-term, controlled release of the HIV microbicide TMC120 from silicone elastomer vaginal rings, *J. Antimicrob. Chemother.* 56 (5) (2005) 954–956.
- R.K. Malcolm, K.-L. Edwards, P. Kiser, J. Romano, T.J. Smith, Advances in microbicide vaginal rings, *Antivir. Res.* 88 (Supplement 1) (2010) S30–S39.
- K.M. Gupta, S.M. Pearce, A.E. Poursaid, H.A. Aliyar, P.A. Tresco, M.A. Mitchnik, P.F. Kiser, Polyurethane intravaginal ring for controlled delivery of dapivirine, a nonnucleoside reverse transcriptase inhibitor of HIV-1, *J. Pharm. Sci.* 97 (10) (2008) 4228–4239.
- P.F. Kiser, T.J. Johnson, J.T. Clark, State of the art in intravaginal ring technology for topical prophylaxis of HIV infection, *AIDS Rev.* 14 (1) (2012) 62–77.
- A. Novak, C. de la Loge, L. Abetz, E.A. van der Meulen, The combined contraceptive vaginal ring, NuvaRing: an international study of user acceptability, *Contraception* 67 (3) (2003) 187–194.
- R.K. Malcolm, Modified-Release Drug Delivery Technology, in: M.J. Rathbone (Ed.), Informa Healthcare, New York, 2008, pp. 499–510.
- M. Arimilli, Synthesis, in vitro biological evaluation and oral bioavailability of 9-[2-(phosphonomethoxy)propyl]adenine (PMPA) prodrugs, *Antivir. Chem. Chemother.* 8 (6) (1997) 557–564.
- T.J. Johnson, K.M. Gupta, J. Fabian, T.H. Albright, P.F. Kiser, Segmented polyurethane intravaginal rings for the sustained combined delivery of antiretroviral agents dapivirine and tenofovir, *Eur. J. Pharm. Sci.* 39 (4) (2010) 203–212.
- R.W. Kormsmeier, S.R. Lustig, N.A. Peppas, Solute and penetrant diffusion in swellable polymers. I. Mathematical modeling, *J. Polym. Sci. Part B: Polym. Phys.* 24 (2) (1986) 395–408.
- R.W. Kormsmeier, E. Von Meerwall, N.A. Peppas, Solute and penetrant diffusion in swellable polymers. II. Verification of theoretical models, *J. Polym. Sci. Part B: Polym. Phys.* 24 (2) (1986) 409–434.
- J. Siepmann, F. Siepmann, Mathematical modeling of drug delivery, *Int. J. Pharm.* 364 (2) (2008) 328–343.
- W. Bounds, A. Szarewski, D. Lowe, J. Guillebaud, Preliminary report of unexpected local reactions to a progestogen-releasing contraceptive vaginal ring, *Eur. J. Obstet. Gynecol. Reprod. Biol.* 48 (2) (1993) 123–125.
- S. Koetsawang, G. Ji, U. Krishna, A. Cuadros, G.I. Dhall, R. Wyss, J. Rodriguez la Puente, A.T. Andrade, T. Khan, E.S. Kononova, J.P. Lawson, U. Parekh, M. Elstein, V. Hingorani, Wang Na-ning, Yao Zhong-beng, B.M. Landgren, R. Boukhris, Lo Li-lan, S. Boccard, D. Machin, A. Pinol, P.J. Rowe, Microdose intravaginal levonorgestrel contraception: a multicentre clinical trial. II. Expulsions and removals. World Health Organization. Task Force on Long-Acting Systemic Agents for Fertility Regulation, *Contraception* 41 (2) (1990) 125–141.
- E. Weisberg, I.S. Fraser, J. Baker, D. Archer, B.M. Landgren, S. Killick, P. Soutter, T. Krause, C. d'Arcangues, A randomized comparison of the effects on vaginal and cervical epithelium of a placebo vaginal ring with non-use of a ring, *Contraception* 62 (2) (2000) 83–89.
- T. Higuchi, Mechanism of Sustained-Action Medication. Theoretical Analysis of Rate of Release of Solid Drugs Dispersed in Solid Matrices, *J. Pharm. Sci.* 52 (1963) 1145–1149.
- T.J. Roseman, W.L. Higuchi, Release of medroxyprogesterone acetate from a silicone polymer, *J. Pharm. Sci.* 59 (3) (1970) 353–357.
- T.J. Roseman, Release of steroids from a silicone polymer, *J. Pharm. Sci.* 61 (1) (1972) 46–50.
- J. Siepmann, F. Siepmann, Modeling of diffusion controlled drug delivery, *J. Control. Release* 161 (2) (2012) 351–362.
- R.M. Corless, G.H. Gonnet, D.E.G. Hare, D.J. Jeffrey, D.E. Knuth, On the Lambert W function, *Adv. Comput. Math.* 5 (1) (1996) 329–359.
- I.M. Helbling, J.A. Luna, M.I. Cabrera, Mathematical modeling of drug delivery from torus-shaped single-layer devices, *J. Control. Release* 149 (3) (2011) 258–263.
- R. Huston, *Practical Stress Analysis in Engineering Design*, CRC Press, Boca Raton, 2009.
- M.R. Clark, T.J. Johnson, R.T. McCabe, J.T. Clark, A. Tuitupou, H. Elgendy, D.R. Friend, P.F. Kiser, A hot-melt extruded intravaginal ring for the sustained delivery of the antiretroviral microbicide UC781, *J. Pharm. Sci.* 101 (2) (2012) 576–587.
- K.T. Barnhart, K. Timbers, E.S. Pretorius, K. Lin, A. Shaunik, In vivo assessment of NuvaRing placement, *Contraception* 72 (3) (2005) 196–199.
- L. Zema, G. Loreti, A. Melocchi, A. Maroni, A. Gazzaniga, Injection Molding and its application to drug delivery, *J. Control. Release* 159 (3) (2012) 324–331.
- V. Brache, A. Faundes, Contraceptive vaginal rings: a review, *Contraception* 82 (5) (2010) 418–427.
- A. Martinelli, L. D'Ilario, I. Francolini, A. Piozzi, Water state effect on drug release from an antibiotic loaded polyurethane matrix containing albumin nanoparticles, *Int. J. Pharm.* 407 (1–2) (2011) 197–206.
- J. Berriot, F. Lequeux, H. Montes, H. Pernot, Reinforcement of model filled elastomers: experimental and theoretical approach of swelling properties, *Polymer* 43 (23) (2002) 6131–6138.
- R.W. Seymour, S.L. Cooper, Viscoelastic properties of polyurethane block polymers, *J. Polym. Sci. Polym. Symp.* 46 (1) (1974) 69–81.
- D.R. Paul, Elaborations on the Higuchi model for drug delivery, *Int. J. Pharm.* 418 (1) (2011) 13–17.
- G. Truskey, *Transport Phenomena in Biological Systems*, Pearson Prentice Hall, Upper Saddle River, New Jersey, 2004.
- S.S. Abdoal Karim, A.D. Kashuba, L. Werner, Q. Abdoal Karim, Drug concentrations after topical and oral antiretroviral pre-exposure prophylaxis: implications for HIV prevention in women, *Lancet* 378 (9787) (2011) 279–281.
- T.J. Johnson, P. Srinivasan, T.H. Albright, K. Watson-Buckheit, L. Rabe, A. Martin, C.P. Pau, R.M. Hendry, R. Otten, J. McNicholl, R. Buckheit Jr., J. Smith, P.F. Kiser, Safe and sustained vaginal delivery of pyrimidineione HIV-1 inhibitors from polyurethane intravaginal rings, *Antimicrob. Agents Chemother.* 56 (3) (2012) 1291–1299.

Author's personal copy

248

J.T. Clark et al. / Journal of Controlled Release 163 (2012) 240–248

- [41] C. Dobard, S. Sharma, A. Martin, C.P. Pau, A. Holder, Z. Kuklenyik, J. Lipscomb, D.L. Hanson, J. Smith, F.J. Novembre, J.G. Garcia-Lerma, W. Heneine, Durable protection from vaginal simian-human immunodeficiency virus infection in macaques by tenofovir gel and its relationship to drug levels in tissue, *J. Virol.* 86 (2) (2012) 718–725.
- [42] T.J. Johnson, M.R. Clark, T.H. Albright, J.S. Nebeker, A.L. Tuitupou, J.T. Clark, Judit Fabian, R.T. McCabe, N. Chandra, G.F. Doncel, D.R. Friend, P.F. Kiser, A ninety day tenofovir reservoir intravaginal ring for mucosal HIV prophylaxis, *Antimicrob. Agents Chemother.* (2012, accepted manuscript).

Supplementary data

TFV quantification by HPLC

Three gradient HPLC methods (15, 25, and 40 minutes) were used interchangeably to determine the TFV concentrations in release media samples and extractions of ring segments. The 15- and 25-minute methods are modified versions of the 40-minute method, which we have reported previously [16]. For all three methods, samples were injected onto a Luna 4.6 mm x 150 mm (5 μ m) C18 column (Phenomenex, Torrance, CA) with gradients of 50 mM potassium phosphate buffer (pH 6.0) (Line B), and the same buffer with 4.5% (Line A), 30% (Line C) or 51% (Line D) acetonitrile (v/v) at a flow rate of 1.5 mL/min. TFV was detected at $\lambda=260$ nm, with retention times ranging from 6 to 9 minutes. Aqueous solutions with known TFV concentrations were used to generate linear calibration curves (peak area vs. mass injected) for TFV quantification in unknown samples.

Table S1: 40-minute version of the HPLC method used for TFV quantification. This version was typically used for quantification of TFV in HPEU IVR extraction samples.

Time (min)	Flow (mL/min)	Line A (%)	Line B (%)	Line C (%)	Line D (%)
0	1.5	0	100	0	0
10	1.5	100	0	0	0
20	1.5	0	0	100	0
30	1.5	0	0	0	100
33	1.5	0	100	0	0
40	1.5	0	100	0	0

Table S2: 15-minute version of the HPLC method used for TFV quantification. This version was typically used for quantification of TFV in drug release experiments.

Time (min)	Flow (mL/min)	Line A (%)	Line B (%)
0	1.5	0	100
10	1.5	100	0
13	1.5	0	100
15	1.5	0	100

Table S3: 25-minute version of the HPLC method used for TFV quantification. This version was also used for quantification of TFV in drug release experiments.

Time (min)	Flow (mL/min)	Line A (%)	Line B (%)	Line C (%)
0	1.5	0	100	0
10	1.5	100	0	0
15	1.5	0	0	100
18	1.5	0	100	0
25	1.5	0	100	0

Determination of TFV loading in IVRs

To determine the weight fraction of TFV in each batch of injection-molded IVRs, TFV was extracted from 10-20 mg ring segments selected randomly from the batch. These segments were placed in 50 mL volumetric flasks filled partially with dimethyl acetamide (DMA). The flasks were agitated vigorously using a large capacity mixer (Glas-Col®, Terre Haute, IN) until all TFV and polymer was fully dissolved in the DMA. The flasks were filled to volume with DMA, and inverted several times to ensure a uniform solution. Using a calibrated volumetric syringe (Hamilton Company, Reno, NV), a 1.00 mL aliquot of the resulting solution was added to a 5.00 mL volumetric flask that was then filled to volume with 50 mM ammonium acetate buffer (pH 7.0) and vortexed briefly to precipitate the polymer. The amount of TFV in each sample was quantified by the 40-minute HPLC method described above.

Approximation of cumulative TFV release from IVRs

Since the release rates of TFV from HPEU IVRs were not directly measured for each day of incubation, it was necessary to interpolate the daily release data to build a cumulative release profile. This was completed using a linear interpolation in OriginPro 8 graphing software (OriginLab Corp., Northampton, MA), yielding an uninterrupted release rate profile, Q^* . The cumulative TFV release profile was then determined by taking discrete sums of $Q^*(t)$:

$$M^*_{TFV}(n) = \sum_{i=1}^n Q^*(i) \quad (S1)$$

The PLDT, as shown in Equation 2a, of M^* were calculated and plotted against time for subsequent analysis.

MATLAB code for release data extrapolation

The function "lsmivrfit.m" can be used to extrapolate daily release data forward using a modified form of Equation 4:

$$\frac{M}{M_0} = 1 - \frac{M_r}{M_0} = 1 - e^{-\left(W_{-1} \left(\frac{\beta(t-t_{lag})-1}{e} \right) + 1 \right)} \quad (S2)$$

if release rates have been measured for the first 7 days. The function also will compute the product " $Deff^*\omega_s$ " which can be used to estimate effective diffusivity if the drug-matrix solubility (ω_s) is known.

```
function [ Q,Deffws ] = lsmivrfit( Mexp,tf,M0,ro,wt,M1exp )
```

```
%Mexp is a column vector containing fractional cumulative release from days  
%3 through 7
```

```
%beta is the time constant derived from PLD release transform fits in units  
%(d^-1)
```

```

%tf is the release duration in days

%M0 is the initial IVR drug load in arbitrary units

%ro is the outer IVR radius in centimeters

%wt is the weight fraction loading

%M1exp is the experimentally determined fractional release on day 1

%Q is the predicted daily release rate profile

Mres=1-Mexp;
texp=(3:1:7)';
Mpld=zeros(length(Mres),1);

for i=1:length(Mres)
    Mpld(i)=(Mres(i)*log(Mres(i)))-Mres(i)+1;
end

pldfit=polyfit(texp,Mpld,1);

beta=pldfit(1);
M1=1-(exp(lambertw(-1,((beta-1)/exp(1))))+1));
PLDlactual=((1-M1exp)*log(1-M1exp))-(1-M1exp)+1;
PLDlmodel=((1-M1)*log(1-M1))-(1-M1)+1;
tlag=(PLDlmodel-PLDlactual)/beta;

t=(0:1:tf);
t=t-tlag;
t(1)=0;

Mfrac=1-(exp(lambertw(-1,((beta*t)-1)/exp(1))))+1));
for i=1:tf
    Q(i)=M0*(Mfrac(i+1)-Mfrac(i));
end

Q=Q';

Deffws=((beta*wt*(ro^2))/4)/86400; % in cm2/s

end

```

CHAPTER 3

ENGINEERING A SEGMENTED DUAL-RESERVOIR POLYURETHANE INTRAVAGINAL RING FOR SIMULTANEOUS PREVENTION OF HIV TRANSMISSION AND UNWANTED PREGNANCY

Justin T. Clark, Meredith R. Clark, Namdev B. Shelke, Todd J. Johnson, Eric M. Smith,
Andrew K. Andreasen, Joel S. Nebeker, Judit Fabian, David R. Friend, Patrick F. Kiser

PLOS ONE 2014; 9(3): e88509

Reproduced with permission from PLOS

Engineering a Segmented Dual-Reservoir Polyurethane Intravaginal Ring for Simultaneous Prevention of HIV Transmission and Unwanted Pregnancy

Justin T. Clark¹, Meredith R. Clark², Namdev B. Shelke¹, Todd J. Johnson¹, Eric M. Smith¹, Andrew K. Andreasen¹, Joel S. Nebeker¹, Judit Fabian¹, David R. Friend², Patrick F. Kiser^{1,3*}

1 Department of Bioengineering, University of Utah, Salt Lake City, Utah, United States of America, **2** CONRAD, Department of Obstetrics and Gynecology, Eastern Virginia Medical School, Arlington, Virginia, United States of America, **3** Department of Biomedical Engineering, Northwestern University, Evanston IL, United States of America

Abstract

The HIV/AIDS pandemic and its impact on women prompt the investigation of prevention strategies to interrupt sexual transmission of HIV. Long-acting drug delivery systems that simultaneously protect women from sexual transmission of HIV and unwanted pregnancy could be important tools in combating the pandemic. We describe the design, *in silico*, *in vitro* and *in vivo* evaluation of a dual-reservoir intravaginal ring that delivers the HIV-1 reverse transcriptase inhibitor tenofovir and the contraceptive levonorgestrel for 90 days. Two polyether urethanes with two different hard segment volume fractions were used to make coaxial extruded reservoir segments with a 100 μm thick rate controlling membrane and a diameter of 5.5 mm that contain 1.3 wt% levonorgestrel. A new mechanistic diffusion model accurately described the levonorgestrel burst release in early time points and pseudo-steady state behavior at later time points. As previously described, tenofovir was formulated as a glycerol paste and filled into a hydrophilic polyurethane, hollow tube reservoir that was melt-sealed by induction welding. These tenofovir-eluting segments and 2 cm long coaxially extruded levonorgestrel eluting segments were joined by induction welding to form rings that released an average of 7.5 mg tenofovir and 21 μg levonorgestrel per day *in vitro* for 90 days. Levonorgestrel segments placed intravaginally in rabbits resulted in sustained, dose-dependent levels of levonorgestrel in plasma and cervical tissue for 90 days. Polyurethane caps placed between segments successfully prevented diffusion of levonorgestrel into the tenofovir-releasing segment during storage. Hydrated rings endured between 152 N and 354 N tensile load before failure during uniaxial extension testing. In summary, this system represents a significant advance in vaginal drug delivery technology, and is the first in a new class of long-acting multipurpose prevention drug delivery systems.

Citation: Clark JT, Clark MR, Shelke NB, Johnson TJ, Smith EM, et al. (2014) Engineering a Segmented Dual-Reservoir Polyurethane Intravaginal Ring for Simultaneous Prevention of HIV Transmission and Unwanted Pregnancy. PLoS ONE 9(3): e88509. doi:10.1371/journal.pone.0088509

Editor: Gilda Tachedjian, Burnet Institute, Australia

Received: September 3, 2013; **Accepted:** January 7, 2014; **Published:** March 5, 2014

Copyright: © 2014 Clark et al. This is an open-access article distributed under the terms of the Creative Commons Attribution License, which permits unrestricted use, distribution, and reproduction in any medium, provided the original author and source are credited.

Funding: Funding was provided under cooperative agreement (GPO-A-00-08-00005-00 and AID-OAA-A-10-0006) between the United States Agency for International Development (USAID) and the Eastern Virginia Medical School. This work was supported by a cooperative agreement from The United States Agency for International Development (USAID). USAID had no role in study design, data collection and analysis, decision to publish, or preparation of the manuscript.

Competing Interests: The authors have declared that no competing interests exist.

* E-mail: patrick.kiser@northwestern.edu

Introduction

The global HIV/AIDS pandemic continues to drive advances in biomedical technologies designed to quell the spread of the virus [1]. The recent USFDA approval of oral Truvada[®] for HIV pre-exposure prophylaxis (PrEP) in discordant couples is a major biomedical advance [2]. But clinicians have encountered difficulty in consistently demonstrating PrEP efficacy in prevention trials. In the CAPRISA 004 trial, topical vaginal application of the tenofovir (TFV) 1% gel used episodically before and after intercourse resulted in a 39% reduction in HIV infection in women [3]. But the same TFV gel did not reduce transmission rates when used once daily [4]. The variability in trial outcomes has caused consternation and several thoughtful reviews [5,6,7,8,9]. Yet the progress is evident when simultaneously considering the success of oral Truvada, the modest effect in CAPRISA 004, and alongside the accumulating evidence of the protective effect of TFV from non-human primate studies [10,11,12]. It is now conceptually clear that using oral and topical

antiretroviral (ARV) drugs to interrupt the early events of sexual HIV transmission and dissemination is biologically and biomedically possible. The poor clinical outcomes result from confounding factors that span across behavioral, biological and pharmacological causes. Since the discovery of low rates of adherence in the Carraguard trial [13] and subsequently in the VOICE trial [4] it has been clear that infrequent use of gels by women likely has been a significant factor contributing to the low rates of effectiveness observed in most gel PrEP trials to date. For many reasons, trial participants are not sufficiently motivated to use the prevention products as instructed. Therefore, if PrEP is to be a technological success, new PrEP modalities are desperately needed that are easier to use and more desirable to women, and are supported by high user demand.

There are two main approaches being explored to increase user demand for PrEP, to either increase device duration or to make devices that are multifunctional and satisfy more than one user need. It is observed across many types of pharmaceutical products

that user adherence and dose duration are positively correlated [14,15]. To this end much effort has been directed toward long-acting injectable ARV [16] and ARV eluting intravaginal rings (IVR) [17,18] for PrEP. Adding multiple functions, indications or purposes is also receiving attention as a method for improving user demand. Hormonal contraception is a well established technology in many low income countries impacted by the HIV pandemic. This has motivated the development of biomedical devices, and in particular long-acting IVR [19,20,21] that elute both contraceptive hormones and ARV. The development of multipurpose prevention technologies (MPT) could be ground breaking as there are no approved products that use two drugs to simultaneously address multiple indications. Yet the literature and the drug store shelf are replete with examples of fixed dose drug combinations designed to treat a single indication that were developed to improve ease of use, patient compliance and outcomes [22,23].

As one might expect, there are a host of contraceptive agents and ARV under evaluation for use in MPT. The progestin levonorgestrel (LNG) is a leading contraceptive agent with a long history of clinical use in topical and oral administration. The Mirena® intrauterine system releases up to 20 µg LNG per day for 5 years. The WHO also developed a silicone reservoir IVR that released approximately 20 µg LNG per day for 90 days [24]. In a large multi-center clinical trial, the LNG IVR was over 95% effective in preventing unintended pregnancy. Tenofovir (TFV) is the leading ARV for many reasons including its approval for PrEP, its long clinical safety record (tenofovir prodrug formulations are currently used by 3.5 million people), extended duration of cellular levels following dosing and stability. But simultaneous dosing of TFV and LNG at relevant levels from simple, monolithic IVR is a challenge due to differences in their properties and target release rates, mandating the investigation of customized IVR designs.

We recently demonstrated the three-month zero-order delivery of TFV from a hydrophilic polyether urethane (HPEU) reservoir IVR [25]. In this report we describe the engineering and design of a segmented dual-reservoir IVR for the controlled delivery of TFV and LNG for 90 days. This manuscript illustrates the challenges of designing and integrating a solid, non-swellable LNG-releasing polyether urethane (PEU) reservoir into the existing swellable HPEU reservoir technology. We used a combination of *in silico*, *in vitro* and *in vivo* methodologies to study, engineer and evaluate the combination IVR. We present new insights regarding the use of the chemically diverse class of elastomeric PEU in reservoir-type dosage forms to deliver chemically diverse molecules at greatly divergent release rates. The work resulted in an IVR that gives nearly time-independent vaginal delivery of TFV and LNG for three months.

Design

All clinically-used IVR in the U.S. employ reservoir technologies, however HIV prevention researchers have often investigated simpler matrix IVR designs to reduce manufacturing complexity and cost [26,27,28,29]. Reservoir IVR are more attractive from a pharmacokinetic perspective as they can provide constant drug levels in the reproductive tract over extended durations [25]. Matrix IVR intrinsically provide high initial release rates, followed by continuously attenuated rates over time [17]. This is generally undesirable for PrEP applications, because the maintenance of preventative ARV levels for the intended IVR duration will require an excess of ARV exposure at early times during the release profile, presenting potential safety concerns. Furthermore, design limitations hindering the attainment of sufficient drug release rates can render it impossible to achieve high drug levels throughout the release profile and may result in increased

probability of HIV acquisition late in the release profile of a matrix ARV-eluting IVR. These pharmacological limitations drive the investigation of reservoir IVR technologies that have the potential to provide precise and tunable control over the drug release rates for as long as several months.

TFV and LNG exhibit approximately 7-log and 4-log differences in their partition/distribution coefficients and aqueous solubilities, respectively (Figure 1A and 1B), precluding their simultaneous solubilization and controlled release from a single polymeric compartment. To address these differences in molecular properties, we utilized chemically diverse polyether urethanes (PEU) capable of solubilizing and delivering TFV and other ARVs with varying physicochemical properties [30,31,32,33]; an ability not generally afforded by the traditionally used silicone and poly(ethylene-co-vinyl-acetate) elastomers. Poly(ethylene oxide) can be added alongside the poly(tetramethylene oxide) soft segment typically used in PEU to create hydrophilic poly(ether urethanes) (HPEU) that swell in aqueous solution and can solubilize hydrophilic drugs when hydrated. Furthermore, PEU and HPEU are otherwise chemically identical and can be readily melt-welded to form mechanically sound IVR.

In addition to their disparate chemical properties, TFV and LNG also require vastly different release rates for their respective pharmacological effects. Our group designed an HPEU hollow-tube reservoir IVR to release 10 mg TFV per day [25], which we similarly targeted for the TFV/LNG IVR. However, as described above much lower release rates of LNG are employed for topical microdose contraception. We chose targets of 10 and 20 µg LNG per day, similar to the Mirena® intrauterine system and WHO's silicone LNG IVR. To address the challenge of delivering these diverse molecules at divergent release rates we designed a two-segment reservoir IVR system [31] containing an analogous TFV reservoir segment [25] and a PEU reservoir segment containing dissolved LNG. We desired to create a platform technology from which three devices, all with the same overall size (5.5 mm and 55 mm cross-sectional and outer diameters, respectively), could be fabricated to deliver ~10 mg TFV per day with LNG daily doses of either 0 (TFV-only), 10 or 20 µg.

Generally, drug release rates (dM/dt) from end-capped cylindrical reservoir devices, like IVR or IVR segments can be varied by changing the segment length (l), core drug concentration (c_m) or the outer, rate controlling membrane (RCM) thickness (represented by the subtraction of outer and inner cross-sectional radii, $r_o - r_i$). A steady-state description, assuming constant c_m , is easily derived from Fick's laws and is ubiquitous in the design of reservoir IVR [34,35]:

$$\frac{dM}{dt} = \frac{2\pi l D c_m}{\ln\left(\frac{r_o}{r_i}\right)} \quad (1)$$

where D is the effective diffusivity of the drug in the RCM material. To achieve the membrane-controlled release described in Equation 1, the drug-loaded core must be well-mixed so that the drug concentration remains uniform throughout the core and at the core/membrane boundary. For a solid polymer system, like the LNG segment, this is achieved by choosing a core polymer with much higher drug diffusivity than that of the RCM polymer. Specifically for PEU, drug flux can be hindered by increasing the volume fraction of crystalline hard segments. This is also easily maintained for a hollow-tube system like the TFV segment [25], because of the large differences in diffusivity between the liquid core and the porous membrane of the wall.

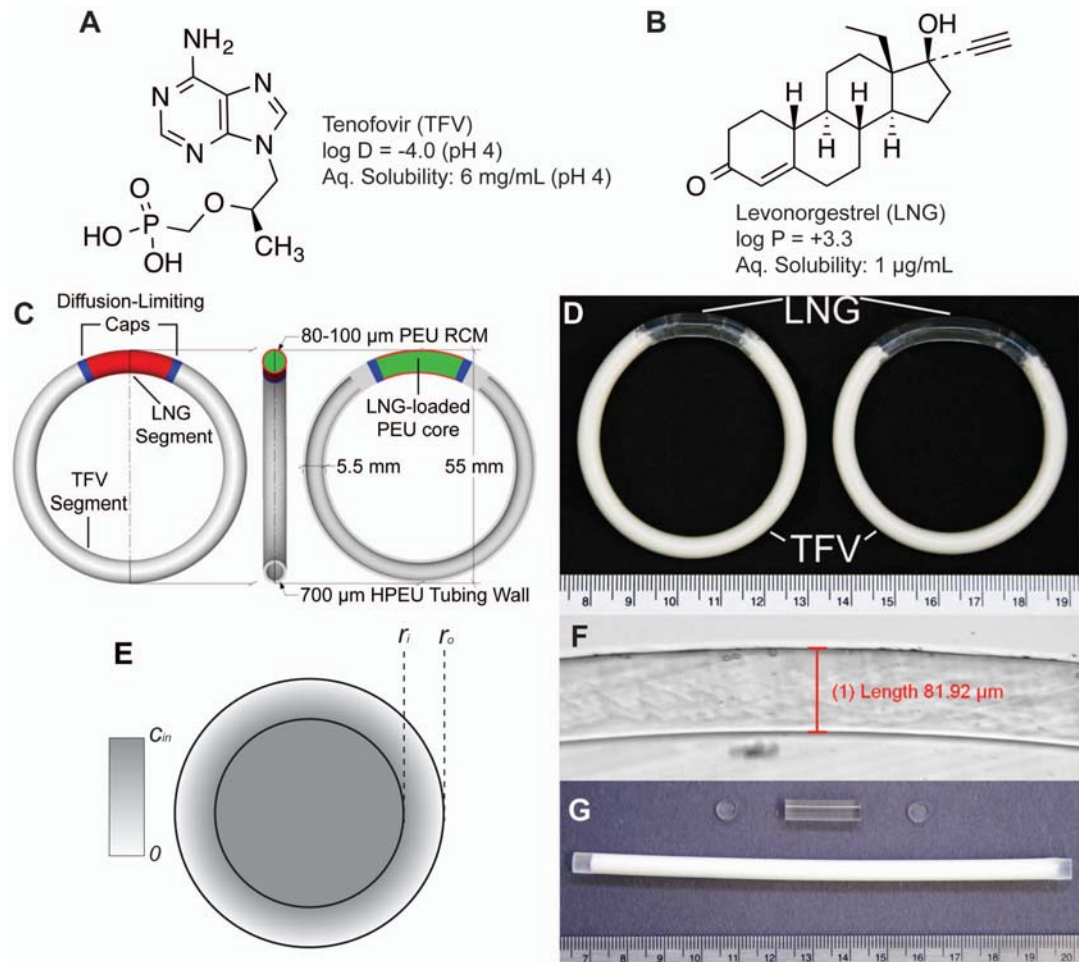


Figure 1. IVR Design Overview. Structural formulae of (A) the HIV-1 nucleotide reverse transcriptase inhibitor tenofovir (TFV) and (B) the progestin contraceptive levonorgestrel (LNG). (C) A design schematic of the full TFV/LNG IVR, shown in the 20 mm LNG segment configuration illustrating the LNG-loaded core (green), the rate-controlling membrane (RCM, red), diffusion-limiting end-caps (blue) and the hollow HPEU tube containing TFV-loaded paste (gray). (D) Photographs of TFV/LNG IVR in the 10 mm (left) and 20 mm (right) LNG segment configurations. (E) Illustration of a reservoir cross-section with outer and inner radii r_o and r_i , and core drug concentration c_m . (F) Photomicrograph of the LNG segment cross-section showing microscopic measurement of RCM thickness. (G) Component parts of the TFV/LNG IVR: a TFV paste-filled HPEU tube (bottom), a co-axially extruded LNG-loaded reservoir segment (top) and two diffusion-limiting end-caps (left and right).
doi:10.1371/journal.pone.0088509.g001

We chose to modify LNG release rates by changing the length of the LNG-segment. We desired to minimize LNG segment length to allow for minimal change in TFV dose between devices, but also sought to minimize the core LNG concentration because of potential physical stability issues of supersaturation and recrystallization on the IVR surface [36]. Thus, we arrived at a target release rate $1 \mu\text{g}/\text{mm}/\text{day}$ for the LNG segment, leading to two IVR prototypes with segments of 10 and 20 mm length to deliver $10 \mu\text{g}$ and $20 \mu\text{g}$ LNG per day, respectively. A diagram of the 20 mm configuration is shown in Figure 1C, and a photograph showing both IVR configurations (with either 10 mm or 20 mm LNG segments) is shown in Figure 1D. We also added diffusion-

limiting end-caps between the two segments (Figure 1C, shown in blue) to prevent circumferential diffusion of LNG from the solid PEU reservoir (green/red) to the hollow HPEU tubing in the TFV-releasing segment (gray). The end-caps are composed of the same PEU used to create the RCM.

Theory

Mathematical models of drug transport can aid the *in silico* design of drug delivery systems [37] including IVR [26,38]. TFV release occurs at a constant rate as predicted by Equation 1, due to an excess of un-dissolved drug which maintains a constant TFV core concentration [25]. For the LNG segment in the TFV/LNG

IVR, two issues confound the simple description of drug release presented in Equation 1. First, if LNG is equally distributed throughout the cross-section (core and membrane) at $t=0$, then the device will initially behave as a matrix device, resulting in a period of burst release, which we refer to as the ‘burst regime’, prior to the onset of steady-state release [34]. Second, as LNG is completely dissolved in the PEU core, the drug source (c_m) diminishes with time as drug is released, even after steady-state is achieved. We refer to this pseudo-steady-state (PSS) period as the ‘steady state regime’. We derived a comprehensive model which addresses both of these issues. Throughout, we assume the drug is completely dissolved at equal concentration in both the core and outer membrane at $t=0$, and that equipartitioning exists between the core and RCM polymer. Axial diffusion is neglected because the loss of LNG to the end-caps occurs on a much longer time-scale than that of drug release.

Radial drug release from cylindrical matrices. Diffusion-limited drug release of a purely dissolved drug from a cylinder with no axial diffusion is presented in the literature [39]. At early times (up to ~ 20 – 30% of cumulative release), the following first-term approximation predicts fractional cumulative release:

$$\frac{M(t)}{M_0} = \frac{4}{r_o} \sqrt{\frac{Dt}{\pi}} \quad (2)$$

where M is cumulative release, M_0 is the initial load of the device (or the cumulative release at infinite time), D is the effective drug-matrix diffusivity, and r_o is the radius of the cylinder. Equation 2 will describe drug release in the burst regime for a solid reservoir with initial homogeneous drug concentration.

Computation of burst duration. We compute the burst regime duration assuming the device will proceed as a matrix until its initial steady state profile is reached. The steady-state profile is then integrated to obtain the mass loss required to complete the burst. First we solve Fick’s Second Law in the steady-state form with a $c=c_0$ boundary at $r=r_i$ and a sink outer boundary ($c=0$ at $r=r_o$) (depicted in Figure 1E):

$$c(r) = \frac{c_0 \ln\left(\frac{r}{r_o}\right)}{\ln\left(\frac{r_i}{r_o}\right)} \quad (3)$$

We now integrate the right-hand-side of Equation 3 from r_i to r_o and scale appropriately to determine the mass remaining in the RCM at the beginning of the steady-state regime (m_{eq}):

$$m_{eq} = \int_{r_i}^{r_o} c(r) dV = 2\pi l \int_{r_i}^{r_o} rc(r) dr = \pi l c_0 \left(\frac{r_o^2 - r_i^2}{2 \ln\left(\frac{r_o}{r_i}\right)} - r_i^2 \right) \quad (4)$$

To avoid confusion, in this manuscript a capital “ M ” will represent to the cumulative drug mass released from the device, while a lower-case “ m ” will represent the drug mass remaining in various compartments of the device. By subtraction we compute the total burst release (M_b):

$$M_b = m_{RCM,t=0} - m_{eq} = \pi l c_0 \left(r_o^2 - \frac{r_o^2 - r_i^2}{2 \ln\left(\frac{r_o}{r_i}\right)} \right) \quad (5)$$

Combining Equation 5 with Equation 2 and solving for t , we obtain the burst duration or length of the burst regime (t_b):

$$t_b = \frac{\pi r_o^2}{16D} \left(1 - \frac{r_o^2 - r_i^2}{2r_o^2 \ln\left(\frac{r_o}{r_i}\right)} \right) \quad (6)$$

There is some approximation in the computation of Equation 6, as concentration profiles in a matrix device following release of M_b and in a reservoir system at steady-state are likely not identical. Some time is required for the system to adjust from the matrix to the reservoir profile when the system becomes constrained by the core boundary condition, during which additional drug is depleted from the core. Depending on the relationship between outer boundary flux during this transitional period and the predicted reservoir flux at when $c=c_0$, Equation 11 (below) will over- or underestimate release rates during this period. This phenomenon is discussed further in the Supporting Information (see Table S1 and Figures S1 and S2 in File S1)

Pseudo-steady-state adjustment for variable core concentration. To effectively describe the attenuation of drug release rates in the steady-state regime, we employ a PSS technique which allows c_m in Equation 1 to vary with time. First, we must replace c_m with an expression which depends on the mass remaining in the device (which we denote as m) and the geometry of the device. However m must represent the total system drug mass (core and membrane):

$$m = M_{core} + M_{eq} = \pi l c_{in} \left(\frac{r_o^2 - r_i^2}{2 \ln\left(\frac{r_o}{r_i}\right)} \right) \quad (7)$$

Solving Equation 7 for c_{in} and substituting into Equation 1 yields a simple ODE, although we must first replace dM/dt , which represents the rate of mass being released from the system, with the rate of mass loss from the system (dm/dt , equal to $-dM/dt$):

$$\frac{dm}{dt} = -am \quad a = \frac{4D}{r_o^2 - r_i^2} \quad (8)$$

Solving the ODE, applying the initial condition $c=c_0$ at t_b gives an expression for the mass remaining in the steady-state-regime. Taking a time-derivative and applying the negative sign we obtain an expression for attenuated release rates as a function of time in the steady-state regime:

$$\frac{dM}{dt} = \frac{2\pi l D c_0}{\ln\left(\frac{r_o}{r_i}\right)} e^{-a(t-t_b)} \quad (9)$$

Equation 9 can be integrated to obtain cumulative release in the steady-state regime:

$$M(t) = M_b + \frac{2\pi l D c_0}{a \ln\left(\frac{r_o}{r_i}\right)} \left(1 - e^{-a(t-t_b)} \right) \quad (10)$$

We now have a simple exponential time constant (a) to describe release rate attenuation. A PSS reservoir model was previously described for cylinders [40], but was complicated by consideration

of axial release from the device, and did not consider the error in the depletion of drug from the outer membrane.

Complete two stage drug release model. We now have a complete, piece-wise description of cumulative drug release from the LNG segment, depending only on drug-polymer diffusivity in the RCM and device geometry:

$$M(t) = 4r_o l c_0 \sqrt{\pi D t} \quad t < t_b \quad (11a)$$

$$M(t) = M_b + \frac{2\pi l D c_0}{a \ln\left(\frac{r_o}{r_i}\right)} \left(1 - e^{-a(t-t_b)}\right) \quad t \geq t_b \quad (11b)$$

as described previously [26], daily release rates then are readily computed by subtraction. It should be noted that, as Equation 2 is a first-term approximation valid only at early times for a matrix device, Equation 11 will lose accuracy for proportionally thicker RCM (lower values of r_i/r_o). This is further discussed in the Supporting Information (File S1).

Materials and Methods

Materials

Aliphatic polyether urethanes Tecoflex EG-85A, Tecoflex EG-60D, Tecoflex EG-65D, Tecoflex EG-100A and the hydrophilic Tecophilic HP-100A-60 were purchased from Lubrizol Advanced Materials (Wickliffe, Ohio). Additionally, PEU-1 (73A-77A shore hardness), PEU-2 (59D shore hardness) and HPEU-35 (78A shore hardness, 37% equilibrium water absorption) were provided by DSM-PTG (now a subsidiary of DSM Biomedical, Berkeley, California). TFV was provided by Gilead Sciences (Foster City, California), and micronized LNG was obtained from Industriale Chemica (Saronno, Italy) or Haorui Pharma-Chem Inc. (Edison, New Jersey). USP grade glycerol was purchased from Spectrum Chemicals and Laboratory Products (New Brunswick, New Jersey). Solutol HS 15 was obtained from BASF (Florham Park, New Jersey). All water used was either USP grade or double deionized (DDI) through an 18 mΩ*cm filtration system. All other solvents were HPLC or ACS grade unless noted.

LNG and TFV quantification by HPLC analysis

TFV and LNG quantification were performed using a 1200 Series HPLC (Agilent Technologies, Santa Clara, California) equipped with a diode array detector. TFV was quantified in *in vitro* release samples by a 15-minute gradient method described previously [25,26]. Various HPLC methods were used to quantify LNG in unknown samples. In all cases a Zorbax ODS 4.6×250 mm, 5 μm column was used and LNG was quantified at 240 nm. For drug extraction samples a 5 minute isocratic run of 20:80 (v/v) DDI H₂O:acetonitrile (ACN) was used, whereas a gradient method was used to quantify LNG in *in vitro* release samples. A longer gradient method was used to quantify LNG in samples containing both TFV and LNG due to interference from TFV elution. Both gradient methods are described in detail in the Supporting Information (see Tables S2 and S3 in File S1).

Dissolution testing of matrix devices to determine LNG-PEU diffusivities

Drug-polymer effective diffusivity was determined using matrix-type PEU segments to aid in the design of the LNG segment and evaluation of RCM polymers. LNG was compounded by roll-coating and hot melt extrusion in each polymer using a Haake

Minilab extruder (Thermo Scientific, Tewksbury, Massachusetts) to an approximate final diameter of 5 mm. Next, 2 mm length segments were excised from the extrudate batch and subjected to the extraction method below to determine the LNG loading for each batch. Segments approximately 15 mm in length were then cut and end-capped as described previously [27]. Before capping, the exact length and diameter of each segment were measured with digital calipers and the exact mass of each segment was measured with an analytical balance. Segments were subjected to release testing in sodium acetate buffer (pH 4.2) with 2% Solutol HS 15 [30] for 7 days at either 23°C, 37°C or 50°C. Aliquots of release media were collected daily and analyzed by HPLC. Daily release data were summed sequentially to determine cumulative release, which was normalized to the initial LNG mass in each segment. Linear regressions of cumulative data against the square-root-of-time were performed from day 3 to day 7 (some non-linearity was observed on days 1 and 2).

As discussed above, diffusion-controlled release from a cylindrical matrix device wherein the drug is completely dissolved and axial transport can be neglected can be approximated by a simple relation at early-times (Equation 2). If the expected linearity of fractional cumulative release (M/M_0) against the square-root-of-time is observed experimentally, Equation 1 can be re-arranged to estimate the effective diffusivity:

$$D = \frac{\pi k^2 r_o^2}{16} \quad (12)$$

where r_o is the cross-sectional radius of the device and k is the slope of the linear regression of fractional cumulative release against the square-root-of-time.

LNG Segment and IVR fabrication

A diagram detailing the TFV/LNG IVR manufacturing scheme is shown in the Supporting Information (Figure S3 in File S1). To fabricate LNG reservoir segments, LNG was first dissolved in either PEU-1 or EG-85A by hot-melt extrusion. PEU-1/EG-85A pellets were roll-coated with LNG powder (up to 2% w/w) and flood-fed into a KETSE 12/36 twin-screw extruder (TSE) (C.W. Brabender, South Hackensack, New Jersey) and cut using a Micropelletizer (Randcastle Extrusion Systems Inc., Cedar Grove, New Jersey). The pelletized extrudate was then subjected to extractions and HPLC analysis to determine drug content as described below. In some cases, LNG-loaded pellets were then mixed with placebo pellets to the desired average LNG loading (~1.3% w/w). LNG-containing reservoir strands were then fabricated by co-axial extrusion. The TSE was connected to a 3/4" single screw extruder (SSE) w/advanced torque rheometer drive (C.W. Brabender) at a 90° angle using a custom-designed mandrel crosshead (Guill Tool, West Warwick, Rhode Island). The LNG-loaded pellet mixture was starve-fed gravimetrically into the TSE using a KCL-24-KQx4 loss-in-weight feeder (K-Tron, Pitman, New Jersey) while PEU-2 or EG-65D pellets were flood fed into the SSE to form an outer rate controlling membrane (RCM) around the LNG-loaded PEU core. In some studies, EG-60D was used as an RCM polymer in place of EG-65D. The coated extrudate was passed through a water trough followed by cold air drying using an Air Wipe cooling ring connected to a Adjustable Spot Cooler vortexing tube (Exair, Cincinnati, Ohio) and fed to a conveyor belt, from which coaxial strands approximately 2–3 feet in length were manually cut. The feed rate of PEU-1, the SSE screw speed and the conveying speed were modulated to form a cylindrical reservoir extrudate with target dimensions of 5.5 mm outer diameter and 5.3 mm inner diameter

(0.1 mm RCM thickness). In some experiments the RCM thickness was varied between 0.05 and 0.15 mm. To facilitate LNG diffusion into the RCM, thus mitigating the lag-times required to achieve steady-state release, strands were treated for 14 days at 40°C/75%RH prior to end-capping. In some cases heat treatment was varied between 4 and 76 days at 40°C/75%RH to assess the kinetic effects on lag/burst behavior during drug release. If segments were fabricated for inclusion in full TFV/LNG IVR, heat treatment was performed on the full IVR instead of the parent co-axial strand as described below. Segments of either 10 or 20 mm length were cut from their parent strands. A process flow diagram for LNG-loading co-axial extrusion is presented in the Supporting Information (Figure S4 in File S1). Exact lengths and diameters of LNG segments were measured by a digital caliper or thickness gage. Exact RCM thicknesses were determined by cutting thin slices of co-axial strand (either throughout the batch or proximal to individual samples) and imaging by bright field microscopy (Figure 1F). Four measurements per cross-section were taken using cellSens Standard software (Olympus, Center Valley, Pennsylvania) and averaged to determine a representative thickness for a given sample or batch. To prevent significant leakage of LNG into the TFV segment, LNG-loaded segments were end-capped with 2 mm length, 5.5 mm diameter EG-65D or PEU-2 caps using an HPS-EM induction welding system (PlasticWeld Systems, Inc., Newfane, NY). End-caps were cut from circular 5.5 mm EG-65D strands extruded using the SSE.

End-sealed TFV segments were fabricated by filling hollow hot-melt extruded HPEU-35 or HP-100A-60 tubes (5.5 mm outer diameter, 4.2 mm inner diameter, 145 or 155 mm length) with 2.1 to 2.3 g TFV/glycerol/water paste (62:36:2 w/w) and end-sealing by induction welding, as described previously [25]. Component parts of the TFV/LNG IVR (filled TFV segments, LNG segments and end-caps) are shown in Figure 1G. To form TFV/LNG IVR, capped LNG segments were welded to sealed TFV segments using a HPS-20 induction welding system with a split-die configuration (PlasticWeld Systems, Inc., Newfane, NY). TFV segments with 131 and 141 mm lengths (post-sealing) were paired with the capped 20 and 10 mm LNG segments, respectively, to form IVR with 55 mm outer ring diameter (Figure 1D). To form a more circular ring shape, IVR were annealed in custom-fabricated aluminum molds for approximately 15 minutes at 65°C. IVR were heat-treated for 14 days at 40°C/75%RH in sealed aluminum pouches prior to *in vitro* release testing.

Prior to any melt processing, all PEU or HPEU resins were dried overnight in a CAFM series compressed air dryer (Dri-Air, East Windsor, Connecticut) to less than 0.05% H₂O (w/w) as determined using a C30 Coulometric Karl Fischer Titrator (Mettler-Toledo, Columbus, Ohio).

Drug extractions to estimate LNG content and *in vivo* release

LNG was extracted from polymer segments to determine the LNG loading in each batch of co-axial extrudate. Several 2 mm long pieces were cut from various locations throughout the batch. Each piece was placed in a 5 mL volumetric flask, which was filled with 3 mL dichloromethane (DCM). Flasks were agitated on a High Capacity Mixer (Glas-Col, Terre Haute, Indiana) overnight to dissolve the PEU and LNG. Following dissolution, flasks were filled to volume with DCM. Flasks inverted several times to ensure good mixing. To precipitate PEU from the solution, 1.00 mL of the DCM solution was transferred to a 10 mL volumetric flask using a calibrated glass syringe. The 10 mL flask was then filled to volume with acetonitrile (ACN) and vortexed for 5 seconds. Aliquots of the resulting supernatants were then passed through a

0.2 µm PTFE syringe filter into HPLC vials for analysis. The same extraction procedure was also performed on 50 mg samples of LNG-loaded PEU-1/EG-85A pellets to assess the drug loading prior to co-axial extrusion.

The same procedure was also used to determine the average LNG mass loaded per device used in the rabbit PK study (see methods below), except that a 25 mL volumetric flask was used in place of a 5 mL flask for the first dissolution step. When full segments with end-caps were extracted, it was necessary to further cut the segment into 2–3 mm pieces before dissolution. These extractions were also performed after *in vivo* testing to estimate average LNG release rates.

In vitro release testing of LNG segments and TFV/LNG IVR

LNG-containing PEU segments and TFV/LNG IVR were subjected to *in vitro* drug release testing. Samples were immersed in aqueous buffer sink for up to 90 days in 250 mL or 500 mL I-Chem glass jars (Thermo Scientific, Rockwood, Tennessee) in an incubated shaker cabinet set to 37°C and 80 rpm. Media were changed daily and media volumes were adjusted throughout the studies to ensure a sufficient sink for both TFV and LNG. TFV and LNG concentrations were not allowed to exceed 20% of their solubility in the release media. Typically, 25 mM sodium acetate buffer (pH 4.2) was used as the testing media, although Gibco (Life Technologies, Carlsbad California) 1× phosphate buffered saline (pH 7.4) was used for parallel *in vitro* release studies in the rabbit PK study to approximate the neutral vaginal pH typically observed in rabbits. Aliquots of release media were collected 23–25 hours from the previous media change and analyzed by HPLC at several points throughout each study to determine daily TFV and LNG release rates. To assess the validity of the model presented above, release rate profiles were compared to predictions from Equation 11. Some TFV/LNG IVR were also evaluate at an 200 rpm shaking speed to assess the adequacy of the standard 80 rpm in maintaining sink conditions. For *in vitro-in vivo* comparison, numerical integrations of *in vitro* release profiles were performed by trapezoidal approximation to generate time-averaged release rates.

Evaluation of LNG containment by PEU end-caps

To evaluate the potential effectiveness of PEU end-caps in preventing LNG transport into the TFV segment, the full TFV/LNG IVR was rendered in COMSOL Multiphysics 4 and Fickian diffusion simulations were performed using the “Transport of Diluted Species” package. A diffusivity of 7.3×10^{-11} cm²/s was applied to the RCM and end-cap compartments based on an experimental measurement of LNG diffusivity in PEU-2. An LNG diffusivity of 3.0×10^{-9} cm²/s was applied to the core compartment and the tubing compartment of the TFV segment representing a typical softer PEU at 37°C (see Table 1), as the exact diffusivity in these compartments should not affect diffusion provided that the value is sufficiently high in the core for LNG to be well-mixed and sufficiently high in the tubing wall so that it acts as a sink. End-cap lengths of 1, 2 and 3 mm were evaluated, while the LNG segment length was fixed at 20 mm and the overall dimensions were fixed at 5.5×55 mm (cross-sectional and outer ring diameters). The RCM thickness was set to 100 µm, and was not loaded with LNG. An initial LNG loading of 42 mol/m³ (~1.3%w/w, assuming a matrix density of 1.05 g/cm³), was applied to the core compartment. A free tetrahedral mesh was applied throughout the IVR, with higher node resolution in and near the RCM and near the segment/end-cap interface. Time-dependent effective diffusivity simulations, governed solely by Fick’s 2nd Law, were carried out for approximately 5 years.

Table 1. Measured LNG effective diffusivities for various PEUs, calculated using Equation 12. Data represents N between 3 and 8, mean \pm SD.

Polymer	LNG Effective Diffusivity ($\text{cm}^2/\text{s} \times 10^{-10}$)
Tecoflex EG-85A	47 \pm 3
Tecoflex EG-100A	2.0 \pm 0.1
Tecoflex EG-60D	1.1 \pm 0.1
Tecoflex EG-65D	0.51 \pm 0.06
PEU-1	17 \pm 3
PEU-2	0.78 \pm 0.06

doi:10.1371/journal.pone.0088509.t001

Volume integrals of the end-cap and TFV segment compartments were performed every 7 days for the duration of the model and normalized to the initial mass of LNG loaded in the system.

To experimentally validate the model presented above, TFV/LNG IVR (HPEU-35/PEU-1/PEU-2) were stored at 40°C for either 1, 3 or 6 months. IVR stored at -80°C were used as controls. IVR were dissected, and separate LNG extractions, as described above, were performed on the end-caps and TFV plug sections (first ~5 mm of the TFV segment on either side of the LNG segment). As can be seen in Figure 1D, it is difficult to discern where the exact cap/segment interface is on the final IVR. Masses of the dissected LNG segments were compared to the initial segment mass before end-capping, and an adjustment was made to the LNG mass extracted from the end-caps based on the segment mass discrepancy and the initial LNG loading of the coaxial extrudate batch.

Extension testing of TFV/LNG IVR

To assess mechanical robustness of the TFV/LNG IVR before and after 31 day *in vitro* release testing, we performed destructive extension tests to determine the tensile load and resulting extension required to cause joint failure. IVR were tested using an Instron 3342 with 500 N load cell and O-ring testing apparatus with Bluehill Lite software control (Instron, Norwood, Massachusetts). IVR were placed on the testing apparatus with the LNG segment oriented vertically and stretched at a rate of 5 mm/s until failure was observed, at which point the net extension and net load were recorded. The failure type of each IVR was also recorded.

Pharmacokinetic testing of LNG-loaded segments in rabbits

Both 10 mm and 20 mm end-capped LNG-loaded PEU-1/PEU-2 reservoir segments were implanted into New Zealand white female rabbits (age 4–8 months) to assess *in vivo* device performance and LNG pharmacokinetics. This study was carried out in accordance with the U.S. Department of Agriculture's (USDA) Animal Welfare Act (9 CFR Parts 1, 2 and 3) and the Guide for the Care and Use of Laboratory Animals of the National Institutes of Health. The protocol was approved by the Institutional Animal Care and Use Committee of MPI Research (USDA Research License Number: 34-R-0031).

Preoperative and surgical procedures were performed as described previously [41]. Briefly, LNG-loaded segments were placed in the proximal, columnar epithelial region of the vagina, such that the distal end of the segment was approximately 7 to 12 cm from the introitus. Up to three 3-0 or 5-0 Prolene sutures were used to secure the segment to the outer ventral wall. All

surgery was performed under analgesia and anesthesia, and all efforts were made to minimize suffering.

Animals weighed between 2.9 and 4.2 kg at implantation. Body weights of test subjects were recorded periodically during implantation. Groups of 6 animals were each administered either 10 or 20 mm segments, for either 28 or 90 days (4 groups total). In the 28-day groups, plasma was collected at 4 hours, 8 hours, and 1, 2, 3, 7, 14, 21 and 28 days post-implantation. In the 90-day groups, plasma was collected at 44, 60, 74 and 90 days post-implantation. Approximately 1 mL blood was drawn from the jugular vein of all animals at each time-point and stored in tubes containing tripotassium EDTA. Tubes were stored on wet ice until centrifuged under refrigeration, at which point samples were aliquoted into cryovials and stored at -50°C to -90°C until analysis could be performed. LNG was quantified in plasma samples by a validated LC-MS/MS method (described in the Supporting Information, see Tables S4 and S5 in File S1). To assess total LNG plasma exposure and device dose dependence, area under the curve (AUC) values were calculated from individual plasma data using WinNonlin Phoenix (Pharsight, St. Louis, Missouri). AUC was calculated from implantation to 28 days post-implantation (AUC₀₋₂₈) for the 28 day groups and from 44 to 90 days post-implantation for the 90-day groups (AUC₄₄₋₉₀).

All test subjects were euthanized at study's end (either day 28 or day 90) by an intravenous overdose of sodium pentobarbital solution followed by exsanguination. Approximately 500 mg of cervical tissue was collected from all animals during necropsy, snap frozen in liquid nitrogen and stored at -50°C to -90°C until LNG extractions could be performed. LNG was extracted from tissue and again quantified by a validated LC-MS/MS method (described in the Supporting Information, see Table S6 in File S1).

LNG segments were recovered post-study during necropsy. Time-averaged *in vivo* LNG release rates were estimated by subtracting the residual LNG mass recovered by extraction (method described above) from the estimated initial LNG mass loaded (batch average LNG loading multiplied by segment mass prior to end-capping), and dividing the net mass by the study duration. In addition, the average cumulative release values from the 28 day and 90 day groups were subtracted to determine the average release rate for the latter portion of the study.

Results and Discussion

LNG Diffusivity in PEUs

We measured effective diffusivities (D) for LNG in rate-controlling PEU by analyzing LNG release from cylindrical matrices and applying Equation 12. Figure 2A depicts examples of linear regressions of release against the square-root-of-time for PEU-1 and PEU-2 ($R^2 > 0.998$). Diffusivity correlated negatively with manufacturer-reported flexural modulus for Tecoflex PEUs (Figure 2B). The mechanical properties of PEU can be controlled by modulating the molar ratio of the macrodiol (e.g. poly(tetramethylene oxide)) to the chain extender (typically a monomeric diol, e.g. 1,4-butanediol) [42]. Thus, the reduced diffusivity of a dissolved molecule, like LNG, in stiffer PEU, e.g. Tecoflex EG-60D and EG-65D, is likely a result of the lower volume fraction of the amorphous soft segment domains that allow LNG transport [43]. Figure 2C depicts the effect of temperature on LNG diffusivity. Interestingly, diffusivity increased 15-fold in the higher-modulus PEU-2 between 23°C to 50°C, but only 3-fold in PEU-1. This could result from differences in phase transition behavior of the crystalline hard segments between harder and softer PEU. Table 1 contains a summary of LNG diffusivities in various PEU tested. The lower diffusivity in PEU-2 at 23°C vs. 37°C

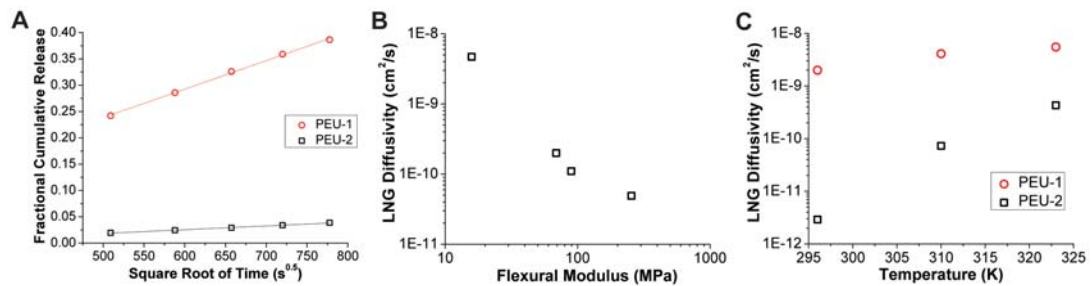


Figure 2. Determination of LNG effective diffusivities in PEU. (A) Example square-root-of-time fitting for PEU-1 and PEU-2 used to estimate LNG-PEU diffusivity values (Eqn. 12). (B) Log-log correlation between LNG diffusivity and reported flexural modulus for Tecoflex PEUs and (C) effect of temperature on LNG diffusivity in PEU-1 and PEU-2. doi:10.1371/journal.pone.0088509.g002

necessitated heat treatment to allow LNG to load into the RCM, thus eliminating the undesirable lag time required to achieve steady-state release.

Mathematical Modeling of LNG *in vitro* release

The model for drug release presented in Equation 11 proved useful in the design of the LNG reservoir segment by allowing accurate prediction of 90-day release rate profiles. Figure 3A depicts the full two-stage model (Eqn. 11) result in comparison to LNG release from PEU-1/PEU-2 segments stored at elevated temperature to homogenize LNG concentration across the device (as per the model assumption). The experimental *in vitro* release data agreed with the full two stage model ($R^2 = 0.74$) with a mean prediction error of 17%. This correlation confirmed that our diffusivity measurements in rate-controlling PEU were sufficiently accurate for release rate prediction in the device design process, allowing us to screen potential RCM polymers for LNG diffusivity using simple cylindrical matrices produced on a small-scale batch extruder.

Use of the two-stage model has a practical limitation as the burst regime of the model is only accurate when complete RCM loading is achieved. Therefore, much of the remaining *in vitro* release data presented herein does not demonstrate the full burst predicted by the model. However, as demonstrated below the latter model regime was still useful regardless of the burst magnitude. The burst mass (M_b) is then practically regarded as the maximal burst release that could be achieved from a given system.

Figures 3B and 3C depict the effects of RCM thickness and drug-polymer diffusivity on steady-state regime LNG release, predicted using Equation 11b, from 5.5 mm diameter solid reservoirs. As shown in Equation 8, the release rate time constant (a) varies with the ratio between diffusivity and RCM cross-sectional area. At a fixed diameter, diffusivity or RCM thickness are positively correlated with the magnitude of drug release, but also with the rate of drug release attenuation, as any increase in drug flux results in more rapid depletion of the core drug concentration. The burst duration (t_b , Eqn. 6), is also shown as a function of RCM thickness and diffusivity in Figures 3D and 3E. The burst duration is inversely proportional to diffusivity, while the relationship between burst duration and RCM thickness is not clear from Equation 6 as $r_o - r_i$ is not readily factored. As expected, the RCM thickness also correlates with M_b (Figure 3F). Figures 3B–3F illustrate the complex relationship between burst duration, maximal burst mass and PSS release rate profile encountered when designing reservoir systems.

In vitro release of LNG from end-capped segments

Experimentally, we evaluated the effects of several RCM design inputs on the LNG release profile, including RCM polymer selection, RCM thickness and duration of heat treatment required to load the RCM with LNG. First, effect of heat treatment was performed on segments fabricated from a LNG-loaded PEU-1 core and PEU-2 RCM by storing samples at 40°C for either 4, 14, 21, 28 and 76 days prior to *in vitro* release testing. As depicted in Figure 4A, a 14-day heat treatment mitigated both burst and lag behavior, and was thus incorporated into the manufacturing process. Furthermore, it was necessary to include a 14-day treatment at 40°C of the hydrophilic PEU used in the TFV segment (manuscript in preparation). This allowed us to reduce both procedures to a 14 day annealing of the final TFV/LNG IVR to both stabilize the TFV release rate on subsequent storage and eliminate the lag behavior in the LNG release profile [44].

Almost all reservoir devices will exhibit a drug burst that increases with time as drug is allowed to diffuse into the RCM. This phenomenon is acceptable if the amount of burst release does not result in unsafe drug levels. LNG is given orally as an emergency contraceptive at 1500 μg in a single dose, and our maximum predicted burst (M_b) is over an order of magnitude lower than this dose as shown in Figure 4D. Furthermore, a range of release rates may be acceptable early in the release profile, provided that the eventually PSS release rate in the reservoir-stage is consistent and is consistently efficacious. If highly reproducible burst release profiles are required for other drugs, it may be necessary to manufacture devices with uniform concentration in both compartments to ensure a kinetically stable release profile during storage, either by compounding the drug in both polymers before co-axial extrusion, or by extended heat treatment. This was initially avoided to mitigate the potential for surface re-crystallization. However, in a recent stability study we discovered that LNG does not re-crystallize on the surface of the TFV/LNG IVR (to be reported in an upcoming manuscript).

Next, we evaluated the release of LNG from reservoir segments fabricated with an 1.3% (w/w) LNG-loaded EG-85A core and varying thickness of either EG-65D or EG-60D RCM (Figures 4B and 4C) (all samples heat-treated for 14 days at 40°C). Based on these data and the diffusion model, we selected an 80–85 μm thick EG-65D RCM to target 20 $\mu\text{g}/\text{day}$ release on day 45 (the middle of the delivery profile), while also minimizing release rate attenuation throughout the reservoir-stage. The batch with the closest RCM (84 μm EG-65D) was tested for a full 90 days and compared to the model in the steady-state regime (Figure 4D). The reservoir-stage model (Equation 11b) and experimental data

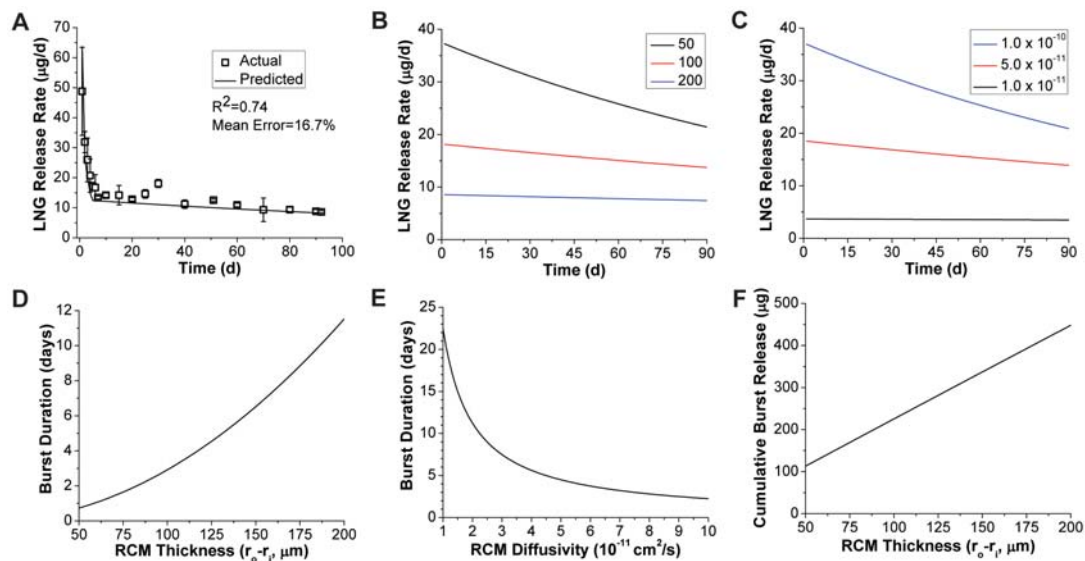


Figure 3. Model for dissolved drug release from cylindrical reservoirs. (A) Accuracy of the two stage drug release model (Eqn. 11) for LNG segments stored 76 days at 40°C to completely equilibrate LNG loading throughout the cross-section. Experimental data represent N=3, mean \pm SD. Effects of (B) EG-65D RCM thickness (in μm) and (C) diffusivity (in cm^2/s) on the reservoir-stage model (Eqn. 11b) for 20 mm length segments with 5.5 mm diameter. Effects of (D) PEU-2 RCM thickness, and (E) diffusivity on the burst duration (t_b) predicted by Equation 6. For panels C and E RCM thickness was fixed at 100 μm . (F) Maximal burst amount (M_b) shown as a function of RCM thickness. doi:10.1371/journal.pone.0088509.g003

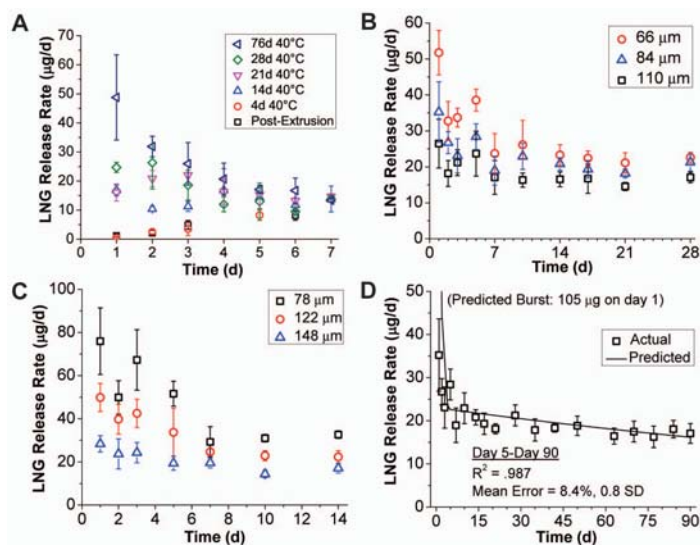


Figure 4. *In vitro* release of LNG from reservoir segments. (A) Effect of partial LNG loadings in the RCM on lag/burst behavior in LNG *in vitro* release kinetics for 10 mm length PEU-1/PEU-2 segments, achieved by 40°C storage for varying duration. *In vitro* LNG release from 20 mm length, 5.5 mm diameter co-axially extruded EG-85A segments with (B) EG-65D or (C) EG-60D RCMs of various thicknesses. (D) Full 90 day *in vitro* release kinetics from the 84 μm EG-65D RCM group with model comparison (Eqn. 11). All data represent N=5, mean \pm SD except panel A (N=3). Segments in panels B–D were all stored for 14 days at 40°C before testing. doi:10.1371/journal.pone.0088509.g004

exhibited excellent correlation ($R^2 = 0.987$ from day 5 to day 90), with mean error of 8.4%, or 0.8 experimental standard deviations.

In vitro release of TFV and LNG from full two-segment IVR

In vitro release of TFV and LNG from full IVR for 90 days is shown in Figures 5A and 5B. From day 2 to day 90, IVRs released TFV and LNG at near-constant rates of approximately 7.5 ± 0.1 mg TFV and 21 ± 2 μ g LNG per day ($N = 5$ time-averaged IVRs, mean \pm SD), a significant achievement given the disparity in drug properties and release rates.

Based on our recent sheep study comparing pharmacokinetics of the TFV-only IVR (similar *in vitro* release rate) and the TFV 1% gel [25], we hypothesize that a device with this constant TFV dose may protect women against HIV transmission. Also, based on previous data from the WHO silicone LNG IVR [24], we hypothesize that these LNG release rates can provide effective contraception. Given our understanding of how to predict release rates from this system, as well as the adaptability of the segmented IVR design, the release rates of TFV and LNG could be modified should human PK testing suggest different doses are needed.

TFV/LNG IVR evaluated at an increased shaking speed of 200 rpm released 23 ± 1 μ g LNG per day over 14 days ($N = 3$ time-averaged IVRs, mean \pm SD), compared to 20 ± 2 μ g LNG per day at 80 rpm ($N = 5$). This comparison suggests that an 80 rpm shake speed sufficiently disrupts the unstirred layer, resulting in sink conditions appropriate for the model presented in Equation 11.

Prevention of LNG diffusion between segments with PEU end-caps

One of the design challenges with developing multi-segment drug delivery systems is the potential for drug diffusion between compartments during storage of the drug product. While diffusion of TFV from the hollow core compartment is hindered by its poor solubility in HPEU [26], LNG diffuses effectively through PEU and thus its “leakage” into the TFV segment is expected. Therefore, we designed end-caps to prevent LNG diffusion into the TFV segment to maintain both LNG release rate magnitude and control in the TFV/LNG IVR following product storage. We evaluated the feasibility of using end-caps made from the same polymers as the LNG-segment RCM (PEU-2 and 65D), but aimed to minimize the end-cap length due to their mechanical rigidity (EG-65D has a flexural modulus of 255 MPa) and the fact that a large cap would eliminate additional length from the TFV

segment. We modeled the complex multi-compartment nature of the problem by rendering a full TFV/LNG IVR performing finite-element simulations of Fickian diffusion (Figures 6A–B). Simulations were carried out for 5 years at 37°C, rather than the usual 40°C, due to availability of drug-polymer diffusivities at 37°C from studies presented above. Volume integrals were performed in both the end-cap and TFV segment compartments and normalized to the initial drug load in the 20 mm LNG segment. As depicted in Figures 6C and 6D, the 1 mm, 2 mm and 3 mm end-cap simulations predicted full LNG containment (no LNG in the TFV segment) for 203, 749 and 1484 days at 37°C, respectively. The 2 mm cap configuration ultimately was chosen because complete LNG containment was achieved in the model for 2 years at 37°C, at which time only 6% of the total LNG load had escaped into the end-caps. In Figure 6D, we show that the subsequent leakage into the whole TFV segment, proceeds at a linear but minimal rate (approximately 1% of total LNG load per year for 2 mm caps), suggesting that performance and chemical stability (depending on the quantitative metric used) may be achieved for much longer than 2 years in the 2 mm configuration. The end-caps also function as RCM, where thickness can modulate LNG flux at the TFV/LNG segment interface through the concentration gradient across the segment. Encouragingly, EG-65D (used in our current lead design) exhibits even lower LNG diffusivity than PEU-2 (Table 1), likely lengthening complete containment times from those observed in these simulations.

In an attempt to experimentally approximate the diffusion simulations, TFV/LNG IVR were stored for 6 months at 40°C and the caps and TFV segment plugs were subjected to LNG extractions at various times. The results are shown in Figure 6E. Reasonable agreement was observed between the theoretical and experimental LNG content in the caps, even with the temperature disparity (37°C to 40°C from model to experiment). Trace amounts of LNG (< 5 μ g total or $< 0.1\%$ of total load) were detected in the TFV segment plugs, but this likely was not due to leakage through the end-caps as no increase was observed in LNG levels over time.

An “ideal” multi-segment IVR would be thermodynamically stabilized by caps formed from a material miscible with the polymers used and impermeable to all components in the formulation. Here we have demonstrated a practical, kinetically-stabilized system using a material already present in the IVR.

IVR extension testing

Mechanical integrity is an important design consideration for any IVR. In this particular IVR design, we were faced with the

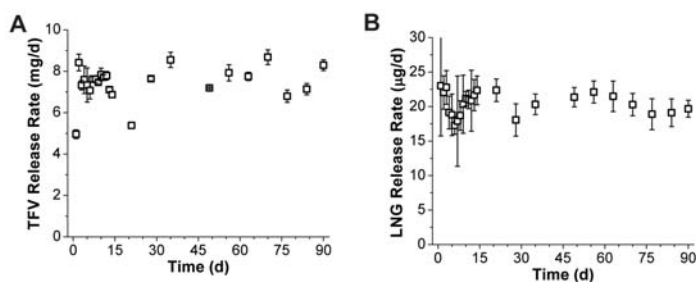


Figure 5. *In vitro* release of TFV and LNG from full two-segment IVR. *In vitro* release of (A) TFV and (B) LNG for 90 days from final TFV/LNG (20 mm) IVR prototypes using Tecophilic and Tecoflex polymers (HP-100A-60 TFV reservoir tube, EG-85A LNG reservoir core and EG-65D LNG reservoir RCM and end-caps). LNG reservoir RCM thicknesses were measured between 74 and 85 μ m. All data represent $N = 5$, mean \pm SD. doi:10.1371/journal.pone.0088509.g005

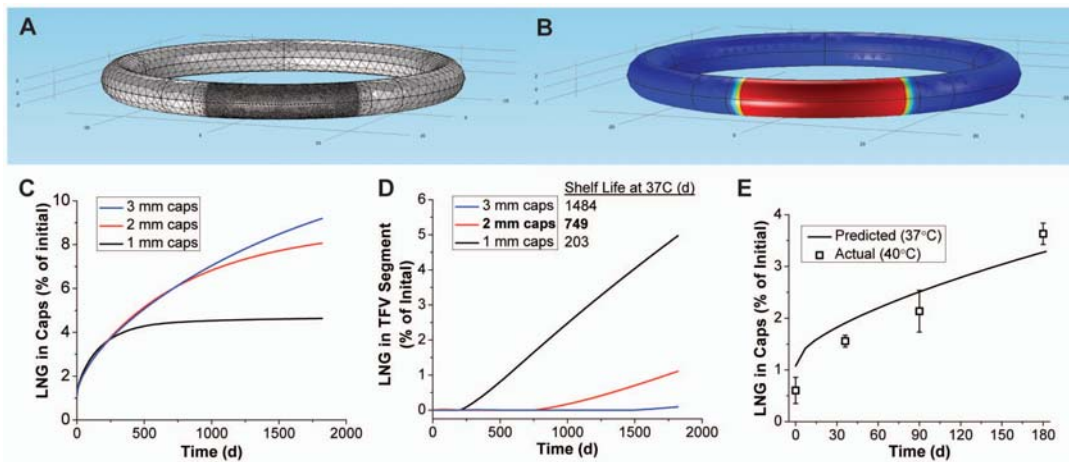


Figure 6. Prevention of LNG diffusion between segments by PEU end-caps. An example (A) finite-element mesh and (B) outer surface model result from the IVR storage diffusion model. The model result represents approximately 2 years storage at 37°C for an IVR with 2 mm length PEU-2 end-caps, where red represents maximum scaled LNG concentration, and blue represents zero LNG. Quantitative results show LNG leakage into the (C) end-caps and (D) entire hollow-tube in the TFV segment during storage by volume integrals of the COMSOL model. Shelf life was determined as the last time-point of complete LNG containment (none detected in the TFV segment). (E) Experimental determination of LNG loss into the caps as a function of TFV/LNG IVR (PEU-1/PEU-2 LNG segments) storage time at 40°C and comparison to the COMSOL result for 37°C storage. doi:10.1371/journal.pone.0088509.g006

additional challenge of welding swellable HPEU (TFV segment) to rigid, non-swellable PEU (capped LNG segments) while maintaining mechanical integrity both in dry and hydrated ring states. To evaluate this, we performed O-ring extension tests (Figures 7A and 7B) on full IVR after production (dry) and subsequent 31 day *in vitro* release testing (hydrated). As shown in Figures 7C and 7D, all IVR (N=15) in the dry group endured at least 190 mm extension and 250 N (56.2 lbf) load before failure, and 9 of the 15 rings remained intact following extension to the limit of our instrument (approximately 330 mm deformation). IVR in the wet group exhibited extension and tensile load of 141 ± 47 mm and 239 ± 58 N (N=15, mean \pm SD) at failure, with all IVRs enduring at least 74 mm extension and 152 N (34.2 lbf) tensile load before failure. Thus, a reduction in joint integrity was observed when IVR were soaked in aqueous media, however these data demonstrate that the IVR are still mechanically sound and would require intentional and excessive user-applied stress to separate the segments. In the dry group, all observed failures (6 of 15) occurred between the cap and the LNG segment, whereas, in the hydrated group, an equal number of joint failures occurred between the cap and the LNG solid reservoir versus the cap and the TFV tube plug (7 of each). The remaining hydrated ring experienced a HPEU tubing rupture near the tube seal, but at the highest observed load at failure in the hydrated group (354 N/79.6 lbf). Given the mismatch in the HPEU tube, which exhibits 58% equilibrium swelling by mass, and the non-swellable PEU assembly (caps and LNG reservoir), the mechanical joint integrity observed in dry and hydrated IVR is remarkable and illustrates the utility of the PEU/HPEU platform in sophisticated drug delivery systems.

PK testing of the LNG segment in rabbits

Results from the rabbit pharmacokinetic study are shown in Figure 8. Figure 8A depicts *in vitro* LNG release rates from the same batch used in the rabbit study. On average, 10 and 20 mm segments released 12.6 and 26.4 μg LNG per day *in vitro*,

respectively, over the 90 day study. Segments consistently released more LNG *in vivo* than *in vitro* as shown in Figure 8B. Release rates were higher *in vivo* for both the 10 and 20 mm segment groups, however this disparity was diminished in the 90-day group with respect to the 28-day group. In fact, when subtracting the average *in vivo* cumulative LNG release of the 28-day group from the 90-day group, the result was very similar to the time-averaged *in vitro* release rate in both groups (10 mm: 13.5 *in vivo* vs. 12.0 $\mu\text{g}/\text{day}$ *in vitro*, 20 mm: 24.0 *in vivo* vs. 25.3 $\mu\text{g}/\text{day}$ *in vitro*). This indicates that a higher burst release of LNG occurred *in vivo* than *in vitro*, but that the eventual steady-state regime profile was nearly identical. In all cases, average release rates varied nearly two-fold *in vivo* between the 10 mm and 20 mm segment groups.

LNG plasma results, presented in Figure 8C, strengthened the observation of an additional burst not detected *in vitro*. An approximately 3-fold drop was observed in plasma LNG concentration from the 4 hour to the 7 day time point, while levels remained relatively stable from day 7 to day 28. Plasma levels also dropped markedly from day 28 to day 44 (25% in the 10 mm group and 37% in the 20 mm group), but this may be due to anatomical differences in the two animal groups as plasma was collected from the 28 day group for the first 28 days, and from the 90 day group from day 44 to day 90. Comparatively, plasma levels stabilized from day 44 onward. It is worth noting that test subject body masses increased 14% and 16% over 90 days in the 10 mm and 20 mm test groups, respectively. This may have caused additional attenuation of plasma profiles not expected from the *in vitro* release rate profiles alone. Mean plasma AUC_{0-28} values of 110421 and 218315 $\text{pg}^*\text{hr}/\text{mL}$ (ratio: 1.98) and AUC_{44-90} values of 154726 and 261354 $\text{pg}^*\text{hr}/\text{mL}$ (ratio: 1.69) were calculated for the 10 mm and 20 mm segment groups, respectively, indicating a dose dependent pharmacokinetic response. This and the agreement of *in vitro* and *in vivo* release rates between day 28 and day 90 suggest that sink conditions exist for LNG *in vivo*, allowing for

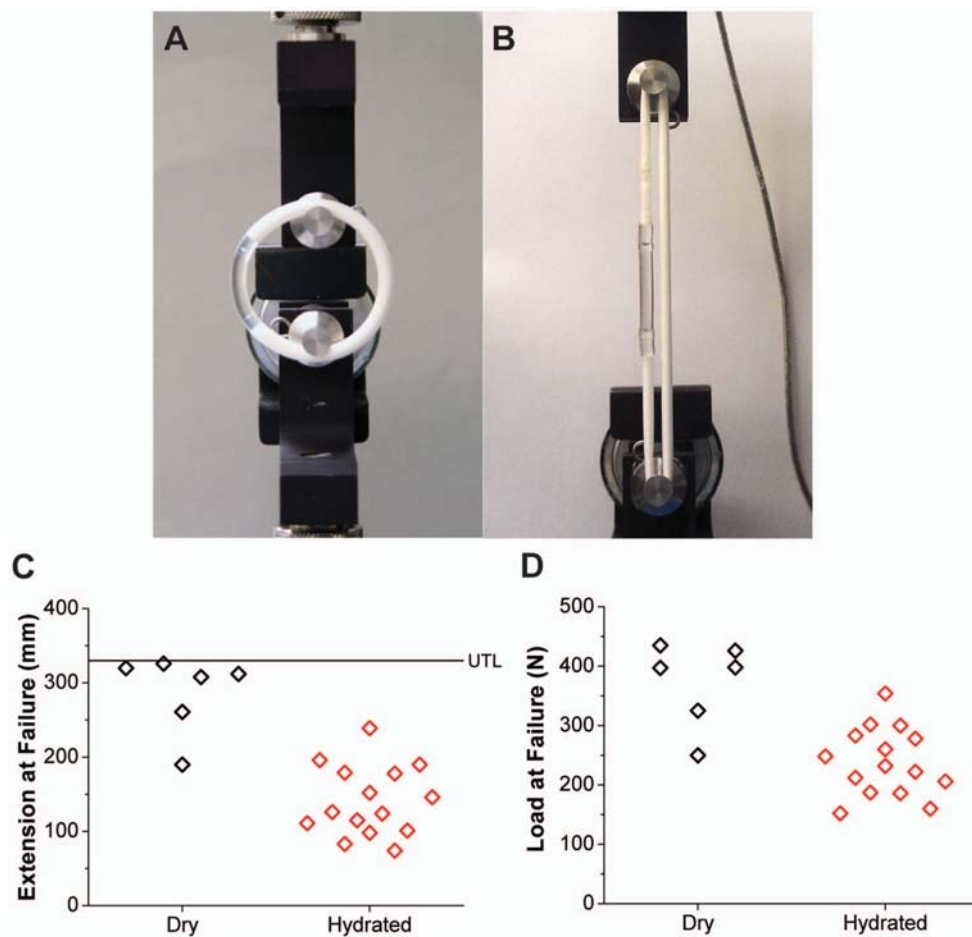


Figure 7. IVR extension testing. (A,B) Extension testing of a full TFV/LNG IVR to 101 mm extension and 145 N (32.6 lbf) load. (C) Extension and (D) load at TFV/LNG IVR both before (“dry”) and after (“hydrated”) 31 day *in vitro* release testing (N = 15 IVR per group). Nine of the 15 IVR in the dry group did not fail below the upper test limit (UTL, ~330 mm extension). doi:10.1371/journal.pone.0088509.g007

direct control of LNG pharmacokinetics through polymer selection and device geometry.

Since topical microdose progestin contraception is achieved largely through local effects [45], the pharmacokinetic profile of LNG concentration in the cervical tissue are a potentially more important predictor of eventual device performance. Figure 8D depicts LNG concentrations in cervical tissues collected at day 28 or day 90. Some samples in the 10 mm groups were below the limit of quantification (0.75 ng LNG/g tissue), which hindered a detailed analysis of the data. However, the median value differed two-fold between the 10 and 20 mm groups on day 28 (4.01 vs. 2.02 ng/g), providing further evidence of dose-dependent PK. Also, LNG levels did not differ significantly between tissues taken on day 28 or day 90 ($p = 0.10$, two-tailed, heteroscedastic t-test), confirming near-zero-order LNG release *in vivo* following the burst.

The rabbit model is useful for early *in vivo* testing of vaginal delivery systems [27,41], although rabbit vaginal histology varies

greatly from that of the human vaginal vault. Furthermore, the exact magnitude of the plasma profile is likely of little significance as LNG pharmacokinetics will vary between species [46]. However, this study confirmed that near zero-order behavior was achieved *in vivo* following the burst period, and that two biologically distinct LNG doses were in fact achieved from the 10 mm and 20 mm length devices.

Conclusions

Multi-purpose drug delivery systems will need to deliver a physically and chemically diverse set of molecules to target an equally diverse set of indications. Accordingly, there is a need for polymeric materials with a range of properties that are equally chemically diverse. Through successful use of HPEU and PEU in the same device, we have demonstrated that biomedical polyurethanes have potential to fulfill this need for many multi-functional IVR formulations. We have described the design and engineering

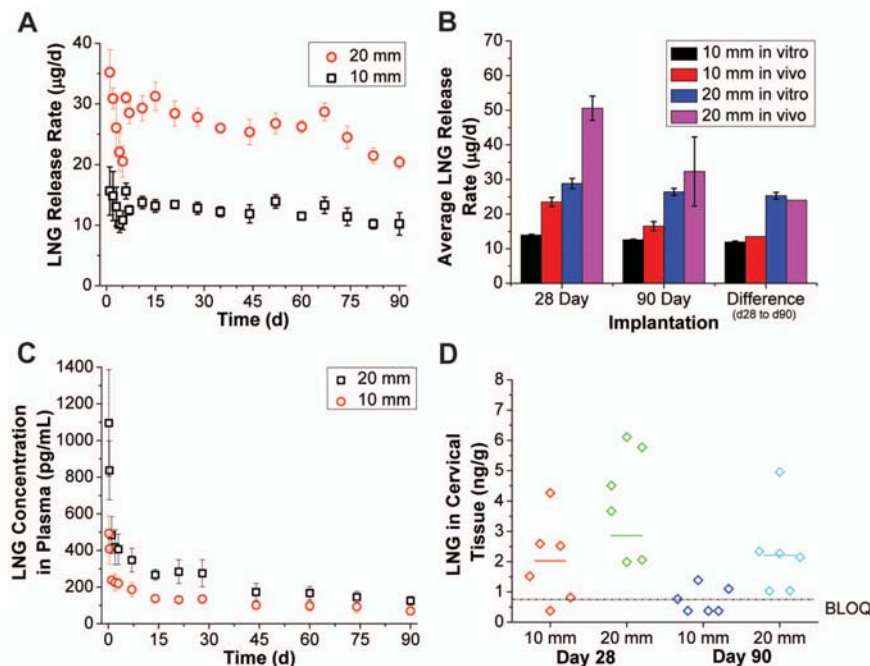


Figure 8. LNG pharmacokinetics in a rabbit model. Pharmacokinetic (PK) testing of end-capped 10 or 20 mm PEU-1/PEU-2 LNG segments in New Zealand white rabbits. (A) Parallel *in vitro* release data for the same LNG segment lot used in the study and (B) comparison with *in vivo* data for the 28 and 90 day study groups. A subtraction of the mean LNG recovery between study groups was performed to directly compare *in vitro* and *in vivo* behavior from day 28 to day 90. (C) Plasma LNG levels measured during the rabbit PK study for 10 and 20 mm LNG segment implantations. (D) Individual and median (bar) LNG levels determined from extractions of cervical tissue. Some samples in the 10 mm study groups were below quantification (BLOQ: <0.750 ng LNG per g tissue). BLOQ data points are graphed as LOQ/2 (0.375 ng/g). *In vitro* data represents N=5, mean \pm SD and *in vivo* data represents N=6, mean \pm SD (except for the *in vivo* "difference" data points, which are subtractions of mean values). doi:10.1371/journal.pone.0088509.g008

of a two-segment, dual-reservoir TFV/LNG IVR, with focus on the LNG segment, its incorporation into the full device, and the evaluation of its performance using a combination of *in silico*, *in vitro* and *in vivo* methodologies. Our two-stage, mechanistic drug release model provides an improvement to existing models of cylindrical reservoirs with dissolved drug in the literature and enabled the rational design of the long duration LNG segment. We demonstrated the near-zero-order release of LNG at clinically relevant levels both *in vitro* and *in vivo*. We have also presented design challenges specific to this system, including the prevention of drug diffusion between compartments during long-term storage. Through extension testing we have shown the IVR to be mechanically sound in both the dry and hydrated states. This IVR is the first long-acting multifunctional drug delivery system in clinical development and may prove to be an important advancement for women to control their reproductive health. The co-delivery of two drugs as physicochemically diverse as TFV and LNG and at such different release rates, sustained for 90 days, demonstrates the adaptability of this dual-reservoir polyurethane

technology. The platform is easily configured to deliver other drugs [12] and a wide range of doses or combinations for other women's health challenges.

Supporting Information

File S1 Supporting Information.
(DOCX)

Acknowledgments

The rabbit PK study and bioanalysis were performed at MPI Research Inc. under the supervision of M. Melissa Peet and Devon Kyle.

Author Contributions

Conceived and designed the experiments: JTC MRC TJJ DRF PFK. Performed the experiments: JTC NBS TJJ EMS AKA JSN JF. Analyzed the data: JTC MRC PFK. Wrote the paper: JTC MRC PFK.

References

- Folkers GK, Fauci AS (2010) Controlling and ultimately ending the HIV/AIDS pandemic: a feasible goal. *JAMA* 304: 350–351.
- Baeten JM, Donnell D, Ndase P, Mugo NR, Campbell JD, et al. (2012) Antiretroviral prophylaxis for HIV prevention in heterosexual men and women. *N Engl J Med* 367: 399–410.
- Abdool Karim Q, Abdool Karim SS, Frohlich JA, Grobler AC, Baxter C, et al. (2010) Effectiveness and Safety of Tenofovir Gel, an Antiretroviral Microbicide, for the Prevention of HIV Infection in Women. *Science* 329: 1168–1174.
- Marrazzo J, Ramjee G, Nair G, Palanee T, Mkhize B, et al. (2013) Pre-exposure Prophylaxis for HIV in Women: Daily Oral Tenofovir, Oral Tenofovir/

- Emtricitabine, or Vaginal Tenofovir Gel in the VOICE Study (MTN 003) (Paper 26LB). 20th Conference on Retroviruses and Opportunistic Infections. Atlanta, Georgia.
5. Heneine W, Kashuba A (2012) HIV prevention by oral preexposure prophylaxis. *Cold Spring Harbor Perspect Med* 2: a007419/007419/007413.
 6. Shattock RJ, Rosenberg Z (2012) Microbicides: topical prevention against HIV. *Cold Spring Harbor Perspect Med* 2: a007385/007381-a007385/007317.
 7. Friend DR, Kiser PF (2013) Assessment of topical microbicides to prevent HIV-1 transmission: Concepts, testing, lessons learned. *Antiviral Res* 99: 391–400.
 8. Hankins CA, Dybul MR (2013) The promise of pre-exposure prophylaxis with antiretroviral drugs to prevent HIV transmission: a review. *Curr Opin HIV AIDS* 8: 50–58.
 9. van der Straten A, Van Damme L, Haberer JE, Bangsberg DR (2012) Unraveling the divergent results of pre-exposure prophylaxis trials for HIV prevention. *AIDS* 26: F13–19.
 10. Dobard C, Sharma S, Martin A, Pau CP, Holder A, et al. (2012) Durable protection from vaginal simian-human immunodeficiency virus infection in macaques by tenofovir gel and its relationship to drug levels in tissue. *J Virol* 86: 718–725.
 11. Singer R, Mawson P, Derby N, Rodriguez A, Kizima L, et al. (2012) An intravaginal ring that releases the NNRTI MIV-150 reduces SHIV transmission in macaques. *Sci Transl Med* 4: 150ra123.
 12. Smith JM, Rastogi R, Teller RS, Srinivasan P, Mesquita PMM, et al. (2013) An intravaginal ring eluting tenofovir disoproxil fumarate completely protects macaques from multiple vaginal SHIV challenges. *Proc Natl Acad Sci* 110: 16145–16150.
 13. Skoler-Karpoft S, Ramjee G, Ahmed K, Alini L, Plagianos MG, et al. (2008) Efficacy of Carraguard for prevention of HIV infection in women in South Africa: a randomised, double-blind, placebo-controlled trial. *Lancet* 372: 1977–1987.
 14. Iskedjian M, Einarson TR, MacKeigan LD, Shear N, Addis A, et al. (2002) Relationship between daily dose frequency and adherence to antihypertensive pharmacotherapy: evidence from a meta-analysis. *Clin Ther* 24: 302–316.
 15. Kruk ME, Schwalbe N (2006) The relation between intermittent dosing and adherence: preliminary insights. *Clin Ther* 28: 1989–1995.
 16. Andrews C, Gettie A, Russell-Lodrigue K, Moss L, Mohri H, et al. (2013) Long-acting parenteral formulation of GSK1265744 protects macaques against repeated intrarectal challenges with SHIV (Paper 24LB). 20th Conference on Retroviruses and Opportunistic Infections. Atlanta, Georgia.
 17. Kiser PF, Johnson TJ, Clark JT (2012) State of the art in intravaginal ring technology for topical prophylaxis of HIV infection. *AIDS Rev* 14: 62–77.
 18. Fetherston SM, Malcolm RK, Woolfson AD (2010) Controlled-release vaginal ring drug-delivery systems: a key strategy for the development of effective HIV microbicides. *Therapeutic Delivery* 1: 785–802.
 19. Malcolm RK, Fetherston SM (2013) Delivering on MPTs: addressing the needs, rising to the challenges and making the opportunities. *Contraception* 88: 321–325.
 20. Friend DR (2012) Drug delivery in multiple indication (multipurpose) prevention technologies: systems to prevent HIV-1 transmission and unintended pregnancies or HSV-2 transmission. *Expert Opin Drug Delivery* 9: 417–427.
 21. Friend DR (2011) Intravaginal rings: controlled release systems for contraception and prevention of transmission of sexually transmitted infections. *Drug Delivery Transl Res* 1: 185–193.
 22. Wertheimer AI (2013) The economics of polypharmacology: fixed dose combinations and drug cocktails. *Curr Med Chem* 20: 1635–1638.
 23. Connor J, Rafter N, Rodgers A (2004) Do fixed-dose combination pills or unit-of-use packaging improve adherence? A systematic review. *Bull World Health Organ* 82: 935–939.
 24. Koetsawang S, Ji G, Krishna U, Cuadros A, Dhall GI, et al. (1990) Microdose intravaginal levonorgestrel contraception: a multicentre clinical trial. I. Contraceptive efficacy and side effects. *World Health Organization. Task Force on Long-Acting Systemic Agents for Fertility Regulation. Contraception* 41: 105–124.
 25. Johnson TJ, Clark MR, Albright TH, Nebeker JS, Tuitupou AL, et al. (2012) A 90-day tenofovir reservoir intravaginal ring for mucosal HIV prophylaxis. *Antimicrob Agents Chemother* 56: 6272–6283.
 26. Clark JT, Johnson TJ, Clark MR, Nebeker JS, Fabian J, et al. (2012) Quantitative evaluation of a hydrophilic matrix intravaginal ring for the sustained delivery of tenofovir. *J Control Release* 163: 240–248.
 27. Clark MR, Johnson TJ, McCabe RT, Clark JT, Tuitupou A, et al. (2012) A hot-melt extruded intravaginal ring for the sustained delivery of the antiretroviral microbicide UC781. *J Pharm Sci* 101: 576–587.
 28. Malcolm K, Woolfson D, Russell J, Tallon P, McAuley L, et al. (2003) Influence of silicone elastomer solubility and diffusivity on the in vitro release of drugs from intravaginal rings. *Journal of Controlled Release* 90: 217–225.
 29. Nel A, Smythe S, Young K, Malcolm K, McCoy C, et al. (2009) Safety and pharmacokinetics of dapivirine delivery from matrix and reservoir intravaginal rings to HIV-negative women. *Journal of acquired immune deficiency syndromes* 51: 416–423.
 30. Johnson TJ, Srinivasan P, Albright TH, Watson-Buckheit K, Rabe L, et al. (2012) Safe and sustained vaginal delivery of pyrimidine nucleoside HIV-1 inhibitors from polyurethane intravaginal rings. *Antimicrob Agents Chemother* 56: 1291–1299.
 31. Johnson TJ, Gupta KM, Fabian J, Albright TH, Kiser PF (2010) Segmented polyurethane intravaginal rings for the sustained combined delivery of antiretroviral agents dapivirine and tenofovir. *Eur J Pharm Sci* 39: 203–212.
 32. Mesquita PM, Rastogi R, Segarra TJ, Teller RS, Torres NM, et al. (2012) Intravaginal ring delivery of tenofovir disoproxil fumarate for prevention of HIV and herpes simplex virus infection. *J Antimicrob Chemother* 67: 1730–1738.
 33. Gupta KM, Pearce SM, Poursaid AE, Aliyar HA, Tresco PA, et al. (2008) Polyurethane intravaginal ring for controlled delivery of dapivirine, a nonnucleoside reverse transcriptase inhibitor of HIV-1. *J Pharm Sci* 97: 4228–4239.
 34. van Laarhoven JA, Krufft MA, Vromans H (2002) In vitro release properties of etonogestrel and ethinyl estradiol from a contraceptive vaginal ring. *Int J Pharm* 232: 163–173.
 35. Saltzman WM (2001) Engineering principles for drug therapy. New York: Oxford University Press.
 36. van Laarhoven JA, Krufft MA, Vromans H (2002) Effect of supersaturation and crystallization phenomena on the release properties of a controlled release device based on EVA copolymer. *J Control Release* 82: 309–317.
 37. Siepmann J, Siepmann F (2008) Mathematical modeling of drug delivery. *Int J Pharm* 364: 328–343.
 38. Helbling IM, Luna JA, Cabrera MI (2011) Mathematical modeling of drug delivery from torus-shaped single-layer devices. *J Control Release* 149: 258–263.
 39. Vergnaud J (1993) Controlled Drug Release of Oral Dosage Forms. Boca Raton: CRC Press.
 40. Siepmann J, Siepmann F (2012) Modeling of diffusion controlled drug delivery. *J Control Release* 161: 351–362.
 41. Clark MR, Kiser PF, Loxley A, McConville C, Malcolm RK, et al. (2011) Pharmacokinetics of UC781-loaded intravaginal ring segments in rabbits: a comparison of polymer matrices. *Drug Delivery and Translational Research* 1: 238–246.
 42. Szycher M (1985) Extrudable Polyurethane for Prosthetic Devices Prepared from a Diisocyanate, a Polytetramethylene Ether Polyol, and 1,4-Butane Diol. United States Patent 4,523,005.
 43. Elabd YA, Sloan JM, Tan NB, Barbari TA (2001) Effect of Penetrant-Polymer Interactions on Molecular Diffusion in Conformational Isomers of a Heterogeneous Polymer. *Macromolecules* 34: 6268–6273.
 44. Kiser PF, Johnson TJ, Clark JT, Shelke N, Rastogi R (2013) Intravaginal Devices for Drug Delivery. WO Patent Application PCT/US2012/047649.
 45. Rose S, Chaudhari A, Peterson CM (2009) Mirena (Levonorgestrel intrauterine system): a successful novel drug delivery option in contraception. *Adv Drug Deliv Rev* 61: 808–812.
 46. Dusterberg B, Humpel M, Speck U (1981) Terminal half-lives in plasma and bioavailability of norethisterone, levonorgestrel, cyproterone acetate and gestodene in rats, beagles and rhesus monkeys. *Contraception* 24: 673–683.

Supporting Information

Drug Release Model Validation Using Finite-Element Simulation

In order to assess the validity of the two-stage drug release model for solid reservoirs presented in Equation 11, we also performed graphical finite element simulations of drug release in COMSOL Multiphysics 4. The "Transport of Diluted Species Package" was used to solve Fick's Second Law on a free triangular mesh applied to two-dimensional, circular cross-sections of cylindrical reservoirs (an example is shown in Figure S1A). Identically to Equation 11, a uniform initial condition ($c_0 = 42 \text{ mol/m}^3$) was applied to the entire cross-section and a sink boundary ($c(r_o) = 0$) was applied to the outer edges of the cross-section. Core drug diffusivity was fixed at $5 \times 10^{-9} \text{ cm}^2/\text{s}$ (not considered in our analytical model as long as it is much larger than the membrane diffusivity). Four different configurations were solved with varying D , r_o and r_i (see Table S1). Simulations were carried out for 90 days, and area integrals were taken of the cross-section at each time-point to determine drug concentration per unit length as a function of time. These integrals were converted to LNG mass units and multiplied by a fixed length of 20 mm. Equation 11 was evaluated for each of the configurations listed in Table S1, and daily release rates of both the finite-element simulation and analytical solutions were calculated by subtraction. The two data sets were then compared by computing the coefficient of determination (R^2) for each configuration.

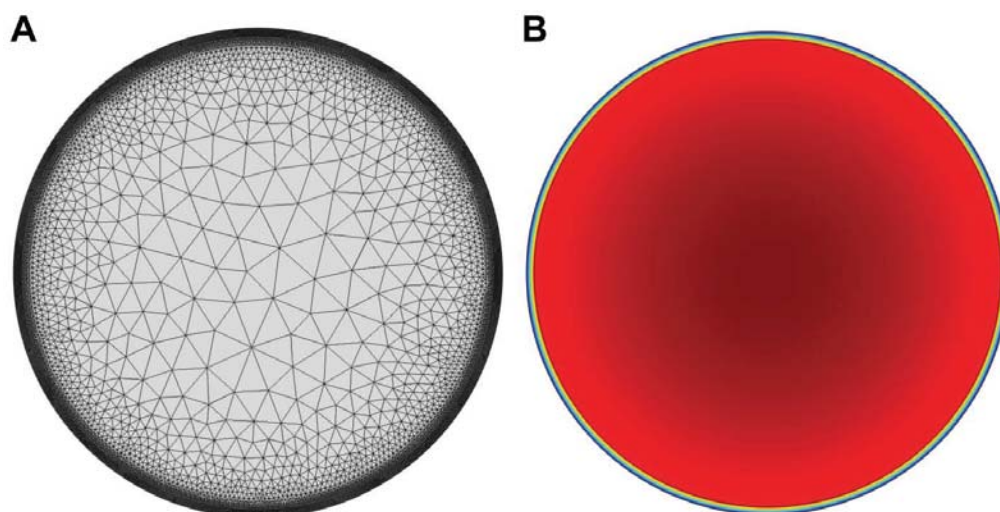


Figure S1: An example (A) finite-element mesh and (B) final concentration profile result from the finite-element drug release simulation, with highest concentration represented by dark red and lowest concentration by purple. (Configuration 'A' shown, see Table S1)

Table S1: Values of outer radius (r_o), inner radius (r_i) and drug polymer diffusivity in the outer membrane (D) for comparisons of the two-stage drug release model (Eqn. 11) to finite-element diffusion simulations.

Configuration	Outer Diameter (mm)	Wall Thickness (μm)	r_o (mm)	R_i (mm)	D (10^{-11} cm ² /s)
A	5.5	90	2.75	2.66	5.0
B	8.0	90	4.00	3.91	1.0
C	3.0	200	1.50	1.30	5.0
D	5.5	200	2.75	2.55	10.0

An example concentration profile at the end of the finite-element simulations is shown in Figure S1B, and comparisons of daily release rate profiles from the finite-element simulations and computed using Equation 11 are shown in Figure S2. Equation 11 generally agreed with the simulations with two exceptions. First, the predicted drug release on day 1 was always significantly lower in the simulations compared to Equation 11. Since a concentration

discontinuity exists on the outer boundary (r_o) at $t=0$, there is bound to be some difficulty in accurately predicting the actual day 1 release using a numerical method. Second, two models generally disagreed during the changeover between the burst and steady state regimes of drug release. As noted during the derivation, our model treats this changeover as an instantaneous switch occurring at (t_b), during which drug fluxes are likely to be underestimated while the concentration profile adjusts to the constraint of the inner boundary at r_i . The models generally agree after this point, except for configuration C, where Equation 11 continued to under-predict the results of the simulation by an average of 18% during the predicted reservoir-stage (from day 19 onward). Based on the configurations that were simulated, the adjustment between the matrix and reservoir concentration profiles likely takes longer for proportionally thicker RCM (higher values of r_i/r_o). This may be due to the first-term approximation used to predict matrix-stage release (Equation 11a), that is increasingly inaccurate for higher values of cumulative release, and only to be used for the first 20-30% of release (13% is released in the matrix-stage in configuration C). As mentioned in the manuscript, this model will be the most accurate for thinner membranes, and a higher order approximation would need to be used to predict matrix-stage release for proportionally thicker membranes, as well as a re-calculation of the burst duration (t_b). Nonetheless, day 2 to day 90 R^2 values were greater than 0.90 for all four configurations, confirming that this is a sufficiently accurate predictor of drug diffusion in cylindrical reservoirs and useful for device design and optimization. Also interesting is that the core does not appear to be completely well mixed in Figure S1B as per our assumption, even with core and membrane diffusivity values that were 100-fold different. However, based on Figure S2A, this does not appear to significantly affect the accuracy of Equation 11 in this setup.

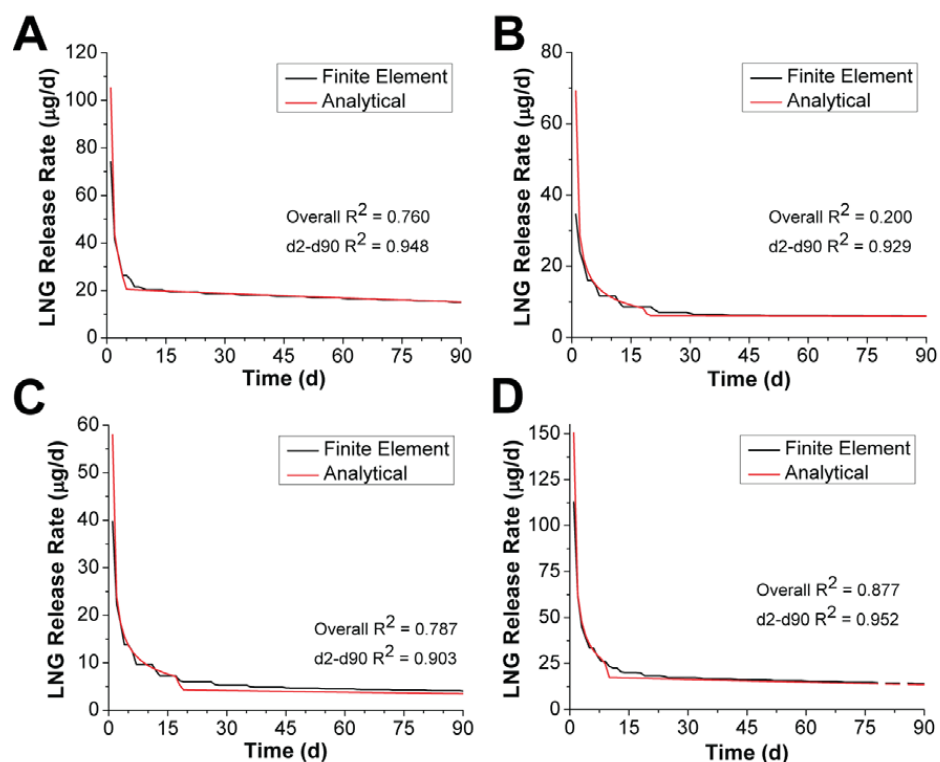


Figure S2: Comparison of a finite-element diffusion model and our analytical model (Equation 11) for drug release from cylindrical reservoirs. Panels A, B, C and D correspond to the "Configuration" column in Table S1.

Gradient HPLC methods for quantification of LNG in *in vitro* release samples

Two gradient HPLC methods were used to quantify LNG in *in vitro* release samples. In both cases a 1200 Series HPLC with a quaternary pump and diode array detector (Agilent Technologies, Santa Clara, California) and a 4.6 x 250 mm, 5 µm Zorbax ODS column (also Agilent Technologies) were used. For samples from LNG segment tests a 7-minute gradient of H₂O and acetonitrile (ACN) was used (Table S2), whereas for samples from full TFV/LNG IVR tests an 18-minute gradient of 0.1% formic acid in H₂O and 0.1% formic acid in ACN was used (Table S3). In both cases, LNG was detected at 240 nm.

Table S2: HPLC gradient profile for detection of LNG alone in *in vitro* release samples. Line A: H₂O, Line B: ACN. A flow rate of 1.1 mL/min was applied throughout the method.

Time (min)	% Line A	% Line B
0.0	30	70
2.0	30	70
2.5	20	80
5.0	20	80
5.5	30	70
7.0	30	70

Table S3: HPLC gradient profile for LNG in TFV/LNG IVR *in vitro* release samples. Line A: 0.1% formic acid in H₂O, Line B: 0.1% formic acid in ACN. A flow rate of 1.0 mL/min was applied throughout the method.

Time (min)	% Line A	% Line B
0.0	100	0
8.0	20	80
13.0	20	80
15.0	100	0
18.0	100	0

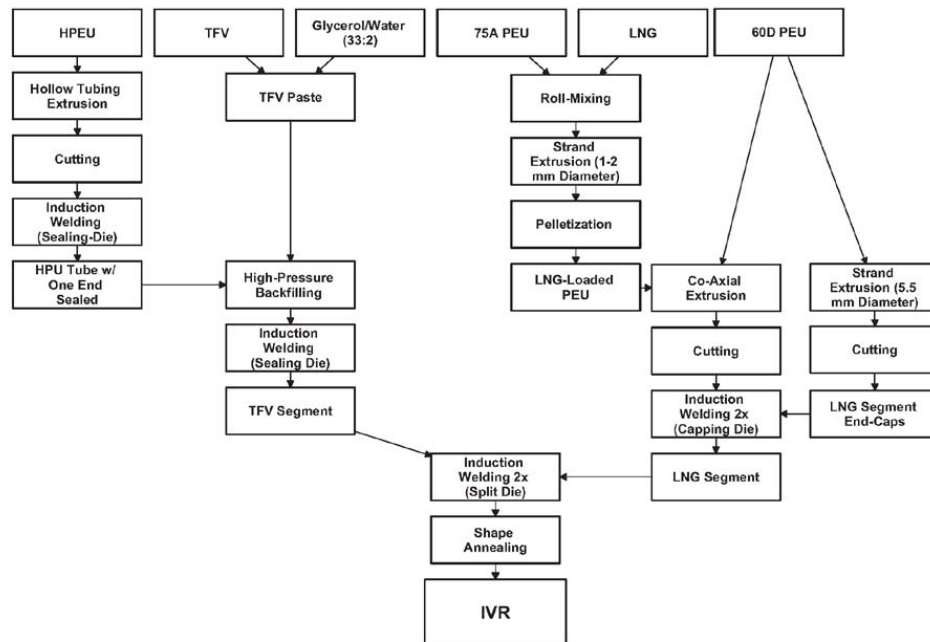


Figure S3: Manufacturing flow diagram for the TFV/LNG IVR.

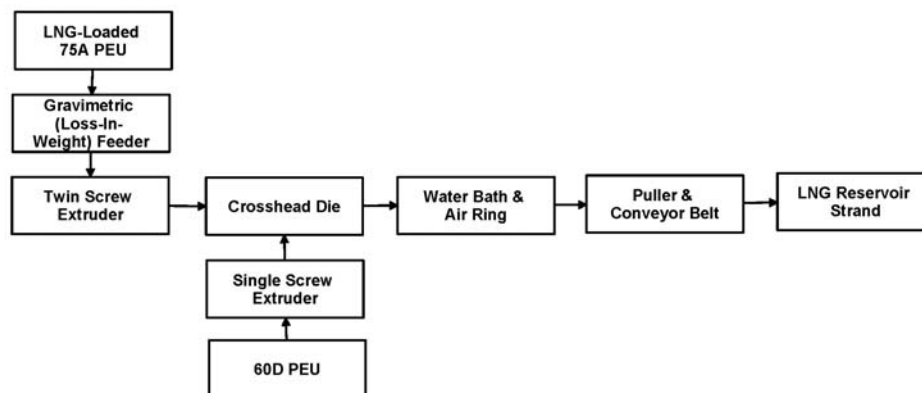


Figure S4: Process flow diagram for co-axial extrusion of LNG-loaded PEU strands.

Extraction of LNG from rabbit plasma samples and quantification by LC-MS/MS

LNG was quantified in rabbit plasma samples by LC-MS/MS during the PK study described in the manuscript. Blood samples were first thawed to room temperature, vortexed briefly and centrifuged at 4000 rpm for 10 minutes at 5°C. 250 µL of each sample was added to a 96-well plate. Also to each well were added 400 µL H₂O and 50 µL of an internal standard containing levonorgestrel-d6 (LNG-d6) (TLC PharmaChem, Inc., Vaughan, Ontario, Canada). In parallel, an Oasis HLB 96-well solid phase extraction (SPE) plate (Waters, Milford, Massachusetts) was conditioned by passing 800 µL MeOH followed by 800 H₂O, another 800 µL MeOH and finally 800 µL dichloromethane (DCM) under minimal vacuum. Sample mixtures were then transferred to the conditioned SPE plate under minimal vacuum (as needed). 800 µL H₂O, followed by 800 µL 40:60 MeOH/H₂O under minimal vacuum was passed through the wells to waste, followed by 5 minutes under high vacuum to dry the SPE beds. 800 µL DCM then was passed through the SPE wells to a 96-well collection plate. High vacuum was again applied to the plate until the SPE beds were visually dry. The DCM eluent was then evaporated under N₂ at 40°C, and reconstituted with 100 µL 50:50 MeOH/H₂O. The entire plate was then vortexed for 1 minute, and samples were again centrifuged at 4000 rpm for 5 minutes at 5°C.

LNG was then quantified in the reconstituted extractants using an 1100 Series HPLC (Agilent Technologies) and a API 5000 mass spectrometer (MS) (AB SCIEX, Framingham, Massachusetts). The HPLC was equipped with a chilled autosampler (set to 5°C), as well as two binary solvent pumps and a 6-port switching valve. Two Betasil C₁₈ 100 x 2.1 mm, 5 µm columns (Thermo Scientific, West Palm Beach, Florida) were used, one as the loading column and one as the analytical column. Gradients of H₂O and ACN (both with 0.1% formic acid) were run on both columns. Pump profiles are shown in Table S4 and the column switching profile is shown in Table S5. Positive daughter ions of LNG and LNG-d6 (245.2 and 251.2 m/z) were detected at approximately 4 minutes.

Table S4: HPLC pump profiles for the plasma LC-MS/MS method. Line A: 0.1% formic acid in H₂O, Line B: 0.1% formic acid in ACN.

Pump 1				Pump 2			
Time (min)	Flow Rate (mL/min)	% Line A	% Line B	Time (min)	Flow Rate (mL/min)	% Line A	% Line B
0	0.3	35	65	0.0	0.6	35	65
2.5	0.3	35	65	1.0	0.6	35	65
2.6	0.6	0	100	1.1	0.3	35	65
4.6	0.6	0	100	5.4	0.3	35	65
4.7	0.6	35	65	5.5	0.6	0	100
10.0	0.6	35	65	6.5	0.6	0	100
				6.6	0.6	35	65
				10.0	0.6	35	65

Table S5: HPLC switching profile for the plasma analysis method. Position A: Pump 1 - autosampler - Column 1 - waste; Pump 2 - Column 2 - MS, Position B: Pump 2 - Column 1 - Column 2 - MS; Pump 1 - autosampler - waste.

Time (min)	Position
0.0	A
1.4	B
2.4	A

Extraction of LNG from rabbit cervical tissue samples and quantification by LC-MS/MS

Rabbit cervical tissue samples were ground with dry ice in a small blade homogenizer to make a finely ground sample. Samples were then stored overnight at -20°C to allow the dry ice to sublime. The ground tissues were then diluted with 80:20 MeOH/H₂O at 100 mg tissue/mL and sonicated for 5 minutes in an ice water bath. Samples were stored at -80°C until analysis could be performed. Samples were again thawed, vortexed and centrifuged at 4500 rpm and 4°C for 10 minutes. The supernatants were transferred to fresh containers prior to aliquoting into 96-well filter plates. To each well, 600 µL ACN, 50 µL of LNG-d6 internal standard and 250 µL of sample were added. Plates were allowed to stand for approximately 5 minutes before applying vacuum and collecting in a 96-well collection plate. The extractants were evaporated and

reconstituted, vortexed and centrifuged as described for plasma extractants above prior to analyzing by LC-MS/MS.

For analysis of tissue extractants, the same LC-MS/MS instrument as above was used except a single-pump, single-column set-up was employed. A 7-minute gradient of 0.1% formic acid in H₂O and 0.1% formic acid in ACN was run through a Betasil C₁₈ 100 x 2.1 mm, 5 μm column. The pump profile is described in Table S6. The same positive daughter ions as above, (245.2 and 251.2) were detected for LNG and LNG-d6 at approximately 2.2 minutes.

Table S6: HPLC gradient profile for LNG detection in cervical tissue using LC-MS/MS. Line A: 0.1% formic acid in H₂O, Line B: 0.1% formic acid in ACN. A flow rate of 0.3 mL/min was applied throughout the method.

Time (min)	% Line A	% Line B
0.0	38	62
2.1	38	62
2.2	5	95
3.7	5	95
3.8	38	62
7.0	38	62

CHAPTER 4

PRECLINICAL EVALUATION OF A MULTIPURPOSE PREVENTION INTRAVAGINAL RING: ASSESSMENTS OF STABILITY AND IN VIVO PERFORMANCE

Justin T. Clark, Namdev S. Shelke, Meredith R. Clark, Todd J. Johnson, R. Tyler
McCabe, Krystin Z. Meidell, Judit Fabian, David R. Friend, Patrick F. Kiser

Manuscript in preparation for submission to the European Journal of Pharmaceutics and
Biopharmaceutics

4.1 Abstract

Women in the developing world desperately need reliable methods to prevent HIV infection and unintended pregnancy. Herein we describe the pharmacokinetic and stability evaluation of a dual-segment reservoir IVR that delivers the anti-HIV drug tenofovir and the progestin contraceptive levonorgestrel at near-constant rates for 90 days. The stability of tenofovir and levonorgestrel, as well as their release rate profiles *in vitro*, were evaluated for up to 5 months at 30°C and 40°C. The sheep model was used for pharmacokinetic testing due to the anatomical similarity between the human and sheep vaginal tract. TFV and LNG were stable in the IVR formulation for up to 5 months at 40°C. Release rates of TFV decreased gradually with storage due to the rearrangement of the hydrophilic polyurethane used to manufacture the TFV-releasing segment, plateauing in the 5-6 mg per day range. Release rates of LNG were stable over 90 days with the exception of an increased burst release due to gradual diffusion of LNG in the outer membrane of the LNG-releasing segment. Rings releasing 8-9 mg TFV per day *in vitro* resulted in sustained TFV levels in sheep vaginal fluid ($\sim 10^5$ to 10^6 ng/g) and tissue ($\sim 10^3$ to 10^4 ng/g) for 90 days following a short lag measured at the 8-hour time-point. Two ring prototypes, releasing 9 or 23 μ g LNG per day *in vitro*, resulted in sustained levels of LNG in the cervical tissue (~ 2 to 20 ng/g) over 90 days. These results demonstrate the potential of the TFV/LNG IVR to become the first long-acting multipurpose prevention device and warrant a clinical investigation.

4.2 Introduction

Although three decades have passed since the discovery of HIV, 35 million people worldwide are still living with HIV infection, with roughly 2.3 million new

infections and 1.6 million deaths occurring annually [1]. The HIV/AIDS pandemic continues to disproportionately affect young women in low-income areas. For example, an estimated 4.3% of women aged 15–24 in Sub-Saharan Africa are living with HIV, compared with 1.5% of men of same age-group. Efforts to encourage safe sex in these populations have experienced limited success due to the unwillingness of men to use condoms [2]. The CAPRISA 004 [3-5] clinical study recently proved the concept of HIV pre-exposure prophylaxis (PrEP), whereby antiretroviral (ARV) drugs are administered either topically or orally prior to sexual exposure to prevent sexual transmission. Women in the CAPRISA 004 study were 39% less likely to become infected with HIV when using a vaginal gel containing the HIV reverse transcriptase inhibitor tenofovir (TFV), both before and after sex. Although the success of CAPRISA 004 was modest, the Partner's PrEP study demonstrated a 75% reduction in HIV transmission between serodiscordant couples when the HIV-negative partner was administered an oral formulation (Truvada) containing a TFV prodrug [6]. Furthermore, several recent studies demonstrated the ability of ARV-containing gels [7, 8] and ARV-releasing intravaginal rings (IVR) [9, 10] to prevent SHIV transmission in nonhuman primates, confirming that PrEP may yet show promise in attenuating the spread of the virus. Unfortunately, the HIV prevention field endured a setback when the VOICE (MTN-003) study failed to demonstrate any statistically significant reduction in HIV transmission across multiple study arms testing the once-daily administration of TFV gel and TFV-containing oral formulations [11]. By measuring TFV levels in plasma, researchers were able to determine that the participants adhered poorly to these once-daily dosing regimen, indicating that the women were unmotivated to protect themselves within the coitally-

independent, once-daily dosing framework. In total, these successes and failures highlight the need to identify and develop of PrEP products that are most desirable to women needing to protect themselves against HIV infection [12].

There is a strong regional correlation between high incidence of HIV infection and unintended pregnancy. Worldwide, 40 % of pregnancies are unintended, resulting in staggering rates of material death in low-income populations [13]. Furthermore, it has been posited that inclusion of a contraceptive component may increase user demand, and subsequently adherence to PrEP products. Accordingly there is an imperative for the rapid development of long-acting, multipurpose prevention technologies (MPT) that simultaneously prevent HIV transmission (and/or other sexually transmitted infections) and unintended pregnancy. IVR have been identified as leading candidates for long-acting MPT products based on the demonstrated acceptability of the contraceptive Nuvaring [14, 15], and the potential for IVR to provide sustained levels of ARV to potential sites of HIV infection for several months [16]. IVR leverage the advantages of local drug delivery (e.g. achieving appropriate drug levels at the site of action while minimizing systemic exposure) while avoiding the messiness and/or inconvenience of other frequently-administered topical vaginal delivery systems (e.g. gels, films, tablets) [17, 18].

We recently reported a dual-reservoir polyurethane IVR for simultaneous delivery of tenofovir (TFV) and the widely-used progestin contraceptive levonorgestrel (LNG) for up to 3 months [19]. This IVR demonstrated release of both TFV and LNG at near constant rates for up to 90 days *in vitro*. We targeted release rates of approximately 10 mg per day for TFV, based on a PK comparison between an IVR containing the same

TFV-releasing technology and the TFV gel. However, we targeted much lower release rates for LNG, either 10 or 20 μg per day based on release rates from LNG-releasing intrauterine systems (IUS) (Mirena® and Skyla®) and the discontinued LNG-releasing silicone IVR [20, 21]. Long-term vaginal administration of a progestin, such as LNG, is an appropriate contraceptive method for incorporation in an MPT due to the remarkably high effectiveness observed with LNG-releasing IUS, which achieve reliable contraception primarily via local effects and without unnecessary systemic hormone exposure.

PK testing of both component segments of the TFV/LNG IVR have been reported: the TFV segment in the sheep PK comparison with TFV gel mentioned above [16], and the LNG segment in the rabbit model [19]. Near zero-order local PK were observed in both studies, motivating the investigation of the full dual-indication device in the sheep model. This manuscript will describe two major efforts in the continued preclinical development of the TFV/LNG IVR: 1) accelerated physical and chemical stability testing and 2) a 90-day PK evaluation in the sheep model. The results herein further demonstrate that our first-in-class long-acting contraceptive/PrEP product has potential to make a significant impact on the reproductive health of women in the developing world.

4.3 Materials and Methods

4.3.1 Materials

As in our previous paper [19], two sets of biomedical PEU were used for the fabrication of TFV/LNG IVR. For stability testing, Tecophilic HP-100A-60 (HP-100A-60), Tecoflex EG-85A (EG-85A), and Tecoflex EG-65D (EG-65D) were obtained from

Lubrizol Advanced Materials (Wickliffe, Ohio). For PK testing, a custom-designed hydrophilic aliphatic polyether urethane (HPEU-35), and two hydrophobic aliphatic polyether urethane (PEU-1 and PEU-2) with shore hardness of 78A, 73A-77A and 59D, respectively, were obtained from DSM Biomedical (Berkeley, CA). Tenofovir (TFV) was supplied by Gilead Sciences (Foster City, CA) and micronized LNG was obtained from Industriale Chimica (Saronno, Italy) or Haorui Pharma-Chem Inc. (Edison, New Jersey). USP grade glycerol and water were purchased from Spectrum Chemical (New Brunswick, NJ). All water used was either USP grade or double de-ionized (DDI). All other solvents and reagents were HPLC or ACS grade, unless otherwise mentioned. Phosphate buffered saline (PBS) was obtained from Life Technologies (Carlsbad, CA).

4.3.2 IVR Fabrication

TFV/LNG IVR were fabricated as described previously [16] [19]. Briefly, for the TFV-releasing segment, HPEU-35 or HP-100A-60 pellets were formed by hot-melt extrusion into hollow tubes with approximately 5.5 mm cross-sectional diameter and 0.7 mm wall thickness. HPEU tubing was cut to two different lengths, 145 mm or 155 mm, for IVR prototypes I and II, respectively (Figure 4.1). Tubes were filled with a TFV/glycerol/water paste (62-65% TFV) using a high-pressure back-filler (Dymax, Torrington, CT) and sealed using a bonding-die induction welder (PlasticWeld Systems, Newfane, NY), resulting in segments with final lengths of 121 or 131 mm, respectively. For the LNG segment, LNG-loaded PEU-1 or EG-85A pellets were first fabricated by roll-coating with LNG powder, hot-melt extrusion, pelletization, and bag mixing. LNG-loaded reservoir strands were obtained by coating a LNG-loaded extrudate with PEU-2 or

EG-65D in a two extruder, co-axial hot melt extrusion set-up. Reservoir strands were approximately 5.5 mm in diameter with approximately 0.1 mm PEU-2/EG-65D rate-controlling membrane (RCM) thickness. For IVRs used in PK testing, LNG-loaded co-axial strands were heat treated for 14 days to mitigate the lag time required for steady state release. Strands were cut to either 20 or 10 mm (for IVR prototypes I and II, respectively) and end-capped using 2 mm length, 5.5 mm diameter PEU-2 or EG-65D polymer discs to prevent LNG diffusion into the TFV segment [19]. Prior to any melt processing, all PEU or HPEU resins were dried overnight in a CAFM series compressed air dryer (Dri-Air, East Windsor, Connecticut) to less than 0.05% H₂O (w/w) as determined using a C30 Coulometric Karl Fischer Titrator (Mettler-Toledo, Columbus, Ohio).

TFV segments and end-capped LNG segments were joined using a split-die induction welder (PlasticWeld Systems, Inc., Newfane, NY). For IVR Prototype I, a 121 mm TFV segment was joined to a 20 mm (24 mm after end-capping) segment, while for Prototype II, a 131 mm TFV segment was joined to a 10 mm (14 mm after end-capping) segment. IVR were annealed in custom-made aluminum molds for 65°C for 10 to 15 minutes to obtain a more circular shape. IVRs used in stability testing were heat treated for 14 days at 40°C in heat-sealed aluminum pouches to simultaneously eliminate the lag-time required to achieve steady state LNG release [19] and stabilize TFV release rates by accelerating the microphase separation of HPEU (manuscript in preparation).

4.3.3 HPLC Quantification of TFV and LNG in Drug Release

and Extraction Samples

TFV and LNG were quantified in *in vitro* release samples using an Agilent (Santa Clara, CA) 1200 series HPLC equipped with a diode array detector. TFV was quantified at 260 nm using a 15-minute gradient of potassium phosphate buffer (pH 6.0) and acetonitrile (ACN) described previously [16]. LNG was quantified using a 4.6 x 250 mm Zorbax C18 5 μ m column (Agilent, Santa Clara, CA) and 240 nm. For polymer extraction samples, a 5-minute isocratic run of 80:20 ACN:water was used, while a 18-minute gradient of 0.1% formic acid in water and 0.1% formic acid in ACN was used to quantify LNG in *in vitro* release samples, both as described previously [19].

4.3.4 In Vitro Drug Release Testing

The release kinetics of TFV/LNG IVR were evaluated *in vitro* under sink conditions as previously described [19]. For IVR undergoing stability evaluation, Prototype I samples were placed in glass jars and immersed in 25 mM sodium acetate buffer (pH 4.2) in an incubated shaker cabinet set to 37°C and 80 rpm. IVR Prototypes I and II were similarly evaluated in parallel to the sheep PK study, except that acetate buffer was replaced with 1X phosphate buffered saline (PBS) (pH 7.4) to mimic the neutral pH of the sheep vaginal tract. Media volumes were selected and modified as needed to ensure that sink conditions (drug concentrations not exceeding 20% of their solubility) were maintained. Release media were changed daily, and aliquots were collected periodically throughout the study. TFV and LNG were quantified in release

media by HPLC as described above. Time-averaged release rates for each IVR were determined using a trapezoidal numerical integration for comparison to *in vivo* data.

4.3.5 Extraction and Quantification of TFV and LNG from IVR

Drug extractions were performed on TFV/LNG IVR were performed as part of the stability and pharmacokinetic studies described below. First, IVR were dissected with a razor blade between the TFV segment plugs and the LNG segment end-caps. TFV extraction from TFV segments were performed as described previously for the TFV-only IVR [16]. Briefly, segments were dissected into several pieces (approximately 5-8 mm in length) and placed into glass jars containing 100 mM sodium phosphate buffer (pH 7.4), which were shaken overnight on a High Capacity Mixer (Glas-Col, Terre Haute, IN) to completely dissolve all TFV present in the ring. For IVR evaluated following *in vivo* testing, TFV segments were first placed at -80°C to avoid spilling of core contents during dissection. Following complete dissolution, the supernatant and multiple rinses of the remaining HPEU tubing fragments were transferred to a 50 mL volumetric flask, which was filled to volume with additional sodium phosphate buffer and agitated briefly. The resulting solution was then volumetrically diluted 100-fold in the same buffer using 100 μ L a calibrated glass syringe (Hamilton Company, Reno, Nevada) and a 10 mL volumetric flask. TFV was quantified in the resulting solution by HPLC as described above. Similar extractions were performed on the source TFV-containing paste for each ring lot to estimate the initial average TFV load for each ring.

LNG was extracted from in LNG segments using a dissolution and precipitation method similar to that described previously [22-24]. LNG segments were cut into several

pieces (approximately 2-3 mm in length), all of which were transferred to a 25 mL volumetric flask, which was filled with approximately 15 mL of dichloromethane (DCM) before undergoing vigorous shaking on the same High Capacity Mixer. Following overnight shaking, flasks were filled to volume with DCM and vortexed vigorously. A 1 mL aliquot of the DCM solution was transferred to a 10 mL volumetric flask, which was filled to volume with ACN to dissolve the LNG present while precipitating the PEU. The supernatant was then subjected to HPLC analysis for LNG quantification as described above.

4.3.6 Stability Evaluation of TFV/LNG IVR

TFV/LNG IVR were stored individually in heat-sealed VF42 Vapor-Flex flat barrier bags (LPS Industries, Moonachie, NJ) and stored at either 30°C/65% relative humidity (RH) or 40°C/75% RH for up to 5 months. Chemical stability was assessed at multiple pull points using the extraction methods described above. For TFV, the total mass extracted was compared at each point to a t=0 baseline, while for LNG, the initial mass of the segment (prior to end-capping) was used to normalize each extracted mass value for a baseline comparison due to the higher dimensional variability observed in the co-axial strands. *In vitro* release testing was performed at each time and temperature for 28 days as described above. We used similarity factors (f_2) to quantitatively assess the stability *in vitro* release profiles. It was first necessary to estimate the cumulative release profile of both TFV and LNG, which was performed by simple summation (for regions of the profile where continuous collection points were available) or by trapezoidal numerical integration (from regions of the profile with gaps in collection data, typically

for days 21 and 28). Similarity factors are typically calculated using cumulative release expressed as a percentage of total drug load in the device [25]. However, since these *in vitro* release tests were not designed to test IVR to exhaustion, we expressed cumulative release as a percentage of the drug released by day 28 in the t=0 group. Similarity factors were then calculated by the following equation:

$$f_2 = 50 * \log \left\{ \left(1 + \left(\frac{1}{n} \right) \sum_{i \leq n} (R_i - T_i)^2 \right)^{-0.5} * 100 \right\} \quad (4.1)$$

where n is the total number of points on the release profile and R and T are the reference and test profiles to be compared. The FDA considers two release profiles to be similar if $f_2 \geq 50$.

We assessed the physical stability of LNG in the co-axially extruded strands and full IVR both visually and using polarized light microscopy to examine the surface of the LNG segment for LNG recrystallization at some time-points.

4.3.7 Pharmacokinetic Evaluation of TFV/LNG IVR in Sheep

Pharmacokinetic studies were carried out at MPI Research (Mattawan, MI) which is accredited by the Association for Assessment and Accreditation of Laboratory Animal Care International (AAALAC International). IVR Prototypes I and II were evaluated in 2- to 5-year-old and 65-80 kg Dorset Crossbred sheep purchased from Buckham's sheep farm (Kalamazoo, MI). Animals were treated under a protocol reviewed and approved by Institutional Animal Care and Use Committee (IACUC) at MPI Research. The sheep were housed in separate indoor pens under fluorescent light provided for approximately 12 hours daily and interrupted for study related activities if required. Animals were allowed free access to hay and commercial rations (Rumilab Diet) except during fasting

periods and water was provided *ad libitum*. Sixteen animals were divided into two groups of 8, one receiving Prototypes I and the other receiving Prototype II. IVR were inserted continuously for 90 days. Prior to insertion, each IVRs was fitted with a medical grade suture thread to allow for easy removal. The exterior of the vagina was treated with chlorhexidine solution and IVR were inserted using gloved hands and a small amount of medical-grade lubricant. Strings fitted to the IVRs were left hanging outside the vagina to visually that samples had not been expelled. Correct ring placement was confirmed by visual examination with the aid of a speculum. Animals were examined daily to confirm that rings had remained in place. Following ring administration, vaginal fluid sponges, vaginal and cervical tissue biopsies, and blood samples were collected periodically for drug content analysis. Preweighed Weck-Cel® sponges (Beaver-Visitec International, Inc., Waltham, MA) were used to collect vaginal fluid from each animal, 8 hours after removal and on days 1, 2, 3, 7, 14, 28, 60, and 90. Samples were also taken on days 91, 92, and 93 (1, 2, and 3 days following IVR removal). Vaginal fluid sponges were collected from proximal vagina (5 to 7 cm from the introitus) and distal vagina (2 to 4 cm from the introitus). Sponges were pressed against the vaginal wall for 1 minute to allow for fluid absorption. The mass absorbed was determined by reweighing sponges following collection and comparing to the initial mass. Kevorkian-Younger biopsy forceps (Miltex, York, PA) were used to collect vaginal and cervical biopsies 8 hours after removal and on days 14, 28, 60, 90, and 93. Prior to all biopsy procedures, animals were anesthetized and the exterior vagina was cleaned using chlorhexidine solution. Tissue samples (approximately 50 mg) were biopsied alternatively from the left or right side from both the proximal and distal vagina. In case of excessive bleeding, direct pressure

was applied with gauze (with or without thrombin), and local analgesic was administered. Approximately 2 mL of blood was collected via the jugular vein at all time points and stored in K₃EDTA-containing tubes and tubes were stored in wet ice until centrifuged. Blood samples were centrifuged at 4°C and the supernatant was collected. Sponges, biopsies, and blood supernatants were stored at -70°C until further bioanalysis could be performed. Animals that expelled rings during the study were immediately administered a fresh ring, with ring treatment continuing to a total of 90 days. PK and drug extraction data obtained from these animals were excluded from analysis (except for one animal that had a ring replaced after 1 hour that was retained for the remainder of the study). A total of 7 and 6 animals retained an IVR for the full 90 days in the Prototype I and II groups, respectively. At study's end, IVR were retrieved from the vaginal tract using the attached suture thread. TFV and LNG were extracted from returned IVR as described above, and time-averaged release rates were determined for each animal by dividing the difference in initial and extracted drug mass by the duration of insertion. For TFV, the initial mass was estimated by multiplying the TFV-containing paste fill mass by the average TFV loading in the paste batch used for the ring lot. For LNG, the initial mass was estimated by multiplying the segment mass (prior to end-capping) by the average LNG weight fraction determined by LNG segment extractions from the same ring batch.

TFV was quantified in vaginal fluid swabs, vaginal tissue biopsies, and plasma samples by extraction and LC-MS/MS procedures described previously [16]. LNG was also quantified in cervical biopsies and plasma samples by extraction and LC-MS/MS procedures described previously for our PK evaluation of LNG segments [19].

4.4 Results

4.4.1 TFV and LNG Chemical Stability

Results of the TFV/LNG IVR chemical stability evaluation are shown in Figure 4.2. TFV and LNG recovery did not significantly decrease during 147 days storage at either 30°C/65% RH or 40°C/75% RH compared to a baseline control. Initially, 1.40 ± 0.03 g TFV was recovered from TFV/LNG IVR, compared to 1.37 ± 0.03 (p=0.06, heteroscedastic t-test) and 1.41 ± 0.04 g (p=0.75) recovered from IVR stored at 30°C/65% RH or 40°C/75% RH, respectively (all N=5, mean \pm SD). LNG loadings were 1.12 ± 0.03 % LNG (w/w) at baseline compared to 1.17 ± 0.01 % (p=0.02, but higher) and 1.16 ± 0.07 % (p=0.29) at 30°C/65% RH or 40°C/75% RH, respectively (all N=5, mean \pm SD).

4.4.2 TFV and LNG Release Rate Stability

Release kinetics of TFV and LNG were evaluated following 31, 92, and 150 days storage at 30°C/65% RH and 40°C/75% RH. These results are shown in Figure 4.3. Following a lag on day 1 and a slight burst on day 2, average TFV was released from IVR at nearly constant rates over 28 days at each time-point as expected [16, 22]. Mean TFV release rates between day 3 and day 28 (N=5) ranged from 5.4 to 7.8 mg/d, 6.5 to 7.9 mg/d, 5.6 to 7.2 mg/d, and 4.7 to 6.8 mg/d following 0, 31, 92, and 150 days storage at 40°C/75% RH, respectively (Figure 4.3C). Release rates generally showed a slight downward trend during increased storage time; however, the 150-day group released more than the 92-day group at 3 collection points (days 14, 21, and 28) and more than the t=0 group on day 21. On average, release rates decreased 22% during 150 days storage at 40°C, with the maximal drop (38%) occurring on day 7, and decreased 12% during 150

days storage at 30°C, with the maximal drop (30%) also occurring on day 7. LNG release also occurred at near constant rates over 28 days at each pull point. LNG release rates varied across the various pull-points, but with no clear trend preserved across the entire kinetic curve. An increase in the initial LNG burst release was observed over the first 3 to 4 days, with the largest change occurring between the t=0 and the 31-day groups at 40°C, but between the 31- and 92-day groups at 30°C. A dip in the release rate profile was observed in the t=0 group but not at any other of the time-points at either temperature. From day 5 onward, mean LNG release rates (N=5) ranged from 13 to 22 µg/d (17 to 22 µg/d discarding day 7 through 9), 22 to 25 µg/d, 18 to 24 µg/d, and 19 to 24 µg/d following 0, 31, 92, and 150 days storage at 40°C/75% RH, respectively. At certain points in the kinetic profile, LNG release was the highest in the 150-day storage group (day 1 and day 21) while on day 21, release was the lowest in the 150-day storage group.

In comparison to the t=0 release rate profile, TFV similarity factors were determined to be 85.5, 62.5, and 53.3 following 31, 92, or 150 days at 40°C, respectively. In comparison to the 31-day profile, TFV similarity factors were determined to be 95.2 and 91.4 following 92 or 150 days at 40°C, respectively. For LNG, similarity factors were determined to be 44.3, 50.1, and 48.6 in comparison to the t=0 group, and 65.7 and 77.2 in comparison to the 31-day group.

4.4.3 TFV and LNG Physical Stability

Both LNG-loaded co-axial reservoir strands and TFV/LNG IVR were monitored visually and by polarized light microscopy for LNG surface recrystallization [23]. Following the initial 14-day heat treatment at 40°C, LNG surface crystals were first

observed following 30 and 38 days at 40°C, 30°C on EG-85A/EG-65D strands stored in sealed pouches (approximate LNG loading 1.3% w/w). However, crystallization kinetics were different for TFV/LNG IVR, also stored in sealed aluminum pouches. As shown in Figure 4.4, no LNG surface crystallization was detectable by polarized light microscopy following 150 days storage at 40°C (164 days total, including heat treatment), which is in direct contrast to the data presented above for LNG strands.

4.4.4 Comparison of TFV and LNG Release Rates *In Vitro* and *In Vivo*

In vitro drug release profiles for TFV and LNG from TFV/LNG IVR (both prototypes I and II) used in the sheep PK study are shown in Figures 4.5A and 4.5B, respectively. Similarly to the data presented above, TFV was released in a zero-order fashion for 90 days following a short lag period on day 1. TFV release rates from Prototype I were consistently lower than prototype II (except on day 21), which was expected as Prototype I contained a 10 mm shorter TFV segment. Time-averaged release rates were 7.7 ± 0.2 and 8.1 ± 0.2 mg/d from Prototypes I and II, respectively (N=5 time-averaged IVR release profiles, mean \pm SD). LNG release proceeded in a near zero-order fashion similarly to above, with a short burst period occurring for Prototype I but not for Prototype II. LNG release rates were between 1.9-fold and 3.6-fold higher at individual time-points from Prototype I in comparison to Prototype II, with the highest of these occurring on day 2. Time-averaged release rates were 23 ± 1 and 9.3 ± 0.5 μ g/d from Prototypes I and II, respectively (N=5 time-averaged IVR release profiles, mean \pm SD), the difference being slightly higher (2.5-fold) than the 2-fold difference expected.

A comparison of time-averaged TFV and LNG release rates *in vitro* and *in vivo* from IVR prototypes I and II is displayed in Figure 4.5C. All data below describe only IVR that remained in for the full 90 day duration (N=7 for Prototype I and N=6 for Prototype II). Extraction of residual TFV from recovered IVR revealed average rates of 12.0 ± 1.7 and 12.6 ± 1.5 mg/d (90.4 ± 12.6 % and 86.4 ± 10.2 % cumulative release, mean \pm SD) from Prototypes I and II, respectively. Even though the standard deviation for the Prototype I group extended beyond 100%, all rings had quantifiable TFV remaining. *In vivo* TFV release was 56% higher than that observed *in vitro* for both Prototypes I and II, which is similar to our previous observations of the TFV-only HPEU reservoir ring [24]. LNG release rates were 31 ± 3 and 14 ± 1 μ g/d (44 ± 4 % and 40 ± 3 % cumulative release, mean \pm SD) from IVR prototypes I and II over 90 days, respectively. *In vivo* LNG release rates were 38% and 49% higher than those observed *in vitro* for Prototypes I and II, respectively.

4.4.5 Pharmacokinetic Evaluation of TFV/LNG IVR in Sheep

TFV vaginal fluid concentrations during 90-day insertions of IVR Prototypes I and II in sheep are shown in Figures 4.6A and 4.6B. In all cases, vaginal fluid levels were relatively steady from day 1 (24 hours) onward, following a short lag observed at the 8-hour time-point, when all mean readings ranged between $1-3 \times 10^4$ ng/g (both proximal and distal, prototypes I and II). From day 1 to day 90, mean TFV concentrations ranged from 1.2×10^5 to 1.4×10^6 ng/g (proximal) and 1.4×10^5 to 8.1×10^5 ng/g (distal) for sheep treated with Prototype I (N=7), and from 3.3×10^5 to 1.9×10^6 ng/g (proximal) and from 2.0×10^5 to 1.9×10^6 ng/g (distal) for sheep treated with Prototype II (N=6).

Mean TFV concentration was generally higher in proximal swabs than distally, for both Prototypes with some exceptions (days 1 and 14 for Prototype I and days 2, 3, and 92 for Prototype II). Although TFV release was slightly higher from Prototype II than from Prototype I, the two datasets were relatively indistinguishable for both proximal and distal swabs. The ratio of mean TFV concentrations between animals treated with Prototype II over Prototype I ranged from 0.3 to 5.2 proximally and from 0.3 to 6.2 distally from day 1 to day 90. The minimum concentrations in any single animal observed between day 1 and day 90 were 2.0×10^3 ng/g (proximal, but with the next highest being 1.6×10^4) and 1.5×10^3 ng/g (distal) for Prototype I, and 1.3×10^3 ng/g (proximal, but with the next highest being 2.5×10^4) and 2.8×10^4 ng/g (distal). With the exceptions of some samples below limit of quantification (LOQ), TFV fluid concentrations were maintained for 3 days beyond ring removal in the 10^2 - 10^4 ng/g range. Since the lower and upper limits of quantification depended on the individual uptake mass of each swab, samples below LOQ (only samples after ring removal, see Figures 4.6A and 4.6B) or above LOQ (only one proximal swab on day 2 for Prototype I) were excluded from analysis, and mean values are not reported for those time-points. An attempt was made to quantify LNG in vaginal fluid swabs, but most readings beyond day 3 were below our limit of quantification for both swab locations and Prototypes, preventing any meaningful analysis.

TFV concentrations in vaginal tissue biopsies were also sustained throughout the 90-day sheep study, as demonstrated in Figures 4.6C and 4.6D. Again a lag was observed at the 8-hour time-point, and as no collections were taken between this and the 14-day collection, the tissue kinetics during the first 2 weeks of treatment are difficult to

elucidate from these data. From day 14 to day 90, mean TFV concentrations in vaginal tissue ranged from 5.8×10^3 to 3.1×10^4 ng/g (proximal) and 2.6×10^3 to 1.4×10^4 ng/g (distal) for sheep treated with Prototype I (N=7), and from 3.3×10^3 to 2.5×10^4 ng/g (proximal) and from 2.2×10^3 to 5.7×10^3 ng/g (distal) for sheep treated with Prototype II (N=6). TFV was still detected in most samples on day 93 (3 days postremoval), with mean TFV concentrations of 120 ng/g (proximal) and 200 ng/g (distal) for Prototype I and 170 ng/g (proximal) and 75 ng/g (distal) for Prototype II. Samples below LOQ were assigned the value of LOQ/2 (10 ng/g) for the calculation of mean values [10]. Mean TFV concentration was always higher in proximal biopsies than in distal biopsies between days 14 and 90, except at day 14 for prototype II, and again the datasets of the two Prototypes were relatively indistinguishable at both biopsy locations. All individual animal readings were above 390 ng/g between days 14 and 90 for both Prototypes and biopsy locations.

LNG concentrations profiles in cervical tissue biopsies are shown in Figure 4.6E. Some samples were below the LOQ for this assay (0.75 ng/g), and were assigned the value of LOQ/2 (0.375 ng/g) for the calculation of mean values [10]. LNG levels were steady from the 8-hour time-point through day 90, and did not exhibit the lag observed in the TFV. Mean LNG concentrations ranged from 2.9 to 14 ng/g in sheep treated with Prototype I (N=7) and 2.4 to 4.9 ng/g in sheep treated with Prototype II (N=6). With the exception of day 90, mean LNG concentrations were higher in sheep treated with Prototype I (N=7) vs. Prototype II (N=6), which was expected as the former was designed to give a 2-fold higher release rate of LNG. In fact, the ratios between mean LNG concentrations between Prototypes I and II were 2.3, 2.0, and 1.8 at 8 hours, day 14,

and day 28, respectively, clearly indicating that the 2.5-fold doses achieved *in vitro* were also achieved *in vivo*. LNG levels were steady over the 90-day period with the exception of the spike observed at day 60 in the Prototype I group, likely resulting from the unusually high value of 65 ng/g achieved in 1 animal. When this value is removed, the mean LNG concentration decreases to 5.6 ng/g, and a Prototype I vs. II ratio of 1.9 is obtained. All readings were below LOQ on day 93 (3 days following ring removal).

TFV was also quantified in blood plasma samples during the 90-day PK study. All readings were below LOQ (1 ng/mL) in plasma 8 hours postinsertion, but TFV was quantified in all samples from day 1 to day 90, with the exceptions of 1 animal in each ring group on day 1 and 2 animals in the Prototype I group on day 90 (again these values were assigned LOQ/2, or 0.5 ng/mL, for statistical calculations). Mean TFV plasma concentrations at day 1 through day 90 ranged between 2.3 and 18 ng/mL for prototype I and between 1.7 and 27 ng/mL for prototype II. C_{max} occurred on day 14 and day 60 for Prototypes I and II, respectively. In both cases, a sharp drop was observed from day 60 to day 90: 12 ± 6 to 5.5 ± 5.5 ng/mL for prototype I and 27 ± 16 to 8.2 ± 3.6 ng/mL for prototype II (all mean \pm SD). TFV was not detected in plasma after 1, 2, or 3 days postremoval for either group.

Generally, LNG concentrations in plasma were below our LOQ (25 pg/mL). For the higher-dose Prototype I group, LNG was detected in plasma for all animals on at the 8-hour time-point, 5 of 7 animals on day 1 and 1 of 7 animals on day 2 with all samples below LOQ thereafter. In the lower-dose Prototype II group, LNG was below LOQ in all samples except for 1 animal at the 8-hour time-point.

4.5 Discussion

4.5.1 IVR Stability

TFV and LNG proved chemically stable in the IVR formulation for up to 5 months under accelerated conditions. No loss of TFV or LNG was observed after storing rings for 147 days at either 30°C or 40°C. Stability testing of TFV/LNG IVR will eventually continue out to at least 2 years at these temperatures to determine the actual shelf life of the product.

TFV and LNG release kinetic profiles remained zero-order or near-zero order throughout the stability evaluation; however, some differences were observed. The average TFV release rate decreased gradually over time. HPEU, such as those used to manufacture the tubing of the swellable TFV segment, undergo gradual microphase separation following extrusion. This physical change results in a reduction of free water in the fluid-filled pores that facilitate transport of TFV through the wall, resulting in a decreased effective diffusivity, and resulting flux of TFV from the reservoir (manuscript in preparation). Ultimately, the TFV release rate is likely to plateau over time as the physical arrangement of the HPEU approaches an equilibrium state. As described in the methods, a 14-day heat treatment was applied to IVR before the start of the stability study. This was done both to drive this HPEU rearrangement toward completion, as well to facilitate LNG diffusion into the membrane of the LNG reservoir segment, as described below. The decay in release rate is greatly enhanced in the presence of the TFV/glycerol/water formulation (data not shown), leading us to hypothesize that glycerol may act as a plasticizer to aid in the migration of polymer chains following its permeation into the tubing wall. Regardless of this gradual migration of the release rate, it should not affect the eventual performance of the IVR, provided that the eventual equilibrium TFV

flux provides a sufficient concentration of TFV in the vaginal tissue to prevent HIV infection from occurring. A more vigorous pretreatment step could be performed to the tubing (e.g., higher temperature or longer time) prior to IVR manufacturing to ensure that the HPEU reaches its equilibrium state, resulting in a more stable release rate. Even though a drop in release rate was noticed, the similarity factor analysis revealed that TFV release rate profiles were quantitatively similar ($f_2 \geq 50$) at all time-points when compared to the $t=0$ data.

The two stage nature of drug release from solid reservoir devices is discussed in detail in a previous manuscript [19]. During the initial matrix-phase, which appeared to last 3 or 4 days, LNG burst release increased in magnitude during IVR storage, but appeared to level off in the 40°C group, meaning that the LNG concentration had likely equilibrated in the wall. However, the burst release on day 1 was well below that predicted by our model [19] for the Prototype I configuration (~100 µg), suggesting that the presence of glycerol on the surface of rings following storage may slightly attenuate the burst. This is a positive result, as the change in burst following 14-day heat treatment (resulting an initial concentration profile similar to that at the beginning of the reservoir phase), to the final equilibrium state was much less than anticipated. Following the matrix-stage, LNG release rates were relatively stable on storage at both temperatures. This result indicates that the microphase separation discussed above, likely also to occur in PEU due to their chemical similarity to HPEU, did not have an effect on diffusion of dissolved LNG molecules through the outer polymer membrane. Based on similarity factor analysis, the 31- and 150-day (40°C) LNG release profiles were slightly dissimilar (44.3 and 48.7) to the $t=0$ profile, however, the 92- and 150-day profiles were both

similar (65.8 and 77.2) to the 31-day profile, quantitatively confirming that the LNG release behavior had reached equilibrium following the initial 31-day storage.

Based on the ability of LNG to crystallize on the surface of reservoir segments, LNG likely exists as a supersaturated solution in the outer rate-controlling PEU at our target LNG loading (~1.2% LNG w/w). At some point during the RCM loading process, possibly even before 14-day heat treatment is completed, the concentration of LNG in the outer interfacial layer of the RCM will become super-saturated and immediately create a chemical potential gradient for recrystallization across the interface. This phenomenon is also encountered with the super-saturated solution of etonogestrel present in NuvaRing® [26], and is the reason for cold-chain storage of the product. Extensive drug surface crystallization is undesirable for any drug delivery system as it may result in an additional burst release of drug and a corresponding reduction in the magnitude of the reservoir release profile in time, provided sufficient drug was allowed to escape from the device core. The presence of glycerol on the outer surface of IVR following storage appears to prevent surface recrystallization of LNG from the LNG segment. This phenomenon was consistent for all IVRs in the 40°C test group following 150 days storage (164 days total, including heat treatment). It is unclear if this 'self-coating' is a permanent solution for surface crystallization, but it is an encouraging improvement to the system and may eliminate the need for either cold-chain storage or application of a spray/dip coating, which also successfully maintained LNG physical stability for reservoir segments (data not shown).

4.5.2 Sheep Pharmacokinetic Study

TFV release was 56% higher *in vivo* than *in vitro* for both Prototype I and II, similar to what we observed with our sheep PK study of the TFV-only IVR [16]. As we only measured the total release over 90 days, it is impossible to determine the exact *in vivo* profile for a head to head comparison with *in vitro* data. However, PK profiles in vaginal fluid swabs were relatively steady over the 90-day period, suggesting that a similar zero-order release profile of greater magnitude was achieved *in vivo*. For reservoir systems, drug release rates vary linearly with dissolved concentration. We hypothesize that the increased release rate may be due to the pH-dependent solubility of TFV. The HPEU tubing is a semipermeable membrane which will allow contents of the endogenous vaginal buffer that are sufficiently small to pass through, and eventually reach equilibrium across the membrane. Even though our parallel *in vitro* release studies were performed in a pH 7.4 buffer, it is possible that an increased buffering capacity of the vaginal buffer present inside the reservoir core during use allowed for more TFV to be dissolved, thus resulting in more rapid TFV flux across the wall. Ultimately, these IVR need to be tested in women to determine the actual *in vitro/in vivo* release rate relationship for this system, but encouraging is that the *in vivo* release rate variability was relatively low within each group (coefficients of variation of 14% and 12% for Prototypes I and II, respectively), indicating that although we may see a higher release rate in women than *in vitro*, the release rate obtained will likely be reproducible. LNG release rates were also higher *in vivo* than *in vitro*. In our previous rabbit PK evaluation of the LNG segment in rabbits [19], the comparison of data between 28-day and 90-day treatment groups, as well as an LNG plasma concentration profile, allowed us to

conclude that, although a higher burst was achieved *in vivo*, the resulting *in vitro* release rates were nearly identical. Again, we only have a single time-point to assess *in vivo* release, but this phenomenon is likely preserved because the LNG segments used in the sheep study IVR were made nearly identically to those used in the rabbit PK study. However, the concentration profile in cervical tissue does not support this assessment at first glance as it is steady with time from 8 hours to 90 days postinsertion. However, one would generally expect a lag (as is observed with the loading of vaginal tissues with TFV), and the presence of an *in vivo* LNG burst may be negated by this physiological lag. The variability in the cervical tissue data may also make the observation of this *in vivo* burst difficult. Regardless, of the presence/absence of this burst, the steady cervical tissue levels throughout the 90-day period are encouraging.

TFV vaginal fluid levels exceeded 10^4 ng/g in nearly all animals at all time-points from 24 hours postinsertion onward for both ring prototypes (with few exceptions in the 10^3 ng/g range and many readings exceeding 10^6 ng/g). Mean values were all in the 10^5 to 10^6 ng/g range, and trend slightly lower, but are comparable to those achieved from the TFV-only variant, which released 17 mg/d *in vivo* vs. the 12-13 mg/d achieved from these combination rings [16]. The partially effective TFV 1% gel has been observed to generate peak vaginal fluid levels in the 10^6 ng/g range in sheep, indicating that this IVR can generate clinically relevant TFV concentrations for extended duration. Furthermore, 10^3 ng/g was identified as a lower cutoff for a higher efficacy group (74% reduction in HIV infection) in the CAPRISA 004 study of the TFV 1% Gel [4] and it is encouraging that all concentration readings in all animals were above this point during the study. However, caution is encouraged when using this 1000 ng/g as a gold standard for TFV

efficacy, as it is unclear from the study reports how long after gel dosing those readings were obtained.

The vaginal tissue compartment is the eventual primary site of action for any product designed to interrupt sexual HIV transmission, and thus is the most important predictor of efficacy in preclinical PK evaluation. Our TFV tissue concentration results were encouraging. The EC₉₉ of TFV has been estimated at 5 µM in cell culture, which equates to approximately 1×10^3 ng/g [27]. All mean TFV tissue concentrations from day 14 to day 90 onward well exceeded this value, although some individual readings were lower. In total the TFV PK data obtained here again confirms that a TFV dose in the 10 mg/d range in a sustained fashion from an IVR is clinically relevant and warrants clinical investigation. However, caution should be used when comparing PK results between women and sheep. Even though the sheep model anatomically approximates the human vaginal tract, it is not clear whether histological differences may result in disparities in drug transport, metabolism, and elimination between species. This principle is well illustrated below for LNG.

Topical microdose administration of progestins primarily achieves contraception through local effects (e.g. the thickening of cervical mucus to prevent sperm transport) [28], and thus our measurement of LNG in the cervical tissue over time during IVR administration is the primary indicator of efficacy in this study. As we noted in our PK assessment of LNG in rabbits [19], the kinetics of the concentration profile are more important than the exact concentration magnitude. Delivery of 10-20 µg/d LNG locally is clinically known to achieve reliable contraception in women, most notably from the Mirena and Skyla IUS, as well as from the WHO LNG IVR. Encouraging here are the

steady levels of LNG achieved over time, as well as the distinguishability of the two doses given by Prototype I and II at most time-points (not statistically, but through the comparison of averages nonetheless). We were not able to quantify LNG in plasma, except in the first few time-points in the study. Our LOQ was 25 pg/mL, well below the ~150-300 pg/mL observed in women using the discontinued 20 µg/day LNG-releasing IVR [21]. This further illustrates that the PK properties of drugs in sheep are not well-enough understood to make direct comparisons between species.

4.6 Conclusions

The TFV/LNG IVR formulation proved to be stable when stored at 40°C for up to 5 months, with the exception of some drift in the average TFV release rate and LNG burst release, both of which less than expected based on our previous investigations of the two phenomena. Our PK assessment in sheep confirmed that this system can achieve clinically-relevant doses of both TFV, which remains the only anti-HIV molecule with clinical efficacy data for HIV PrEP (including its prodrug TDF), and LNG, a long-studied molecule for topical microdose contraception. The TFV/LNG IVR and the TFV-only IVR have been transferred to GMP manufacturing and are currently slated for a Phase I clinical investigation. The TFV/LNG IVR is the first in a new class of exciting, long-acting MPT, any of which may become critical tools in overcoming the PrEP adherence battle through their ability to provide simultaneous contraception and to provide protection for long durations, mitigating the need for on-demand or daily user intervention.

4.7 Acknowledgements

This work was supported by CONRAD of Eastern Virginia Medical School through a cooperative agreement with USAID. The sheep PK study was performed at MPI Research (Mattawan, Michigan) under the supervision of Melissa Peet. Opinions expressed by the authors do not necessarily reflect those of USAID.

4.8 References

- [1] UNAIDS, Global report: UNAIDS report on the global AIDS epidemic 2013, in, Joint United Nations Programme on HIV/AIDS (UNAIDS), 2013.
- [2] United Nations Fund for Population Activities, Comprehensive condom programming: A strategic response to HIV and AIDS, in, 2010.
- [3] Q. Abdool Karim, S.S. Abdool Karim, J.A. Frohlich, A.C. Grobler, C. Baxter, L.E. Mansoor, A.B. Kharsany, S. Sibeko, K.P. Mlisana, Z. Omar, T.N. Gengiah, S. Maarschalk, N. Arulappan, M. Mlotshwa, L. Morris, D. Taylor, Effectiveness and safety of tenofovir gel, an antiretroviral microbicide, for the prevention of HIV infection in women, *Science*, 329 (2010) 1168-1174.
- [4] S.S. Abdool Karim, A.D. Kashuba, L. Werner, Q. Abdool Karim, Drug concentrations after topical and oral antiretroviral pre-exposure prophylaxis: implications for HIV prevention in women, *Lancet*, 378 (2011) 279-281.
- [5] J.A. van Laarhoven, M.A. Krufft, H. Vromans, In vitro release properties of etonogestrel and ethinyl estradiol from a contraceptive vaginal ring, *Int J Pharm*, 232 (2002) 163-173.
- [6] J.M. Baeten, D. Donnell, P. Ndase, N.R. Mugo, J.D. Campbell, J. Wangisi, J.W. Tappero, E.A. Bukusi, C.R. Cohen, E. Katabira, A. Ronald, E. Tumwesigye, E. Were, K.H. Fife, J. Kiarie, C. Farquhar, G. John-Stewart, A. Kakia, J. Odoyo, A. Mucunguzi, E. Nakku-Joloba, R. Twesigye, K. Ngure, C. Apaka, H. Tamooh, F. Gabona, A. Mujugira, D. Panteleeff, K.K. Thomas, L. Kidoguchi, M. Krows, J. Revall, S. Morrison, H. Haugen, M. Emmanuel-Ogier, L. Ondrejcek, R.W. Coombs, L. Frenkel, C. Hendrix, N.N. Bumpus, D. Bangsberg, J.E. Haberer, W.S. Stevens, J.R. Lingappa, C. Celum, Antiretroviral prophylaxis for HIV prevention in heterosexual men and women, *N Engl J Med*, 367 (2012) 399-410.
- [7] C. Dobard, S. Sharma, A. Martin, C.P. Pau, A. Holder, Z. Kuklenyik, J. Lipscomb, D.L. Hanson, J. Smith, F.J. Novembre, J.G. Garcia-Lerma, W. Heneine, Durable protection from vaginal simian-human immunodeficiency virus

- infection in macaques by tenofovir gel and its relationship to drug levels in tissue, *J Virol*, 86 (2012) 718-725.
- [8] U.M. Parikh, C. Dobard, S. Sharma, M.E. Cong, H. Jia, A. Martin, C.P. Pau, D.L. Hanson, P. Guenther, J. Smith, E. Kersh, J.G. Garcia-Lerma, F.J. Novembre, R. Otten, T. Folks, W. Heneine, Complete protection from repeated vaginal simian-human immunodeficiency virus exposures in macaques by a topical gel containing tenofovir alone or with emtricitabine, *J Virol*, 83 (2009) 10358-10365.
- [9] R. Singer, P. Mawson, N. Derby, A. Rodriguez, L. Kizima, R. Menon, D. Goldman, J. Kenney, M. Aravantinou, S. Seidor, A. Gettie, J. Blanchard, M. Piatak, Jr., J.D. Lifson, J.A. Fernandez-Romero, M. Robbiani, T.M. Zydowsky, An intravaginal ring that releases the NNRTI MIV-150 reduces SHIV transmission in macaques, *Sci Transl Med*, 4 (2012) 150ra123.
- [10] J.M. Smith, R. Rastogi, R.S. Teller, P. Srinivasan, P.M. Mesquita, U. Nagaraja, J.M. McNicholl, R.M. Hendry, C.T. Dinh, A. Martin, B.C. Herold, P.F. Kiser, Intravaginal ring eluting tenofovir disoproxil fumarate completely protects macaques from multiple vaginal simian-HIV challenges, *Proc Natl Acad Sci U S A*, (2013).
- [11] J. Marrazzo, G. Ramjee, G. Nair, T. Palanee, B. Mkhize, C. Nakabiito, M. Taljaard, J. Piper, K. Gomez Feliciano, M. Chirenje, Pre-exposure Prophylaxis for HIV in Women: Daily Oral Tenofovir, Oral Tenofovir/Emtricitabine, or Vaginal Tenofovir Gel in the VOICE Study (MTN 003) (Paper 26LB), in: 20th Conference on Retroviruses and Opportunistic Infections, Atlanta, Georgia, 2013.
- [12] D.R. Friend, P.F. Kiser, Assessment of topical microbicides to prevention HIV-1 transmission: Concepts, testing, lessons learned, *Antiviral Res*, (2013).
- [13] D.R. Friend, J.T. Clark, P.F. Kiser, M.R. Clark, Multipurpose prevention technologies: Products in development, *Antiviral Res*, (2013).
- [14] A. Novak, C. de la Loge, L. Abetz, E.A. van der Meulen, The combined contraceptive vaginal ring, NuvaRing: an international study of user acceptability, *Contraception*, 67 (2003) 187-194.
- [15] F.J. Roumen, M.M. op ten Berg, E.H. Hoomans, The combined contraceptive vaginal ring (NuvaRing): first experience in daily clinical practice in The Netherlands, *Eur J Contracept Reprod Health Care*, 11 (2006) 14-22.
- [16] T.J. Johnson, M.R. Clark, T.H. Albright, J.S. Nebeker, A.L. Tuitupou, J.T. Clark, J. Fabian, R.T. McCabe, N. Chandra, G.F. Doncel, D.R. Friend, P.F. Kiser, A 90-day tenofovir reservoir intravaginal ring for mucosal HIV prophylaxis, *Antimicrob Agents Chemother*, 56 (2012) 6272-6283.

- [17] R.K. Malcolm, Vaginal Rings for Controlled-Release Drug Delivery, in: M.J. Rathbone (Ed.) Modified-Release Drug Delivery Technology, Informa Healthcare, New York, 2008, pp. 499-510.
- [18] C.J. Timmer, T.M. Mulders, Pharmacokinetics of etonogestrel and ethinylestradiol released from a combined contraceptive vaginal ring, *Clin Pharmacokinet*, 39 (2000) 233-242.
- [19] J.T. Clark, M.R. Clark, N.B. Shelke, T.J. Johnson, E.M. Smith, A.K. Andreasen, J.S. Nebeker, J. Fabian, D.R. Friend, P.F. Kiser, Engineering a segmented dual-reservoir polyurethane intravaginal ring for simultaneous prevention of HIV transmission and unwanted pregnancy, *PLoS ONE* 9 (2014) e88509.
- [20] S. Koetsawang, G. Ji, U. Krishna, A. Cuadros, G.I. Dhall, R. Wyss, J. Rodriguez la Puente, A.T. Andrade, T. Khan, E.S. Kononova, et al., Microdose intravaginal levonorgestrel contraception: a multicentre clinical trial. I. Contraceptive efficacy and side effects. World Health Organization. Task Force on Long-Acting Systemic Agents for Fertility Regulation, *Contraception*, 41 (1990) 105-124.
- [21] B.M. Landgren, A.R. Aedo, S.Z. Cekan, E. Diczfalusy, Pharmacokinetic studies with a vaginal delivery system releasing levonorgestrel at a near zero order rate for one year, *Contraception*, 33 (1986) 473-485.
- [22] J.T. Clark, T.J. Johnson, M.R. Clark, J.S. Nebeker, J. Fabian, A.L. Tuitupou, S. Ponnappalli, E.M. Smith, D.R. Friend, P.F. Kiser, Quantitative evaluation of a hydrophilic matrix intravaginal ring for the sustained delivery of tenofovir, *J Control Release*, 163 (2012) 240-248.
- [23] M.R. Clark, T.J. Johnson, R.T. McCabe, J.T. Clark, A. Tuitupou, H. Elgandy, D.R. Friend, P.F. Kiser, A hot-melt extruded intravaginal ring for the sustained delivery of the antiretroviral microbicide UC781, *J Pharm Sci*, 101 (2012) 576-587.
- [24] T.J. Johnson, K.M. Gupta, J. Fabian, T.H. Albright, P.F. Kiser, Segmented polyurethane intravaginal rings for the sustained combined delivery of antiretroviral agents dapivirine and tenofovir, *Eur J Pharm Sci*, 39 (2010) 203-212.
- [25] Food and Drug Administration, Center for Drug Evaluation and Research, Guidance for industry: Waiver of in vivo bioavailability studies for immediate-release solid oral dosage forms based on a biopharmaceutics classification system, in, August 2000.
- [26] J.A. van Laarhoven, M.A. Krufft, H. Vromans, Effect of supersaturation and crystallization phenomena on the release properties of a controlled release device based on EVA copolymer, *J Control Release*, 82 (2002) 309-317.

- [27] J. Balzarini, S. Aquaro, C.F. Perno, M. Witvrouw, A. Holy, E. De Clercq, Activity of the (R)-enantiomers of 9-(2-phosphonylmethoxypropyl)-adenine and 9-(2-phosphonylmethoxypropyl)-2,6-diaminopurine against human immunodeficiency virus in different human cell systems, *Biochem Biophys Res Commun*, 219 (1996) 337-341.
- [28] S. Rose, A. Chaudhari, C.M. Peterson, Mirena (Levonorgestrel intrauterine system): a successful novel drug delivery option in contraception, *Adv Drug Deliv Rev*, 61 (2009) 808-812.

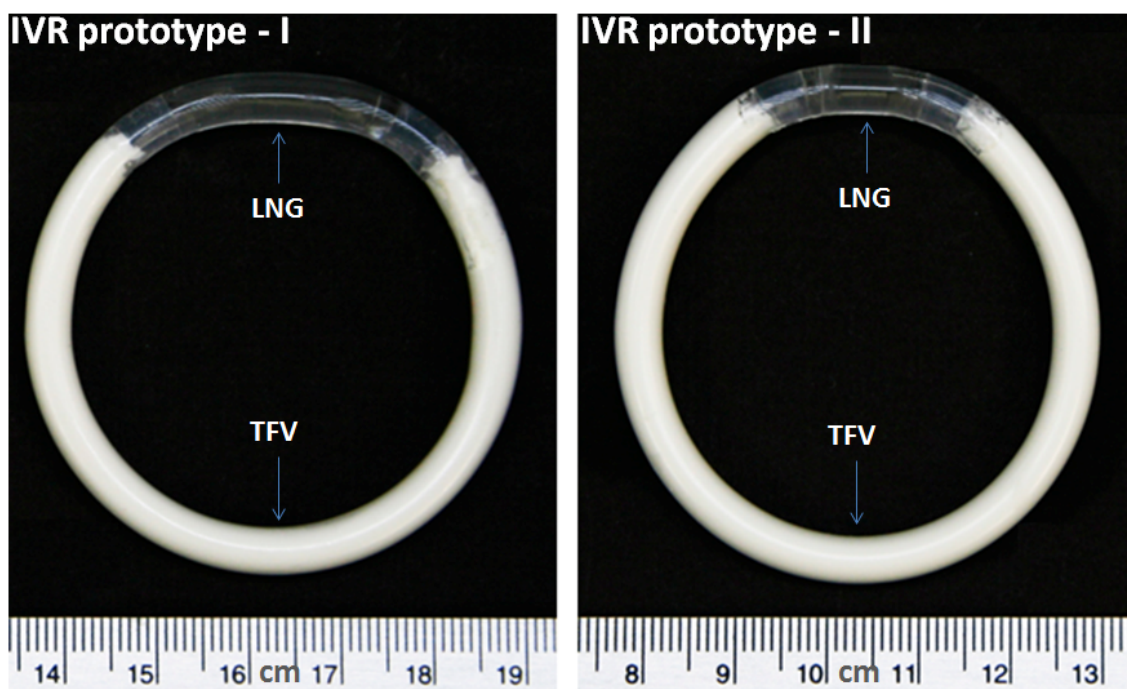


Figure 4.1: Photographs of TFV/LNG IVR Prototypes I and II.

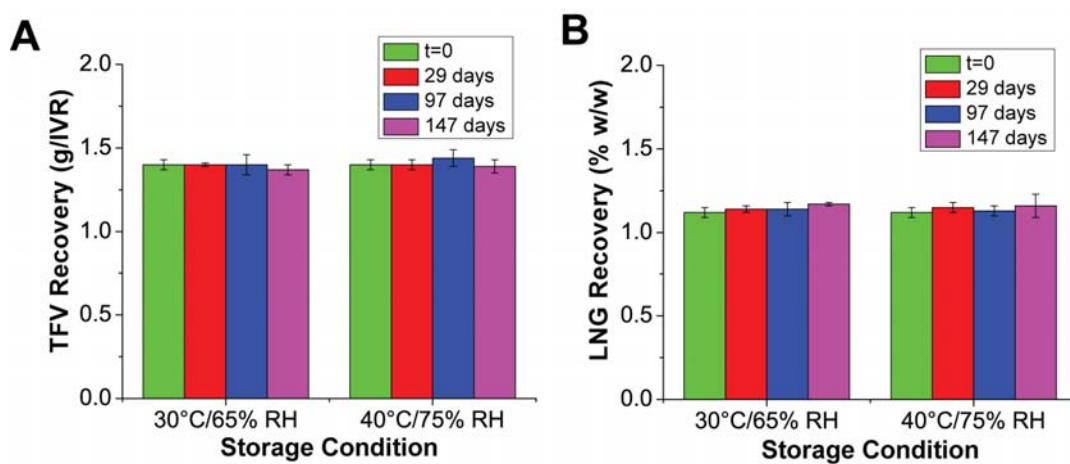


Figure 4.2: Recovery of (A) TFV and (B) LNG by residual extractions from TFV/LNG IVR (Prototype I) following storage at either 30°C/65% RH or 40°C/75% RH for up to 147 days. Data represent N=5, mean \pm SD.

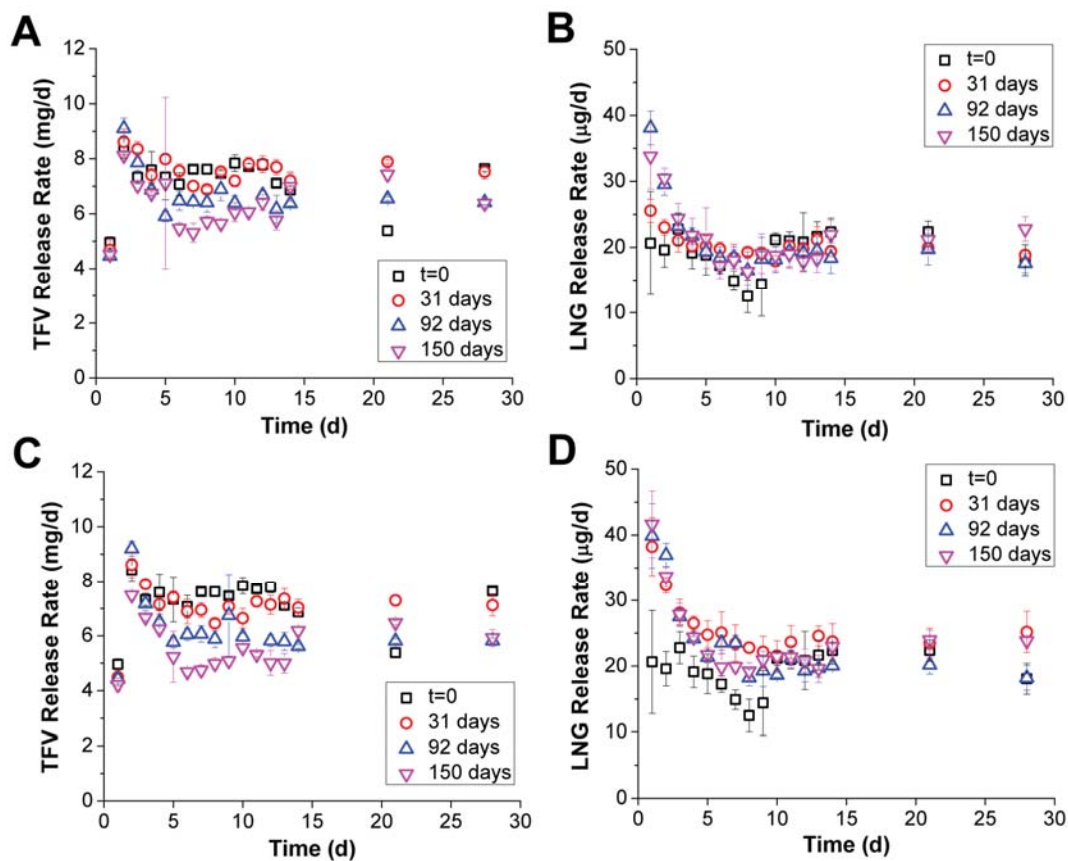


Figure 4.3: *In vitro* release rate profiles of TFV and LNG from TFV/LNG IVR (Prototype I) following storage following storage at either 30°C/65% RH (A, B) or 40°C/75% RH (C, D) for up to 150 days. Data represent N=5, mean \pm SD.

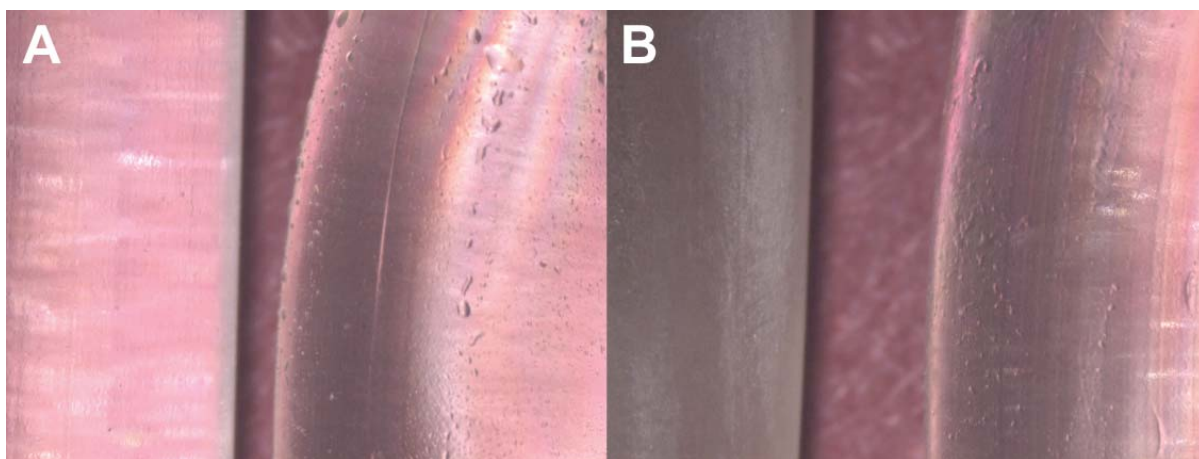


Figure 4.4: Prevention of LNG surface crystallization for 164 days (total) at 40°C by glycerol self-coating on a full TFV/LNG IVR (right), shown in comparison to (A, left) a placebo co-ex segment and (B, left) an uncoated co-ex segment with extensive LNG re-crystallization.

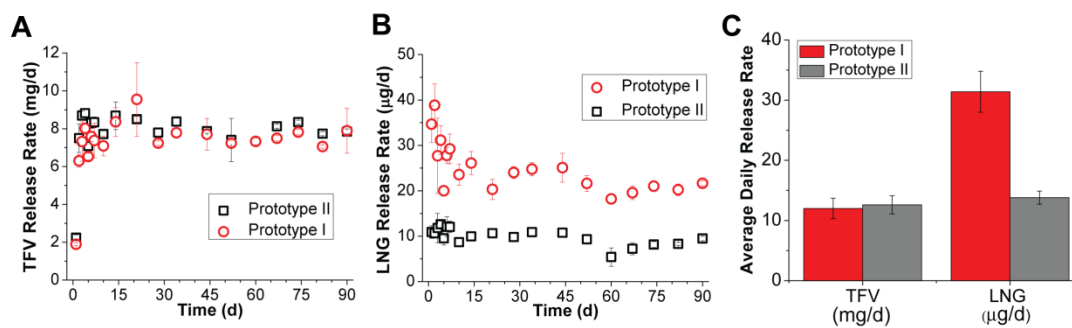


Figure 4.5: *In vitro* release of (A) TFV and (B) LNG under sink conditions from IVR Prototypes I and II. (C) *In vivo* release estimated from residual extractions of IVRs following 90-day insertion in sheep. Data represent mean \pm SD, N=5 (*in vitro*), N=7 (Prototype I *in vivo*) or N=6 (Prototype II *in vivo*).

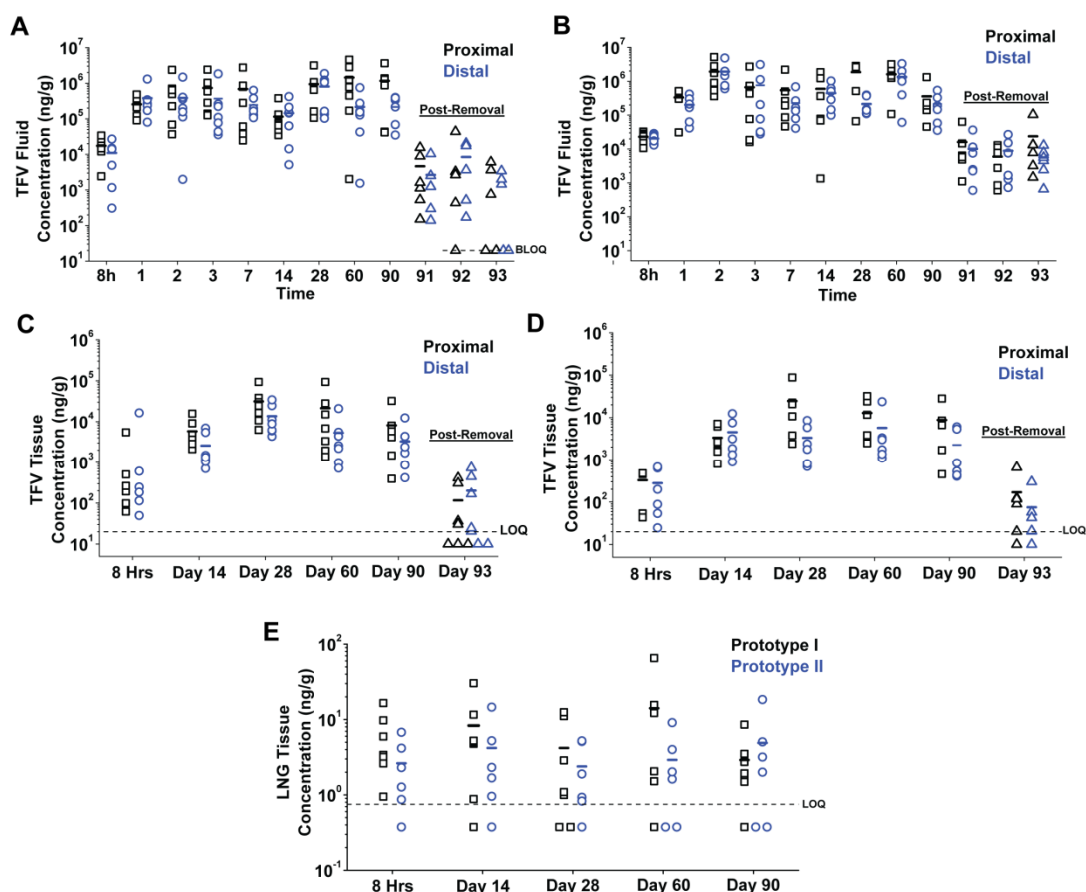


Figure 4.6: Individual animal results of the sheep pharmacokinetic study. Horizontal bars represent mean values. (A,B) TFV levels in vaginal fluid of sheep treated with IVR prototype I (A) or II (B) for 90 days. Some samples were below limit of quantification (BLOQ) during the 72-hour washout period (days 91-93), and mean values were not calculated for these points. Some samples were lost at the study site during days 91-93. (C,D) TFV levels in vaginal tissue biopsies from sheep treated with IVR Prototype I (C) or II (D) for 90 days and (E) LNG levels in cervical tissue biopsies. For tissue data, values below LOQ were plotted as LOQ/2 (10 ng/g TFV and 0.375 ng/g LNG) and assigned that value for calculating mean values.

CHAPTER 5

SUMMARY AND FUTURE DIRECTIONS

5.1 Research Summary and Context

Chapters 2 through 4 summarize a wide array of the research and preclinical development of the HPEU TFV IVR and the dual-segment TFV/LNG multipurpose IVR. In Chapter 2, the first-generation matrix-type injection-molded TFV HPEU IVR was presented as a case study for the rigorous engineering design of matrix-type IVR, with many of the concepts extending to cylindrical matrix-type drug delivery systems in general. Our explicit solution (Equation 2.4) to Roseman and W.I. Higuchi's classic model for cylindrical reservoirs [1, 2] allowed us to accurately extrapolate release rates from 7 out to 90 days, and the mechanical model (Equation 2.6) provided the first insight into the effects of IVR design choices on mechanical properties. Very interesting is the interplay between drug release and mechanical compressibility, which are intimately coupled for matrix devices containing large amounts of undissolved drug. The second-generation of the TFV HPEU IVR, described in detail in the final chapters of the Ph.D. thesis of Todd Johnson (Department of Bioengineering, University of Utah), utilized a hollow reservoir design which allowed for constant drug release rates and mechanical properties over time. This technology was adapted for use in the TFV/LNG IVR.

Chapter 3 described the incorporation of a solid PEU reservoir into the second-generation TFV IVR for the creation of the dual-segment TFV/LNG IVR, the first long-acting system designed to simultaneously prevent HIV infection and unintended pregnancy. When the TFV/LNG IVR project was initiated, we desired to rigorously understand the two-stage nature of release from solid reservoir systems. This behavior was discussed in one of the NuvaRing development papers [3], but not mathematically described. Due to the higher cross-sectional area (i.e. diffusion path) of our reservoir cross-section, the interplay between matrix and reservoir behavior was of even more

importance, with burst durations of up to several days, whereas burst release of etonogestrel from NuvaRing typically occurs in 24 hours. We used a piecewise-approach, as well as a moving concentration boundary, to quantitatively address the knowledge gap in the description of reservoir-type IVR. We also, for the first time, illustrated the importance of drug loading in the rate-controlling membrane. Again, this is potentially more important for our system due to the increased diffusion path and its influence on the lag or burst behavior at early times from reservoir systems. These concepts are universal to any reservoir device, provided that the geometry is well understood and accounted for. Also remarkable is the utilization of an improved two-segment IVR for the simultaneous delivery of microdose progestin and a "macro-dose" of an NtRTI. Use of induction welding technology and the chemically diverse PEU elastomer class allowed us to create a ring that retained impressive mechanical integrity, even following the hydration at swelling of the TFV segment (at least 85% of the ring circumference), around the nonhydrating, rigid LNG segment.

In Chapter 4, we exposed the TFV/LNG IVR to the rigors of preclinical development. The formulation was remarkably stable throughout during 5 months under accelerated conditions, with the exception of some instabilities in the release kinetics of both drugs. However, these instabilities are well understood and were less prominent than expected for this system. During this work, we discovered the unexpected benefit of the glycerin present in the TFV segment leaching out into the packaging on storage and forming a protective coating around the ring, preventing LNG surface crystallization and potentially hindering the burst release. This eliminated the need for application of a surface coating (which was likely also to contain glycerin), and will hopefully eliminate

the need for cold storage of the eventual product (also successfully investigated as a method for prevention of surface crystallization on the LNG segment), a desired trait for developing world-bound products such as these IVR. The TFV/LNG IVR performed well in a sheep PK study, although analytical limitations prevented us from a more complete compartmental PK description for LNG. Nonetheless, these two studies demonstrated the potential of the system to be sufficient for a clinical investigation.

5.2 Discussion and Future Recommendations

In this dissertation, the reader has been exposed to the full range of IVR design and manufacturing complexity: from the monolithic, injection molded, matrix-type first generation TFV IVR in Chapter 2, to the dual-segment, dual-reservoir, dual-indication TFV/LNG IVR in Chapters 3 and 4. No future recommendations will be made regarding the design of the former, as it was replaced by the second-generation TFV reservoir platform [4]. However, some commentary is warranted regarding the theoretical aspects of the work. In this manuscript, we were the first to publish a mathematical model for drug delivery regarding the Lambert-W function [5] (Equation 2.4), and also the first to utilize the 40-year-old Roseman/Higuchi implicit solution for drug release from cylinders for analysis of drug release from an IVR. Higuchi's famous equation for thin films [6], which is the planar analog to Equation 2.4, is sometimes used in the context of drug delivery from IVR [7]. When deriving Equation 1.3/2.4, Roseman noted that the Higuchi equation was a valid approximation at early times, due to the low error in approximating the annulus outside the diffusion front as a thin plane of length equal to the IVR circumference. However, as the diffusion front progresses inward, the geometric error

will result in a deviation from square-root-of-time behavior, necessitating the use of Equation 2.4. A similar phenomenon is encountered for Equation 1.2/3.2 (matrix cylinder diffusion-only model), where a first-term approximation also gives square-root-of-time dependence, but a second negative term, which must be considered after 20-30% of cumulative release, depends linearly on time. It is often acceptable to use simpler models to provide meaningful insight to the design of drug delivery systems, as long as the assumptions made (and some estimate of the resulting error) are understood. An attempt should always be made to construct drug diffusion models from first principles when possible, as the exercise will lead the researcher to a better understanding of the underlying mechanisms at work. Any students seeking to investigate this topic are referred to the review articles of Juergen Siepmann [8-12], including one in particular [13] that served as a catalyst for my Ph.D. work.

Although IVR are generally classified as drug products, they are also medical devices, meaning that concepts beyond typical pharmaceutical formulation need be understood, requiring some engineering expertise. If IVR are to be further investigated and utilized as drug delivery systems, an attempt should be made to couple the compression properties of IVR with the elastic properties of the vaginal wall. Our use of the load at 10% compression (F_{10}) for comparison to existing rings should serve only as a first-order rough method for estimating IVR acceptability. It is thought that the excessive stiffness of the WHO LNG IVR caused vaginal tissue damage and that this was a major factor in the discontinuation of its development [14]. IVR also rely on sufficient retractile force to remain in place and remain effective. The analysis of vaginal biomechanics and

force balance with an inserted IVR would be an excellent project for a biomedical or mechanical engineering student.

There are several ways in which the TFV/LNG IVR could be improved before its full consideration as a clinical product. First, as evidenced by Figures 3.S3 and 3.S4, the manufacturing of this device is quite complex and may be difficult to scale into high-volume manufacturing (e.g. 10^5 - 10^6 units per year). The main process impediment is likely the 6 induction welds required to fabricate the device. Furthermore, each of the two split-die welds used to assemble the final ring require a >1-minute heating cycle. If a single over-molding step could be used to both join the two segments and generate the PEU end-caps, this would eliminate 3 net process steps and greatly streamline the manufacturing. Such a process change may require the preannealing of the two extrudates (HPEU tubing and LNG-loaded PEU) to the correct curvature, which could cause problems with filling of the TFV-loaded paste. Also recommended is the use of milled (i.e. cryo-ground) PEU and a blending with LNG powder. This would likely eliminate the need for roll-coating and the first compounding extrusion prior to co-axial extrusion. We investigated this early in our research but had difficulty in sufficiently drying PEU powders with our equipment due to their extremely high surface area and ability to readily adsorb and retain surface water.

The two-stage model for the LNG segment (Equation 3.11) accurately describes drug release from a solid reservoir where the entirety of the drug load is dissolved at $t=0$. However, as demonstrated in Figure 3.S2 (and experimentally in Figures 3.3A and 3.4D), there is some inaccuracy in the use of an instantaneous changeover between matrix and reservoir behavior. Although this was expected, the change in concentration profiles

between the matrix and reservoir stages could be described, replacing the discontinuity at t_b with a third, intermediate phase. During our research, Siepmann published a similar first-order diffusion-only, "nonconstant activity source" model for reservoir cylinders where drug is allowed to release in all directions [10]; however, in simplifying the model to only consider radial drug release (as occurs in IVR), we were able to elucidate a much simpler exponential time constant (' a '). Equation 3.11 also considers the change in mass of dissolved drug in the RCM (contrary to the model presented in Chapter 2), which increases accuracy. Although algebraically challenging, the time constant obtained when considering the RCM mass change was surprisingly simpler than when it was neglected.

It is not clear why a greater burst release was observed *in vivo* than *in vitro* from the LNG segment in the rabbit PK study (Figure 3.7), and also not clear from the available data whether this occurred in the sheep PK study of the full IVR (Figure 4.6). Adequate volumes were used to maintain sink conditions during *in vitro*, meaning it is nearly impossible for higher flux *in vivo* to occur by passive diffusion alone. LNG likely exhibits better solubility in vaginal fluid than the simple PBS solution used in parallel *in vitro* studies due to the presence of naturally-present solubilizing agents. Even though drug is molecularly dissolved in the rate-controlling PEU, there may be a small amount of LNG at the polymer-fluid interface that can be released by surface erosion, the rate of which would depend on the solubility of drug in media.

A criticism leveled at the hollow HPEU TFV reservoir system is the potential for a bacterial reservoir to form within the liquid core during IVR use, thus potentially being released in the event of a tubing wall failure and resulting in an acute bacterial infection. The potential for bacterial growth in the IVR core both during dry storage and during use

are currently under investigation by Kiser and colleagues. The effective pore size of a hydrated HPEU is likely many orders of magnitude smaller than the smallest dimension of any bacterium present in the vaginal milieu, meaning such bacterial infiltration would have to occur during manufacturing of the TFV segment, or through a tubing wall defect. As vaginal products are not typically manufactured under sterile conditions, there may be a need to quantify bacterial load during the manufacturing of the TFV segment.

A major limitation in the TFV/LNG IVR, and with all PrEP IVR to-date, is that the required prophylactic ARV dose for HIV prevention is not known. Any effective PrEP IVR must result in effective levels at all potential sites of infection throughout the duration of use [15]. As an estimate of potential efficacy, most PK studies to date have quantified ARV levels in large vaginal tissue biopsies and have attempted to compare these data to *in vitro* estimates of efficacy. While these large biopsies can be taken in various longitudinal and circumferential positions in the tract, they represent a depth-average of drug concentration, and do not necessarily represent the exact concentration at the three-dimensional location of an HIV target cell. Further complicating this assessment for TFV is that its active by product, TFV diphosphate (TFV-DP), is formed in cells [16], and thus TFV concentration never represents the true efficacy of a TFV delivery system. We have investigated the measurement of drug TFV concentration as a function of depth in rabbit vaginal tissue cross-sections using MALDI-MS/MS. This type of measurement, coupled with a detailed three-dimensional PK simulation of drug delivery from an IVR, could become a powerful tool to estimate necessary drug release rates for HIV prevention. Geonnotti and Katz performed a vaginal drug transport simulation on a two-dimensional cross-section of the vaginal tract and surrounding tissues, which serves

as a starting point for these efforts [17]. In the Appendix, the reader will find a proposed strategy for modeling drug and virus transport in the vaginal tract following drug release from an IVR. This proposal was written into an NIH grant proposal, which was ultimately funded. The PK modeling effort will be undertaken by Patrick Kiser, Igal Szleifer, and colleagues at Northwestern University.

In summary, this dissertation should illustrate the necessity of incorporating a fundamental physical understanding in a rigorous engineering approach during the conception and design of IVR, and drug/device combinations in general.

5.3 References

- [1] T.J. Roseman, Release of steroids from a silicone polymer. *J Pharm Sci* 61(1) (1972) 46-50.
- [2] T.J. Roseman, W.I. Higuchi, Release of medroxyprogesterone acetate from a silicone polymer. *J Pharm Sci* 59(3) (1970) 353-357.
- [3] J.A. van Laarhoven, M.A. Krufft, H. Vromans, In vitro release properties of etonogestrel and ethinyl estradiol from a contraceptive vaginal ring. *Int J Pharm* 232(1-2) (2002) 163-173.
- [4] T.J. Johnson, M.R. Clark, T.H. Albright, J.S. Nebeker, A.L. Tuitupou, J.T. Clark, J. Fabian, R.T. McCabe, N. Chandra, G.F. Doncel, D.R. Friend, P.F. Kiser, A 90-day tenofovir reservoir intravaginal ring for mucosal HIV prophylaxis. *Antimicrob Agents Chemother* 56(12) (2012) 6272-6283.
- [5] R.M. Corless, G.H. Gonnet, D.E.G. Hare, D.J. Jeffrey, D.E. Knuth, On the Lambert W function. *Adv Comput Math* 5(1) (1996) 329-359.
- [6] T. Higuchi, Mechanism of Sustained-Action Medication. Theoretical Analysis of Rate of Release of Solid Drugs Dispersed in Solid Matrices. *J Pharm Sci* 52 (1963) 1145-1149.
- [7] K. Malcolm, D. Woolfson, J. Russell, P. Tallon, L. McAuley, D. Craig, Influence of silicone elastomer solubility and diffusivity on the in vitro release of drugs from intravaginal rings. *J Control Release* 90(2) (2003) 217-225.

- [8] J. Siepmann, A. Gopferich, Mathematical modeling of bioerodible, polymeric drug delivery systems. *Adv Drug Deliv Rev* 48(2-3) (2001) 229-247.
- [9] J. Siepmann, N.A. Peppas, Mathematical modeling of controlled drug delivery. *Adv Drug Deliv Rev* 48(2-3) (2001) 137-138.
- [10] J. Siepmann, F. Siepmann, Modeling of diffusion controlled drug delivery. *J Control Release* 161(2) (2012) 351-362.
- [11] J. Siepmann, F. Siepmann, Mathematical modeling of drug dissolution. *Int J Pharm* 453(1) (2013) 12-24.
- [12] J. Siepmann, N.A. Peppas, Higuchi equation: derivation, applications, use and misuse. *Int J Pharm* 418(1) (2011) 6-12.
- [13] J. Siepmann, F. Siepmann, Mathematical modeling of drug delivery. *Int J Pharm* 364(2) (2008) 328-343.
- [14] E. Weisberg, I.S. Fraser, J. Baker, D. Archer, B.M. Landgren, S. Killick, P. Soutter, T. Krause, C. d'Arcangues, A randomized comparison of the effects on vaginal and cervical epithelium of a placebo vaginal ring with non-use of a ring. *Contraception* 62(2) (2000) 83-89.
- [15] P.F. Kiser, P.M. Mesquita, B.C. Herold, A perspective on progress and gaps in HIV prevention science. *AIDS Res Hum Retroviruses* 28(11) (2012) 1373-1378.
- [16] J. Balzarini, L. Naesens, E. De Clercq, New antivirals - mechanism of action and resistance development. *Curr Opin Microbiol* 1(5) (1998) 535-546.
- [17] A.R. Geonnotti, D.F. Katz, Compartmental transport model of microbicide delivery by an intravaginal ring. *J Pharm Sci* 99(8) (2010) 3514-3521.

APPENDIX

PROPOSED SPATIAL PK MODEL FOR PREDICTION OF DRUG
AND VIRUS TRANSPORT IN THE VAGINAL TRACT

A.1 Context

The following text was adapted from an eventually-funded NIH multiproject program grant (U19), specifically, from one of three specific aims of the "Research Design and Methods" section of a project entitled "Pharmacokinetics and Biodistribution of Antiretrovirals and HIV-1 in Macaques". The two remaining aims, not discussed here, proposed the design and manufacturing of new IVR prototypes and the spatial mapping of drug concentrations following their testing in the pig-tailed macaque (PTM) model, as well as the localization of fluorescently labeled HIV pseudovirions in pig-tailed macaques. The original text was conceived and authored by Justin T. Clark, Igal G. Szleifer, and Patrick F. Kiser.

A.2 Rationale

One of the most significant knowledge gaps in the topical PrEP field has been the lack of a quantitative mechanistic description of drug PK and virus distribution in the vaginal tissue. An experimentally validated model which couples drug release to complex mass transport processes occurring in the FGT and surrounding tissue, as well as with the existing PD data available for ARVs, could become an invaluable tool in the future design of effective microbicide products. We propose to model ARV transport in the FGT using a multiscaled approach. Microscopic, molecular dynamics simulations will be constructed to determine drug and virus mobility in various compartments. Continuum-scale models, based primarily on linear transport theory and MRI of the PTM FGT, will be used to describe bulk ARV transport and determine effective tissue concentrations of drugs and their metabolites as a function of spatial position, time, and release rate from an IVR. Due to the complexities of the FGT and of the governing partial differential

equations (PDE) that describe both diffusive and convective drug transport, as well as chemical reactions and elimination, we will utilize COMSOL or in-house software to numerically resolve ARV concentration profiles within MRI-derived, CAD-generated renderings of the PTM FGT. An array of physiologically relevant constants will be required for the continuum-scale model, including vaginal fluid velocity, effective drug diffusivities through the vaginal epithelium and lamina propria, and rate constants for first-order drug elimination from the tissues into the plasma compartment. These parameters will be obtained by detailed simulations of the molecular dynamics of ARV mobility at the microscale, results of which will be compared to experimental data. We will use a similar multiscaled approach to describe the transport of HIV into the tissue.

A.3 Microscale Molecular Dynamics Simulations

To determine ARV and virus mobility in various FGT domains (i.e. vaginal epithelium, lamina propria), we will construct microscopic models, results from which can be used as inputs into the continuum-scale transport model. We have performed preliminary molecular dynamics simulations on a simple model system. Figure A.1 shows the paracellular distribution of a model drug (A) and virus (B) in a simplified structure mimicking epithelial tissue. It is clear from the graphics shown that there are differences in the mobility and resulting distribution of the model drug as compared to virus. We expect that such mobility modeling within structures derived from histological examination will be instrumental in providing exquisite information as to the microscopic nature of drug and virus distributions within tissues, as well as their effective tissue diffusivities required for the continuum model described below.

A.4 Continuum-scale Transport Model

Using MRI scans generated at the University of Washington we will generate 3D representations of PTM FGT, which will ultimately be rendered in the CAD software package SolidWorks. The continuum-scale model will consist of four principal compartments: (1) drug delivery system (25 mm OD macaque IVR), (2) vaginal lumen, (3) vaginal epithelium, and (4) lamina propria. Additional tissues such as ectocervix will also be included if drug loss into these compartments is determined to have a large impact on model outcomes. This 3D CAD representation of PTM FGT will be imported into COMSOL or custom software for model construction. In general, time-dependent effective bulk transport in biological tissue can be approximated by PDE in the form of Equation A.1 [1], a modified form of the linear transport equation (see Figure A.2 for all equations in this Appendix).

A.5 Establishing the Device/Lumen Boundary

Solutions to the vaginal transport model will depend heavily on drug/virus input boundaries. In the case of water-soluble drugs, it is likely that an effective sink is maintained *in vivo* (see Chapter 4). In this case, we will first estimate the *in vivo* drug release profile, by a combination of residual drug analysis from removed devices and analysis of drug release *in vitro*. We will then introduce a drug-generating torus in the luminal compartment of the rendered FGT, whereby the outer surface is assigned as a steady flux boundary, whose magnitude will be defined as the estimated *in vivo* release rate divided by the outer surface area of the IVR. In previous studies, we have observed that *in vivo* release of hydrophobic ARV may be limited by its solubility in the surrounding media [2, 3]. In this case, an *in vitro* sink will not be a valid method for

release rate determination, and *in vivo* fluxes need be approximated by residual drug in IVRs following PTM studies. Modulation of model *in vivo* fluxes can aid in the determination of optimal ARV release rates from IVR. For virus, we will introduce a sub-domain in the fluid compartment that simulates the volume of viral suspension added in PTM experiments. The PTM vaginal fluid velocity, also measured in these experiments, will then be applied in the longitudinal direction in the luminal compartment. Although advection is thought to be the primary driving force for luminal transport [4], diffusion may also be important in this compartment, especially for circumferential distribution of drug molecules after they are released from the device. It may be necessary to estimate the effective diffusivities of ARVs and HIV in the vaginal fluid layer. Since these diffusivities will likely not be transport-limiting, it may be sufficient to estimate them using the Stokes-Einstein equation and appropriate molecular shape factors [5]. We also plan to study the specific nature of molecular dynamics in the fluid layer to obtain a microscopic understanding of the process. Especially, we expect mucus structure and specific solute-mucus interactions to play a role in viral transport, whereas they may not impact ARV mobility.

A.6 Modeling Transport in the Tissue Compartments

Fluid-tissue partition coefficients and effective tissue diffusivities will be estimated experimentally and using microscopic simulations as described above. Through such measurements we will estimate if there is a difference in partitioning and effective diffusivity between the epithelial layer and the lamina propria. Partition coefficients at the lumen-epithelium boundary will be applied as jump conditions across the rendered surface separating the two compartments. We hypothesize that bulk transport in the

epithelium may be described purely by effective diffusivity Equation A.3. In the lamina propria, a fraction of particle concentration at any given point in the tissue will be eliminated per unit time, yielding Equation A.4 [1]. We will estimate the effective tissue elimination rate constant (k_{l2}) for each drug using Equation A.5 upon zero-order delivery from an IVR (assuming mass-balance in the plasma compartment), where, c_{LP} is the average steady-state concentration in the lamina propria estimated by biopsy extraction and MALDI-MS/MS imaging, K is the terminal elimination rate constant, which can be estimated for PTM, and C_p is the observed steady-state plasma concentration in PTM. It may be possible to describe the transport, cellular uptake, and elimination of HIV in a similar fashion as in Equation A.1. However, experimental determination of rate constants will be more difficult to obtain and results from microscopic simulations will be required. Effective diffusivities of HIV in tissues have been estimated experimentally by methods previously described [6]. Furthermore, molecular dynamics studies will enable us to assess if the effective diffusivity assumption is valid. It may be determined that position-dependent diffusivities need be used to properly describe the bulk motion of ARV and virus. If so, these quantities will be estimated from microscopic simulations.

A.7 Outer Model Boundaries

There will be several types of outer model boundaries employed. The pelvic floor will likely be modeled as an impermeable boundary, although the introitus to the vaginal canal will be modeled as an outflow boundary. Some modeling and experiment will need to be performed to determine the nature of the outer radial boundary. If MALDI imaging and initial model estimates reveal that drug concentrations at a certain depth into the tissue are sufficiently low, then a sink boundary can be employed at some radial distance

from the tract. In analytically approximating one-dimensional steady-state vaginal delivery, Saltzman imposed a semi-infinite boundary condition, which is an equivalent approach [7].

A.8 Conversion of TFV Prodrugs and Formation of TFV-DP

Effective rates of conversion for TFV prodrugs (e.g. TDF) to TFV can be estimated from published data [8]. This will result in a system of equations for simultaneous transport of the two compounds. The system for TDF transport in the lamina propria is shown as an example in Equation A.6a and A.6b. We propose that the relatively small amounts of the active TFV metabolite, TFV diphosphate (TFV-DP), formed in cells will not affect bulk transport of either TFV or its prodrugs. Thus, the average intracellular concentration of TFV-DP at any point can be estimated by probing the model as in Equation A.7 where k_{eq} are the effective equilibrium constants estimated from cell culture experiments. The cellular scale multicomponent mass transfer of the prodrug/TFV/TFV-DP system can be modeled in detail in one or more microscopic simulations, results of which will be used to determine the appropriateness of applying Equation A.7 at the continuum-scale.

A.9 Experimental Model Validation and Further Study

Solutions to 3D concentration profiles for drugs and virions from models outlined above will be compared to data obtained from tissue sections and MALDI experiments. This comparison will provide an opportunity to assess the sensitivity of model outputs to the biological variability of various physiological parameters and to assess the physical validity of assumptions made in model construction. If parametric optimization and

validation are successful, the effects of varying ARV dose regimen, drug properties, and biological variability can be further studied *in silico*. PTM finite element models could also be reconstructed at the human scale to enhance the clinical relevance of this work.

A.10 Expected Outcomes and Potential Pitfalls

Upon completion of this work, we expect to construct a mathematical model capable of quantitatively describing experimental vaginal drug and virus distribution data. If experimental validation is successful, we will be able to estimate the ARV release rates necessary to achieve protective ARV concentrations where HIV and CD4⁺ cells are present. There will likely be high variability in the *in vivo* data, the range of which may have a large impact on model predictions that may limit the utility of the integrated model. In equilibrium constants proposed for TFV-DP formation are embedded cell volume fractions, cellular uptake equilibria, and intracellular phosphorylation rates. If, through comparison of microscopic and continuum-scale modeling, as well as experimental data, this is found not to be a representative approximation of TFV-DP formation, we can further expand this part of the model. This may include a representation of distinct cellular structures and ARV uptake rates in the continuum model to replace the basic representation of the tissue as a spatially averaged homogeneous medium. We will likely find that cycle phase is important in drug and virus transport and drug metabolism. Our data will allow us to construct simulations specifically for follicular and luteal phase situations.

A.11 References

- [1] G.A. Truskey, F. Yuan, D.F. Katz, *Transport phenomena in biological systems*, Pearson Prentice Hall, Upper Saddle River, NJ, 2004.
- [2] T.J. Johnson, P. Srinivasan, T.H. Albright, K. Watson-Buckheit, L. Rabe, A. Martin, C.P. Pau, R.M. Hendry, R. Otten, J. McNicholl, R. Buckheit, Jr., J. Smith, P.F. Kiser, Safe and sustained vaginal delivery of pyrimidinedione HIV-1 inhibitors from polyurethane intravaginal rings. *Antimicrob Agents Chemother* 56(3) (2012) 1291-1299.
- [3] M.R. Clark, T.J. Johnson, R.T. McCabe, J.T. Clark, A. Tuitupou, H. Elgandy, D.R. Friend, P.F. Kiser, A hot-melt extruded intravaginal ring for the sustained delivery of the antiretroviral microbicide UC781. *J Pharm Sci* (2011).
- [4] A.R. Geonnotti, D.F. Katz, Compartmental transport model of microbicide delivery by an intravaginal ring. *J Pharm Sci* 99(8) (2010) 3514-3521.
- [5] I. Tinoco, K. Sauer, J.C. Wang, J.D. Puglisi, *Physical Chemistry: Principles and applications in biological sciences (Fourth Edition)*, Prentice Hall, Upper Saddle River, NJ, 2002.
- [6] C.Y. Gomez, T.J. Hope, Mobility of human immunodeficiency virus type 1 Pr55Gag in living cells. *J Virol* 80(17) (2006) 8796-8806.
- [7] P.Y. Kuo, J.K. Sherwood, W.M. Saltzman, Topical antibody delivery systems produce sustained levels in mucosal tissue and blood. *Nat. Biotechnol.* 16(2) (1998) 163-167.
- [8] L.C. Yuan, T.C. Dahl, R. Oliyai, Degradation kinetics of oxycarbonyloxymethyl prodrugs of phosphonates in solution. *Pharm Res* 18(2) (2001) 234-237.

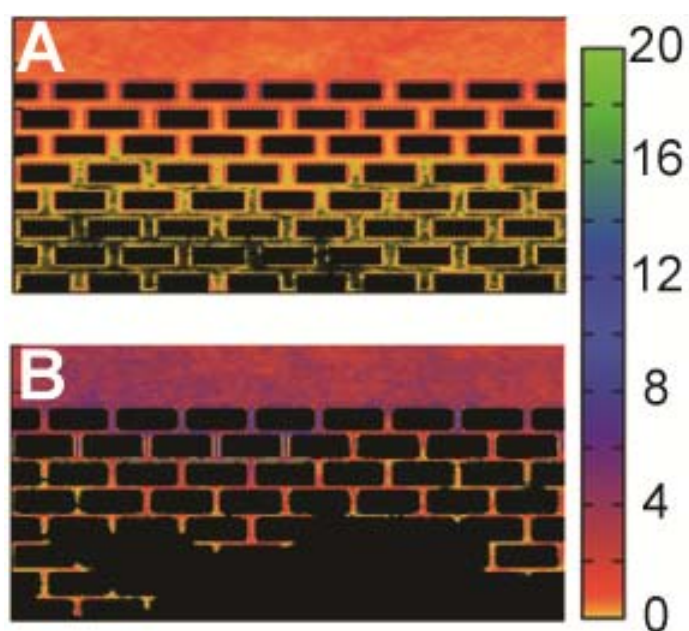


Figure A.1: Distribution of model drug (A) and virus (B) that arise from molecular dynamics simulations of a source (upper part of slab) and a model tissue. Molecular dynamics simulations were carried out using GROMACS.

$$\frac{\partial c}{\partial t} + \mathbf{v}\nabla c = D\nabla^2 c - c \sum k_i - k_{12}c \quad (\text{A.1})$$

$$\frac{\partial c}{\partial t} + \mathbf{v}\nabla c = D_{VF}\nabla^2 c \quad (\text{A.2})$$

$$\frac{\partial c}{\partial t} = D_{VE}\nabla^2 c \quad (\text{A.3})$$

$$\frac{\partial c}{\partial t} = D_{LP}\nabla^2 c - k_{12}c \quad (\text{A.4})$$

$$k_{12}\overline{c_{LP}} - KC_p = 0 \quad (\text{A.5})$$

$$\frac{\partial c_{TDF}}{\partial t} = D_{LP}\nabla^2 c_{TDF} - k_h c_{TDF} - k_{12,TDF}c_{TDF} \quad (\text{A.6a})$$

$$\frac{\partial c_{TFV}}{\partial t} = D_{LP}\nabla^2 c_{TFV} + k_h c_{TDF} - k_{12,TFV}c_{TFV} \quad (\text{A.6b})$$

$$c_{TFV-DP}(\mathbf{x}, t) \approx k_{eq,TFV} c_{TFV}(\mathbf{x}, t) + k_{eq,TDF} c_{TDF}(\mathbf{x}, t) \quad (\text{A.7})$$

Figure A.2: Continuum model for tenofovir. Compartmental description of continuum-scale mass transport in the vaginal epithelium. Shown is a generic linear transport PDE (A.1) describing convection, diffusion, chemical reactions, and elimination, along with reduced forms for the vaginal fluid/mucus (A.2), vaginal epithelium (A.3), and lamina propria (A.4). (A.5) is a simple mass balance argument for the blood compartment following steady state administration. TDF conversion to TFV during transport can be modeled by a coupled system of PDEs (A.6) (an example is shown for the lamina propria compartment). An equilibrium assumption (A.7) may be used to probe the model at any point in space-time to estimate average TFV-DP concentration in tissue.